STUDIES ON IGNITION AND FLAME PROPAGATION OF SOLID PROPELLANTS

FINAL REPORT COVERING THE PERIOD 22 JUNE 1966 THROUGH 22 JUNE 1967

Prepared for

JET PROPULSION LABORATORY
NATIONAL AERONAUTICS AND SPACE ADMINISTRATION
PASADENA, CALIFORNIA
CONTRACT NO. NAS 7-479

United Technology Center
DIVISION OF UNITED AIRCRAFT CORPORATION

UTC 2229-FR
13 November 1967

STUDIES ON IGNITION AND FLAME PROPAGATION OF SOLID PROPELLANTS

Research and Advanced Technology Department
UNITED TECHNOLOGY CENTER
Division of United Aircraft Corporation
Sunnyvale, California

FINAL REPORT
FOR THE PERIOD 22 JUNE 1966 THROUGH 22 JUNE 1967

Prepared for

Jet Propulsion Laboratory
NATIONAL AERONAUTICS AND SPACE ADMINISTRATION
Pasadena, California

Contract No. NAS 7-479

Prepared by:

J. D. Kilgroe
Project Engineer

Approved by:

R. O. MacLaren
Manager
Propulsion Research Branch

Submitted by:

R. S. Brown
Project Manager

C. M. Frey
Manager
Research and Advanced Technology Dept.

ABSTRACT

Studies were conducted to characterize heat transfer mechanisms of solid propellant pyrogen igniters. Experimental data were obtained from previously conducted tests which measured igniter heat transfer to non-reactive walls by firing solid propellant pyrogen igniters into an instrumented copper duct. The effects of mass flow rates and aluminized and nonaluminized igniter propellants were evaluated with two head-end igniter configurations and sonic and supersonic aft-end igniters.

For the fixed duct diameter and ratio of duct-to-igniter jet diameters tested, the most pronounced effect on heat transfer was attributable to igniter mass flow rate. Qualitatively, the higher flow rates resulted in sharper and higher peaks. Although the location of the maxima could not be analytically determined from theoretical considerations, all maxima were observed to be in the neighborhood of 2 port diameters downstream of the igniter exit plane. The amplitudes of the maxima were proportional to the mass flux G for aluminized igniter propellant and $G^{0.3}$ for nonaluminized propellants. The canted head-end igniters displayed significant higher peak-heat fluxes than the axial igniters tested, which is attributed to direct jet impingement upon the duct wall. Considerable differences in the circumferential heat flux in the impingement area persisted until 6 to 7 port diameters downstream of the impingement region.

Correlations are found for the length-dependent head-end igniter data; the correlations reducing to the classical full-developed pipe flow form approximately 10 diameters downstream of the maximum heat transfer point. Methods of determining the location and magnitude of the maximum heat transfer are also presented and discussed.

Correlations based upon the total igniter mass flow rate indicated that for distances greater than 3 port diameters downstream of the igniter exit plane, there was little effect of aluminum in the igniter propellant upon the convective heat transfer coefficient. At the maximum heat transfer points, the aluminized propellants exhibited approximately 20% higher heat coefficients.

No general correlations were found which were believed to be valid for aft-end ignition. Unknown flow dynamics and limited test data prohibited a meaningful generalized correlation.

CONTENTS

CONTENTS (Continued)

ILLUSTRATIONS

ILLUSTRATIONS (Continued)

ILLUSTRATIONS (Continued)

TABLES

SYMBOLS

Nu	Nusselt number = hD/k
Pr	Prandtl number = $\frac{\mu C_p}{k}$
Re	Reynolds number = $\frac{GD}{\mu}$
St	Stanton number = $\frac{h}{C_p G}$
A	Cross-sectional area
a	Constant
b	Constant
C	Specific heat
c	Constant
D	Diameter
e	Constant
f	Constant
Fc	Radiation calorimeter calibration factor
G	Mass velocity = $\dot{w}/A$
g	Constant
T	Temperature
h	Convective heat transfer coefficient
k	Thermal conductivity
k_1, k_2	Constants
K	Constant
l	Thickness

M	Mass of radiation calorimeter slug
P	Pressure
q	heat flux
r	Radius
$\dot{r}_p$	Flame propagation rate
SF	Scale factor
t	Time
$\dot{w}$	Mass flow rate
x	Axial distance along duct measured from end of duct
x'	Axial distance along duct measured from igniter jet impingement point

GREEK SYMBOLS

α	Thermal diffusivity
γ	Ratio of specific heats
ϵ	Emissivity
λ	Wavelength
μ	Viscosity
ρ	Density
ϕ	A function of x'

SUBSCRIPTS

aw	Adiabatic wall conditions
b	Bulk or stream conditions or burning propellant
c	Chamber conditions
cu	Copper

e	Nozzle exit plane
i	Igniter
j	Jet
ign	Conditions in the igniter or igniter exit
m	Average
max	Maximum
rad	Due to radiation
w	Wall conditions
x	Conditions at axial location x (e.g., Nu_x)
∞	Conditions at infinity (e.g., Nu_∞)
o	Initial conditions

1.0 INTRODUCTION

Significant advances have been made during the past decade in the design and use of solid propellant igniters. These advances have resulted from a definition of design principles based on theoretical considerations and experimentally developed criteria. The results of many studies have shown that ignition can be characterized by a knowledge of the thermal energy input to the solid propellant surface and the response of the propellant to this input. Studies have indicated that ignition is established at any point on the propellant surface when runaway reaction conditions are attained (i.e., an autoignition temperature which depends on igniter heat flux and chamber pressure), and that the total ignition event is characterized by the time and spatial variation in attainment of the runaway reaction conditions. Because of spatial input variations to the solid propellant grain resulting from use of different igniter configurations, various locations reach runaway conditions at different times yielding an ignition front which propagates across the surface. The rate of propagation is dependent upon the previous time history heat input to the propellant grain and definition of this time history with location is necessary to characterize the total ignition event. Thus, the important characteristic of any ignition system is the heat flux to the propellant surface produced by the igniter.

A commonly used method of ignition is the pyrogen igniter which contains a small solid propellant charge to provide the thermal energy required for ignition. The energy transfer from the relatively nonreactive exhaust of the pyrogen igniter flowing along the surface of the grain prior to first ignition is controlled primarily by convective heat transfer. This type of

heat transfer is determined by the gaseous boundary layer over the surface of the propellant, which in turn is a function of the gas mass velocity and the structure of the velocity and temperature fields adjacent to the propellant surface. Established convective heat transfer correlations for developing boundary layers are not directly applicable because of the complicated flow dynamics induced by the igniter jet.

The objectives of this program are to analyze and correlate experimental data obtained under National Aeronautics and Space Administration (NASA) Contract No. NAS 7-302 for pyrogen igniters. These correlations were conducted to provide an analytical characterization of the igniter heat input to the solid propellant surface in order to provide information for igniter design and definitions of ignition transients.

2.0 SUMMARY AND UTILITY OF RESULTS

The following paragraphs summarize the more significant results of the present study:

2.1 AXIAL HEAD-END IGNITERS

From test data employing axial head-end igniters, the most pronounced effect was found to result from igniter mass flow rate for the fixed-duct diameter and ratio of duct-to-igniter jet diameters. The higher flow rates resulted in higher heat flux peaks while the lower flow rates displayed reduced maxima and broadened peaks. Maximum heat transfer was observed to be in the region of 2 port diameters downstream of the igniter exit plane. The location of the maxima could not be analytically determined from theoretical considerations. The amplitudes of the heat flux maxima were proportional to the mass flux for aluminized igniter propellant and mass flux to the 0.3 power for nonaluminized propellants.

For the range of parameters studied, it was found that the heat flux at any axial location could be reconstructed by use of the following equations

$$\left(\frac{hD}{k}_{x'}\right) = 0.033\ (1+1.23e^{-0.418x'/D})\ Re^{0.8}\ Pr^{0.3} \qquad (1)$$

(nonaluminized)

and

$$\left(\frac{hD}{k}_{x'}\right) = 0.033\ (1+2.0e^{-0.50x'/D})\ Re^{0.8}\ Pr^{0.3} \qquad (2)$$

(aluminized)

It should be noted that these equations are valid only for jet expansion pressure rates (P_j/P_c) from 20 to 45 and duct-to-jet nozzle diameter ratios (D_d/D_i) from 10 to 15. Adjustment of peak values for length ratios (x'/D)

of less than 2.0 is desirable for Reynolds numbers less than 36,000.

Convective heat transfer upstream of the region of maximum heat flux depends upon the relative igniter and duct configuration. Stagnation areas and zones of recirculation result in ill-defined flow fields which are geometry-dependent. However, for the configurations studied, the head-end heat transfer may be approximated by the equations

$$Nu = 0.033 \; \phi x' \; Re^{0.8} Pr^{0.3} \qquad (3)$$

where

$$\phi x' = 2.23 - 0.7x'/D \; ; \; x'/D \leq 0 \qquad \text{(nonaluminized)} \qquad (4)$$

$$\phi x' = 3.0 - 1.25x'/D \; ; \; x'/D \leq 0 \qquad \text{(aluminized)} \qquad (5)$$

2.2 CANTED HEAD-END IGNITERS

Significantly higher peak heat fluxes resulted when using canted head-end igniters in comparison to the axial igniters. This difference is attributed to direct jet impingement upon the duct wall. The canted igniters produced considerable variations in the circumferential heat flux in the impingement area which persisted for 6 to 7 port diameters downstream of the impingement region.

The maximum heat flux location for all cases corresponds with the region of direct jet impingement and the magnitude of the maximum heat flux was found to be proportional to the igniter mass flow rate. Widely different maximum heat fluxes for two tests with comparable igniter mass flows but differing igniter jet pressure ratios were interpreted as a result of the jet spread at the impingement area and it is concluded that the duct back pressure has a profound effect on the maximum heat flux of impinging jet igniters. This effect should be particularly evident during the

transient ignition period when duct pressure varies considerably.

For the limited data available for correlation, the convective heat flux downstream from the maximum may be determined by the equation

$$Nu_x = \frac{hD}{k} = 0.0278\ (1+k_1 e^{-k_2 x'/D})\ Re^{0.8}\ Pr^{0.3} \qquad (6)$$

where

$\left(\frac{Nu_x}{Nu_\infty}\right)_{max}$ can be determined from figure 1 and

$$k_1 = \left(\frac{Nu_x}{Nu_\infty}\right)_{max} - 1$$

$$k_2 = -\frac{1}{6} \ln (0.1/k_1)$$

Insufficient data in the peak heat flux region were obtained to correlate the results of the aluminized igniter propellant. However, for distances greater than 3 port diameters downstream of the impingement region for the canted nozzle tests, correlations are applicable.

2.3 AFT-END IGNITION

No general correlations were found which were believed to be valid for aft-end ignition. The limited test data were insufficient to permit evaluation of the flow dynamics; therefore, meaningful generalized correlations could not be obtained.

Length-dependent heat flux distributions agreed closely with results reported by other investigators. For the range of configurations tested, the parameters of primary significance were the igniter mass flow rate and nozzle configuration.

Supersonic nozzle igniters displayed superior igniter gas duct

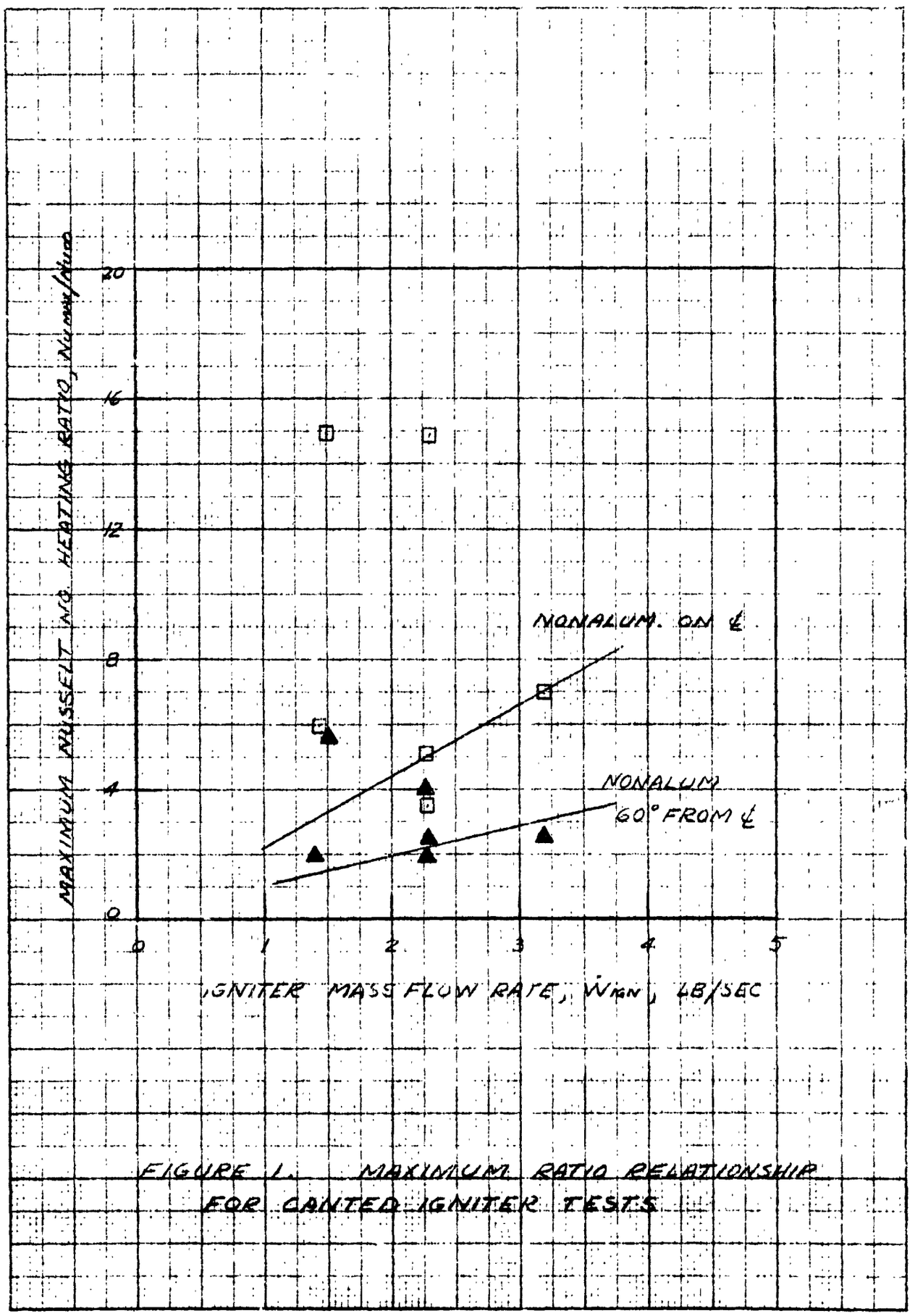

FIGURE 1. MAXIMUM RATIO RELATIONSHIP FOR CANTED IGNITER TESTS

penetration. Heat flux levels for the sonic and supersonic nozzles were comparable for the same igniter mass flow rates, but the points of maximum heat flux corresponding to plume penetrations for the supersonic nozzles were approximately 1 port diameter (upstream of the duct head-end) in comparison with the sonic nozzle tests. The maxima for the supersonic igniters were approximately 2.5 duct diameters from the igniter nozzle exit plane while the maxima of the sonic igniters were in the region of 1.5 diameters.

The maximum convective heat fluxes for aft-end igniters may be calculated by use of developed equations. However, since a general length correlation was not found, it is recommended that the maximum heat flux be calculated and a flux profile be constructed to approximate the axial heat flux distribution.

2.4 RADIATION HEAT FLUX

Radiation heat fluxes generally were found to be less than 10% of the observed convective values. For head-end igniters, the highest values were observed at the center of the duct with reduced levels at the ends. Similar profiles were noted for aft-end igniters, but they were considerably shortened due to the head-end stagnation zone. Adequate determination of radiation flux levels may be obtained by theoretical calculations.

2.5 ALUMINUM CONTENT

Correlations based upon the total igniter mass flow rate indicated that for distances greater than 3 port diameters downstream of the igniter exit plane, there was little effect of alumina in the igniter propellant exhaust upon the convective heat transfer coefficient (h). At the maximum heat transfer points, the aluminized propellants exhibited approximately

20% higher heat coefficients. This heat transfer coefficient at the maximum points is attributed to impingement and condensation of hot alumina particles on the duct wall and possible two-phase flow effects resulting in modifications in the thermal and velocity boundary layers.

3.0 TECHNICAL BACKGROUND

The technical studies conducted on the current program were an extension of solid propellant ignition studies conducted under Contracts No. NAS 7-156, NAS 7-302, and NAS 7-329. In the programs under NAS 7-156 and NAS 7-329, the major emphasis was the analytical development and experimental substantiation of a general theoretical model describing ignition and subsequent flame (ignition) propagation on a propellant grain in environments characteristic of combustion exhaust products from rocket exhaust (pyrogen) and hypergolic type igniters. Under Contract No. NAS 7-302, igniter flow dynamics and heat transfer mechanisms in nonreactive environments were studied to characterize induced heat transfer from pyrogen igniters to solid propellant grain surfaces.

The objective of the current program was to complete reduction and correlation of experimental data generated under NAS 7-302 and incorporate this data with correlations developed under NAS 7-156 and NAS 7-329 into an analytical model suitable for use in igniter design. For clarity of presentation the results of earlier programs are discussed in the following paragraphs as background information for the current program.

3.1 CONTRACT NO. NAS 7-156 - INVESTIGATION OF IGNITION UNDER FLOW CONDITIONS

Under Contract No. NAS 7-156, theoretical analyses were developed to describe the total ignition transient in solid propellant motors. These analyses were based upon experimental observations which indicated that the time required to initiate overall combustion of a solid propellant rocket grain and develop steady-state operating pressure in the motor can be divided into three sequential though somewhat overlapping intervals (see figure 2). During the first phase, the propellant is subjected to the action of a rocket-exhaust, pyrotechnic, or hypergolic igniter alone. When runaway reaction

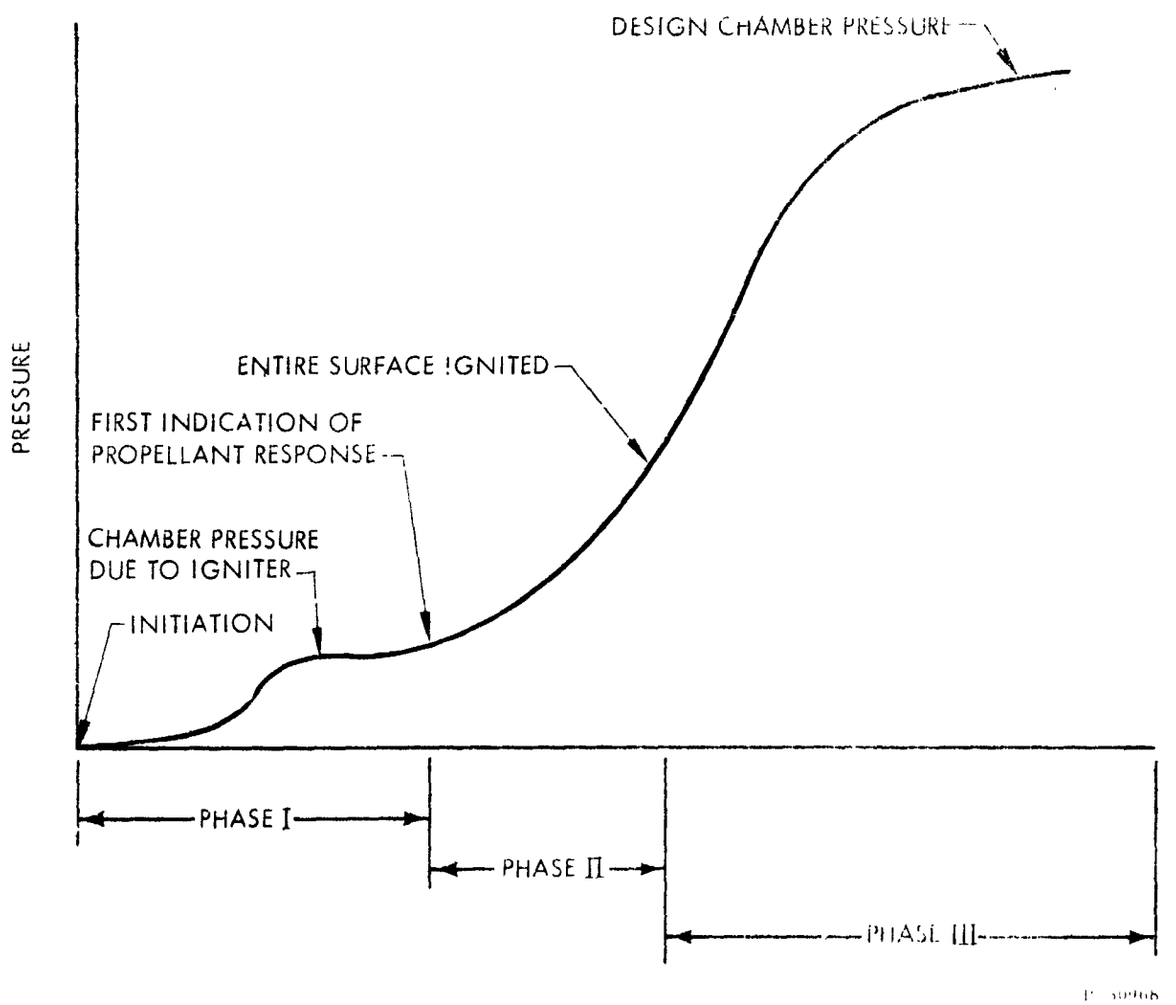

Figure 2. Schematic Diagram of Chamber Pressure Transient During Ignition

conditions are reached at the point of maximum heat transfer, the propellant ignites, initiating steady-state combustion completing the first phase of the motor ignition process. The time interval of this phase is a function of the ignition response of the propellant and the heat-transfer characteristics of the igniter.

In the second phase, the heating of the unignited portion of the propellant surface continues, promoting propagation of the flame across the unignited surface of the grain. During this phase the addition of propellant combustion products to the flowing igniter gases causes the motor pressure to increase. This addition of combustion products modifies the heat transfer characteristics of the igniting environment by disrupting the igniter gas flow patterns; by the increase of mass flow rate; by decreasing the concentration of any hypergolic agents present in the flowing gas; and if the igniter gas temperature differs from that of the propellant combustion products, by a change in the mixed gas temperature. As each location on the propellant surface reaches runaway reaction conditions, combustion is initiated at that location. Initiation of combustion at all points on the propellant surface completes the second phase of the motor ignition process.

During the third phase, the motor chamber continues to fill with propellant combustion products until steady-state pressure has been achieved. The time required to complete this phase is determined by the ballistic accumulation of combustion gases in the motor, the burning rate characteristics of the propellant, and the igniter gas flow.

Fundamental to the theoretical model is the use of the autoignition surface temperature concept as the criterion for propellant ignition. The use of such a concept under many practical conditions has been well

substantiated by studies of Baer and Ryan,[1] Anderson, [2][3] Price, [4] and Beyer [5] which have shown that under most conditions simulating motor ignition,* the autoignition temperature is an invariant quantity. Only under conditions of extremely high flux or low ignition pressure does the variation in ignition temperature become significant. In these cases, suitable modifications can be made in the analysis by using a flux pressure dependent autoignition temperature, thereby satisfying these extreme conditions.

Theoretical analysis was developed to describe the first point of ignition and subsequent ignition propagation on a solid propellant grain. The analysis is based on the solution of the two-dimensional energy equation to simulate the thermal behavior of the solid propellant. The simultaneous solution of the one-dimensional equations describing the axial variation of energy content and oxidizer concentration is used to simulate the behavior of the igniting environment. The equations describing the theoretical model are solved by numerical procedures to yield the temperature history of the propellant surface. From this temperature history and the propellant autoignition temperature, the ignition delay and subsequent ignition propagation rate are computed.

Concurrent with the development of the theoretical model, an experimental program was conducted to measure the rate of flame propagation** across the surface of a propellant sample. Examination of the experimental results in conjunction with numerical solutions of the theoretical model showed ignition

---

* Under normal motor ignition conditions the pressure in the main motor generated by igniter gas flow is of the order of 1 to 3 atm and the flux ranges from 5 to 35 cal/cm^{2}sec.

** Flame propagation as used here is synonymous with ignition propagation.

and ignition propagation are determined by the absolute value of, and by the variation in, the rate of heat transfer along the surface of the grain, both prior to and after first point ignition on the grain surface. Specific results of the theoretical and experimental phases of NAS 7-156, which formed the basis of the previously described ignition model and subsequent investigations, are summarized below:

A. Ignition and ignition propagation phenomena can be described theoretically on the basis of the transient heat-transfer characteristics of the igniting environment. Agreement between theory and experiment is obtained when the heat-transfer and heat-generation characteristics of the igniting atmosphere are known quantitatively or are measured accurately.

B. The rate of ignition propagation across the surface of a solid propellant results from a variation in heat flux with position on the propellant surface. Thus, the important variables controlling the ignition delay and ignition propagation rate are the gas mass velocity, gas temperature, gas composition, gas pressure, port diameter, thermal properties of the propellant, and the propellant ignition temperature.

C. In environments where convective heat transfer dominates the propellant heating, the ignition propagation rate can be scaled by the approximate relation.

$$\dot{r}_p \propto St/\dot{q}^2 \qquad (7)$$

D. The propagation rate was shown to have a maximum value; the maximum being the linear velocity of the flowing gases. This maximum value is observed in hypergolic environments and also in large diameter ports, i.e. 30 in., where convective and radiative heating dominate the process.

E. Convective heat-transfer studies demonstrate that the heat-transfer coefficient during the propagation period is significantly higher than values calculated from normal laminar or turbulent boundary layer relations. This difference is primarily caused by the complex nature of the flow field in the region downstream of the advancing flame.

F. In instances when the temperature of gaseous products from the igniter is significantly different, i.e., greater than 500°C, from the propellant flame temperature, thermal equilibrium between these two streams is not achieved in the flame zone.

G. The absolute value of the convective heat flux from typical head-end rocket exhaust igniters cannot be predicted from currently available heat-transfer correlations.

3.2 CONTRACT NO. NAS 7-329 - INVESTIGATION OF IGNITION PROPAGATION

As a logical extension of these basic studies, theoretical and experimental studies were conducted on ignition propagation phenomena and solid propellant motor ignition conditions. Ignition and ignition propagation resulting from head-end and aft-end rocket exhaust igniter action were determined by means of propellant tripwire plugs mounted in the surface of the motor grain. Ignition-propagation period, convective heat-transfer rates, and igniter-produced convective flux patterns were measured using platinum thin-film flux gages also mounted in the motor grain surface.

Experimental ignition propagation measurements downstream of the point of first ignition in the motor were shown to agree with the predicted results of a previously developed theoretical analysis based on the autoignition temperature concept, if the igniter-produced energy transfer and the ignition-propagation energy transfer can be accurately predicted.

The ignition-propagation energy transfer studies showed that over much of the ignition-propagation period, downstream convective fluxes can be based on the empirical expression

$$h = h_i \left(\frac{\dot{w}_b + \dot{w}_{ign}}{\dot{w}_i} \right)^{0.5} \qquad (8)$$

using the assumption that instantaneous mixing occurs between propellant combustion products and igniter products.

Ignition delays and convective fluxes measured in motor tests were found to agree with laboratory arc-image furnace studies. The agreement between the arc-image furnace data and the motor data indicates the ignition requirements of different propellants can be easily characterized in the laboratory, minimizing the need for more expensive motor ignition studies.

Ignition in the test motor was observed to first occur 1.0 to 2.0 motor port diameters downstream of the head-end axial, single-port igniter nozzle. The igniter heat-transfer measurements showed that maximum convective heat transfer also occurred in this region. The igniters in these tests used converging sonic nozzles which produced rapidly expanded exhaust plumes. Plumes produced by expansion nozzles would tend to be channeled with the resulting point of maximum heat transfer and consequent first ignition point further downstream. Once first ignition was achieved, ignition propagated in both the fore and aft directions. Ignition propagation downstream of the point of first ignition was observed to be much faster than the head-end ignition propagation rate because of the accelerating influence of the addition of propellant combustion products from the ignited areas.

Head-end canted, three-port igniter nozzles produced first ignition (or extreme ablation quickly followed by ignition) in the impingement zones about 1.0 motor port diameters downstream of the igniter nozzle. First ignition was followed by anular upstream and downstream flame spreading. Although first ignition occurred sooner with the canted nozzles than with the axial nozzles, because of the much higher flux levels in the canted nozzle impingement zones, complete motor ignition was achieved only slightly sooner with the canted nozzles.

First ignition and complete motor ignition were both observed to be slightly slower when nonaluminized igniter propellants were used rather than aluminized igniter grains. These tests did not show conclusively whether the higher flux levels and resultant faster ignition achieved by the aluminized igniter products resulted from the higher flame temperatures or from particle impingement and condensation.

Aft-end ignition and ignition propagation were found to be controlled primarily by the igniter-produced flux levels. However, the propagation rates that would be predicted on the basis of the igniter flux levels are slower than the observed flame spreading rates indicating that ignition propagation upstream of the ignited zone is enhanced to a significant degree by the propellant combustion products.

As a result of the studies under Contract No. NAS 7-329 it was concluded that the development of quantitative motor ignition design procedures necessitates knowledge of (1) the ignition requirements of the propellant, (2) the igniter flux distribution, and (3) change of convective flux during ignition propagation. Of these three areas, item (2), quantitative descriptions of typical igniter flux patterns, is most lacking. Until

such relationships are developed, igniter design must necessarily be on an empirical basis.

3.3 CONTRACT NO. NAS 7-302 - HEAT TRANSFER STUDIFS OF SOLID ROCKET IGNITERS

The object of the NAS 7-302 program was to characterize solid propellant pyrogen igniter heat transfer. Experimental work on the program included flow visualization tests for observation of igniter jet plumes by use of a flow duct and Schlieren systems. Data on heat transfer was obtained using igniters of various configurations fired into an instrumented copper duct.

Flow visualization tests indicated that the location of the first Riemann wave for axial head-end igniters was within approximately 10% of the location predicted by an empirical relation of Lewis and Carlson.[6] For aft-end igniters, the shock location was found to be closer to the nozzle than predicted of the method of Lewis and Carlson or based on theoretical distances predicted by Love and Grigsby.[7] The shock locations in the jets from the multiple port (canted) head-end igniters were also closer to the nozzle exits than predicted by reference 6 or 7. High turbulence and high degree of breakdown of igniter jet over a relatively short range was indicated on all tests. There were no indications of high velocity or turbulence in the separated "base" region, suggesting that convective heat-transfer in this region should be small.

The basic test apparatus is described in the following paragraphs to provide a basis for understanding the experimental data. This apparatus, used to model solid propellant motor igniter heat transfer, was an instrumented 8-in.-diameter, 96-in.-long copper duct with an 0.125-in. wall. The copper tube was instrumented to provide data on the spatial and time variation of total heat transfer, radiant heat transfer, and duct static pressure

as shown in figure 3. Duct instrumentation included 16 externally mounted thermocouples, six radiometers, and six pressure transducers. Basic pyrogen igniter configurations tested were: (1) head-end axial igniters, (2) head-end igniters with canted nozzles, (3) supersonic aft-end igniters, and (4) sonic aft-end igniters using both aluminized and nonaluminized igniter propellants. Two duct nozzle orifice sizes were used to vary duct steady-state pressure while maintaining constant duct mass flux (Reynolds number).

Total heat transfer data were obtained from 16 constantan wires peened into the outside surface of the duct to form thermocouple junctions with the pure copper duct. The constantan wires were led to an insulated reference junction box. The igniter duration was sufficiently short so that the maximum errors produced by conduction away from the thermocouple junctions were less than 4% and, in most cases, less than 1%.

Accurate determination of the transient heat transfer during igniter startup requires an instrument with faster response and higher sensitivity than the backside thermocouple. However, attempts made to design and produce an instrument which was capable of accurately measuring the desired transient and yet could withstand repeated uses in the severe duct environment without major repairs were unsuccessful.

The radiation heat flux calorimeters shown in figure 4, as developed at UTC, consist of a copper slug sensing element with a thermocouple soldered onto the backside. The sensing element was approximately 0.020-in.-thick with a diameter of 0.35 in. The thermocouple junction, formed from 4-gauge chromel and constantan wire was silver soldered onto the back of the copper sensing element. Accurate measurements of the mass of the slug, wire, and solder were made so that the heat capacity could be calculated for the

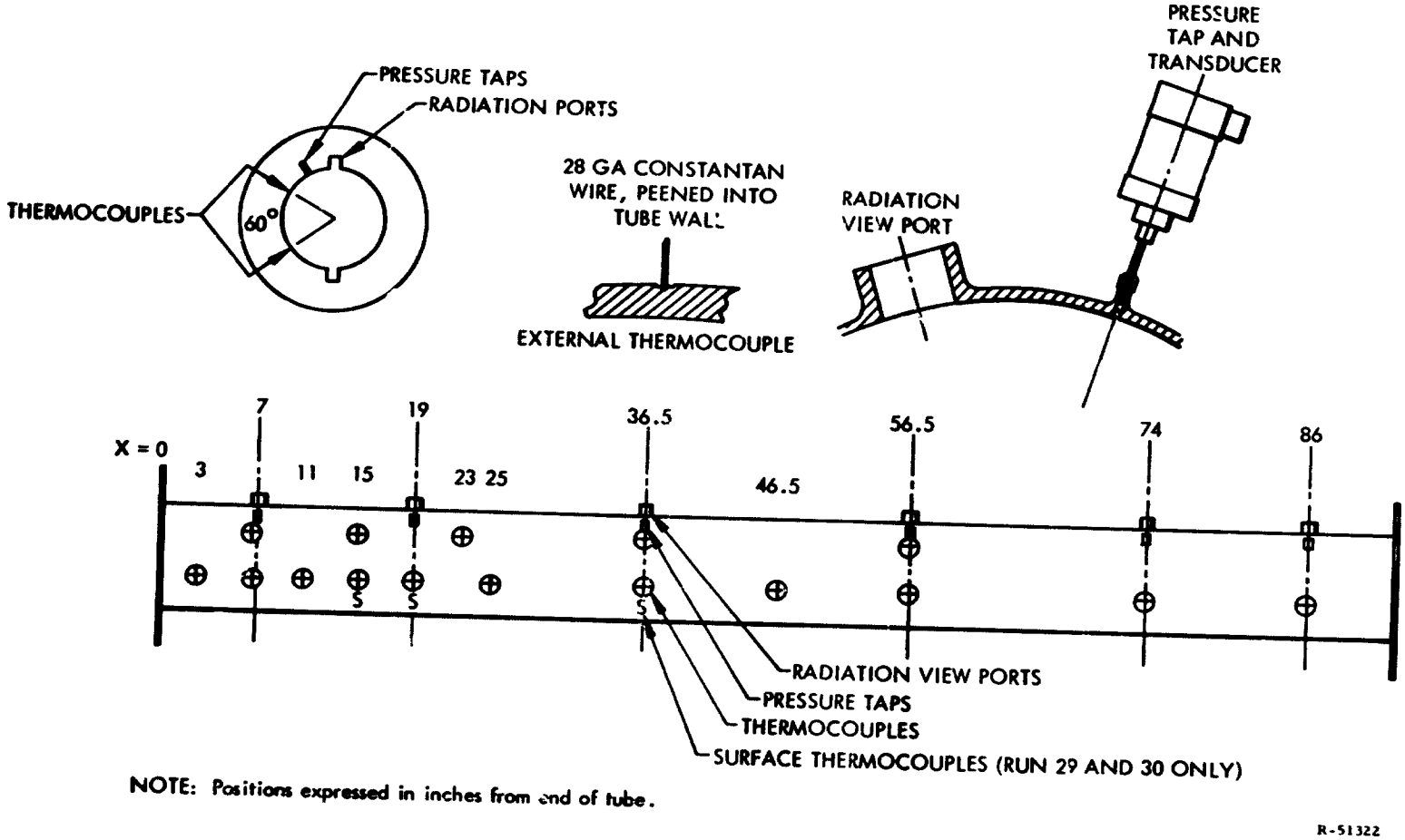

NOTE: Positions expressed in inches from end of tube.

R-51322

Figure 3. Copper Tube Instrumentation

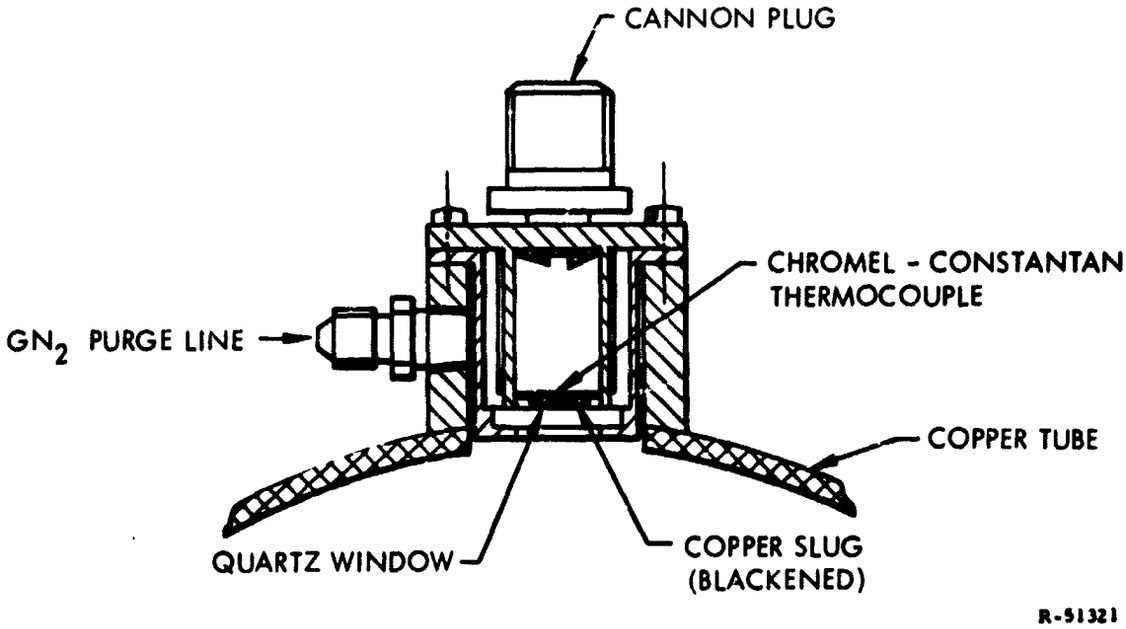

Figure 4. United Technology Center's Radiation Calorimeter

finished slug. The slug was mounted in an aluminum holder and the thermocouple wires led to a standard two-wire electrical connector. The surface of the copper slug was blackened with a very thin coating of flat black paint to minimize the reflectivity. By comparing the results of calibration runs using HyCal gages and UTC gages with no quartz windows installed, it was found that the UTC gage sensing element has an approximate 0.84 to 0.85 surface absorptivity.

The holder was inserted into an aluminum case which contains an O-ring sealed quartz window approximately 0.10-in.-thick. The sensing element was positioned within approximately 0.005 in. of the quartz window. The quartz window transmits approximately 90% of the incident, radiant energy within the band 0.4 μ to 2.2 μ . In other work at United Technology Center (UTC),[8] it was shown that rocket exhaust clouds have a spectral radiation intensity distribution similar to that of a gray body. Therefore, the wavelength of peak radiation intensity may be calculated from classical thermal radiation relationships. Hence, for gas clouds at 5,960° and 5,220°R corresponding to the combustion temperatures of aluminized and nonaluminized igniter propellants, peak radiation intensity is obtained at wavelengths of about 0.8 μ and 1.0 μ , respectively. This is well within the band of peak transmissivity of quartz; therefore, it was concluded that not more than about 10% of the incident radiation was lost due to the absorptance and reflectance of the quartz windows.

The radiometers were calibrated prior to the tests by comparing the heat absorption rate of radiometers to that of the more sensitive (but more delicate) HyCal gage under the same incident radiation. By appropriate correction to the HyCal gage readings, the incident flux calibration for the UTC radiometers was obtained. The resulting calibration factors are shown in table I.

TABLE I

UTC RADIATION CALORIMETERS:
HEAT CAPACITY AND CORRECTION FACTOR

UTC Gage Serial No.	$\frac{mC_p}{A}$ Btu/in^2 -^oF	$\frac{1}{F_c \cdot \text{HyCal}}$
1	6.85×10^{-4}	1.48
2	6.79	1.59
3	6.78	1.55
4	6.60	1.47
5	6.66	1.41
6	6.56	1.47
7	6.77	1.54
8	6.70	1.46
9	6.71	1.44
10	6.64	1.51
11	6.59	1.39
12	6.64×10^{-4}	1.42

Pressure taps were provided at six locations along the duct length as shown in figure 3. An 0 to 100 psia Taber Model A106 transducer was connected to each of the six pressure taps by a short length of tubing as shown in figure 5. Igniter chamber pressure was recorded by an 0 to 1,000 psig Taber pressure transducer.

An electric calibration of the recording circuit for all instrumentation channels was made prior to each test. A sample thermocouple circuit is shown in figure 6. With the calibration switch in the down position, the galvanometer was subjected only to the output from the thermocouple. With the switch in the up position (shown), the thermocouple was taken out of the recording circuit and the calibration circuit was substituted. Measurement of the calibration voltage was made with a potentiometer capable

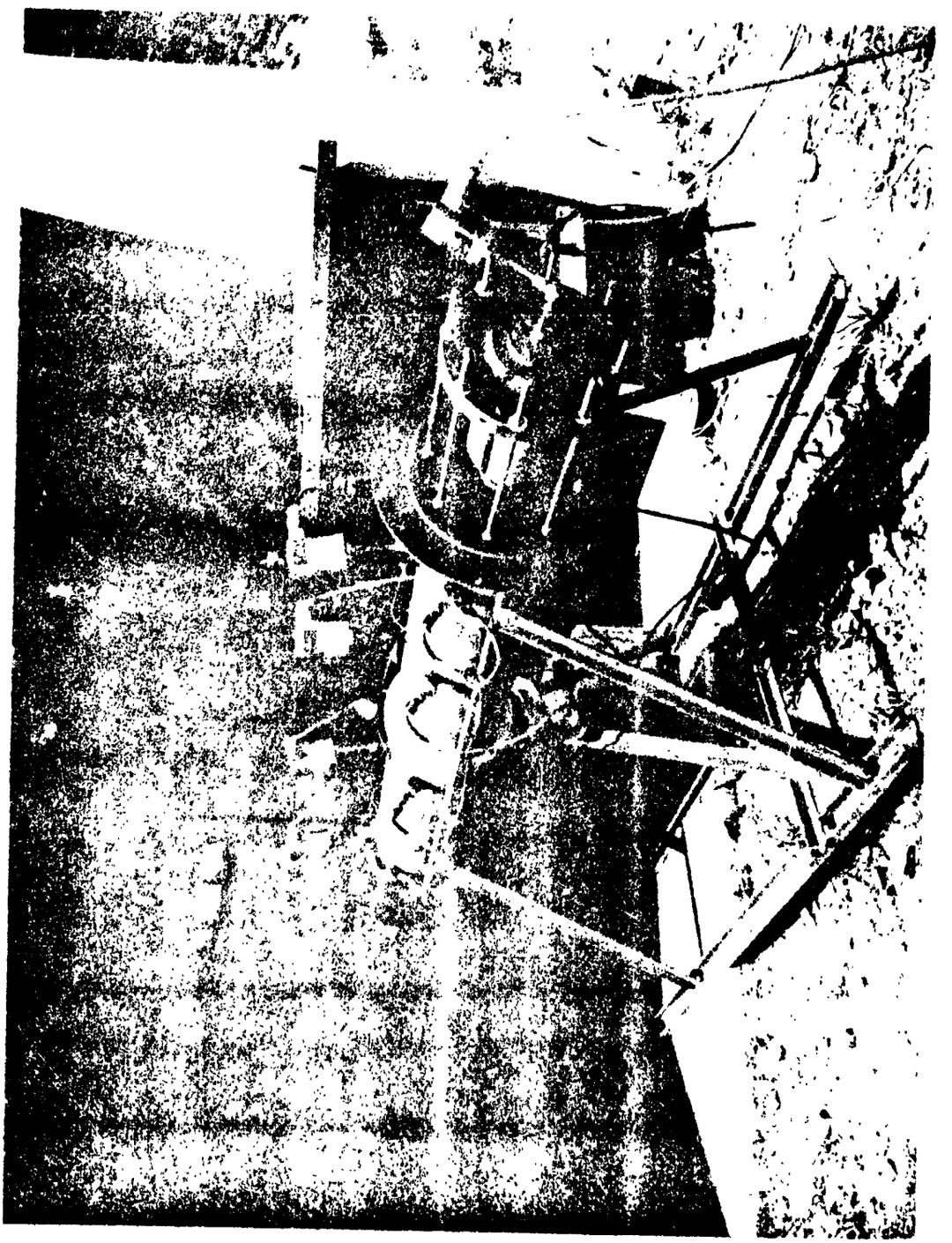

Figure 5. Copper Duct Apparatus

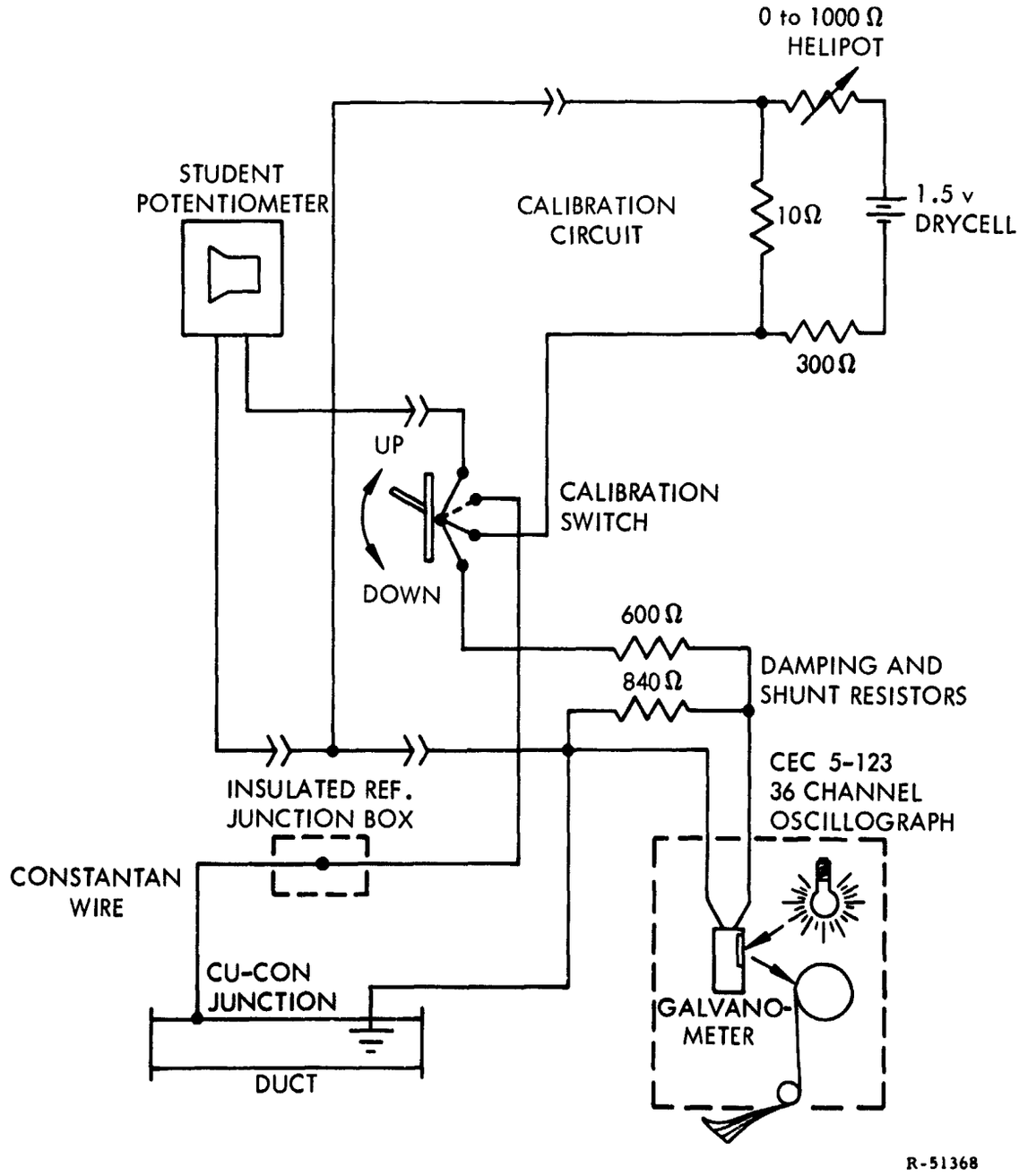

Figure 6. Schematic of Typical Thermocouple Circuit, Including Calibration Circuit

of reading to within 0.001 mw. Two steps in calibration voltage were made prior to each run by varying the 0 to 1,000-ohm helipot setting.

The basic pyrogen igniter used in the test program contained a squib and BKN pellet basket initiator and igniter propellant cast onto phenolic sleeves which fit into the igniter cases. The igniter propellant burning area was varied to provide three design flow rates for durations of 300 msec at a nominal chamber pressure of 1,000 psia. The aluminized (UTP-1095) and nonaluminized (UTX-6937) propellants were selected to provide similar burning rates at 1,000 psia. Table II presents a comparison of constituents and ballistic properties for the two propellants. Equilibrium thermodynamic calculations indicate that the temperature of the combustion products in the chamber will be about 4,760°F for the nonaluminized propellant and about 5,500°F for the aluminized propellant (18.5 moles of Al_2O_3 per 100 g of propellant in the chamber).

TABLE II

IGNITER PROPELLANT PROPERTIES

	Weight, %	
Constituent,	UTP-1095	UTX-6937
PBAA/AN Binder	16.0	16.0
Ammonium Perchlorate	73.0	82.0
Aluminum	10.0	0.0
Iron Oxide	1.0	2.0
Exhaust Combustion Temperature, °R	5,960	5,220
Characteristic Velocity, (c*) ft/sec	5,000	4,900

The igniter cases were of two basic designs to accommodate either axial or canted nozzle inserts and were capable of being mounted either at the closed or open end of the copper duct to simulate head-end or aft-end ignition configurations. Igniter nozzles were sized to maintain a nominal igniter pressure of 1,000 psi for all tests. The head-end axial igniter had three available sonic nozzle inserts to accommodate three flow rates. The head-end configuration with the multiple-port (canted) igniter was also fitted with one of three sets of sonic nozzles to accommodate three mass flow rates. The axial and multiple port igniter configurations are shown in figure 7.

The aft-end igniter could be placed at the duct exit or partially inserted into the duct as shown in figure 8. Nozzle expansion ratios at near optimum expansion and unexpanded (sonic) conditions were tested. Three sizes of aft igniter nozzles were available to provide three igniter flow rates. Orifice plates were attached to the open end of the copper duct to maintain the desired duct pressure. Ten of the 13 aft-end ignition tests were conducted with the igniter inserted approximately 10-1/2 in. into the duct. In these tests, the duct pressure was regulated by adjusting the gap between the igniter and the duct end flanges. The position of the igniter in the aft-end of the duct is shown in figure 8.

During tests employing aluminized igniter propellant, a film of Al_2O_3 was deposited on the duct wall and was found to be heaviest in the vicinity of the jet impingement areas. This film was removed with emery paper and the surface in the vicinity of the thermocouple instrumentation was carefully cleaned prior to each test.

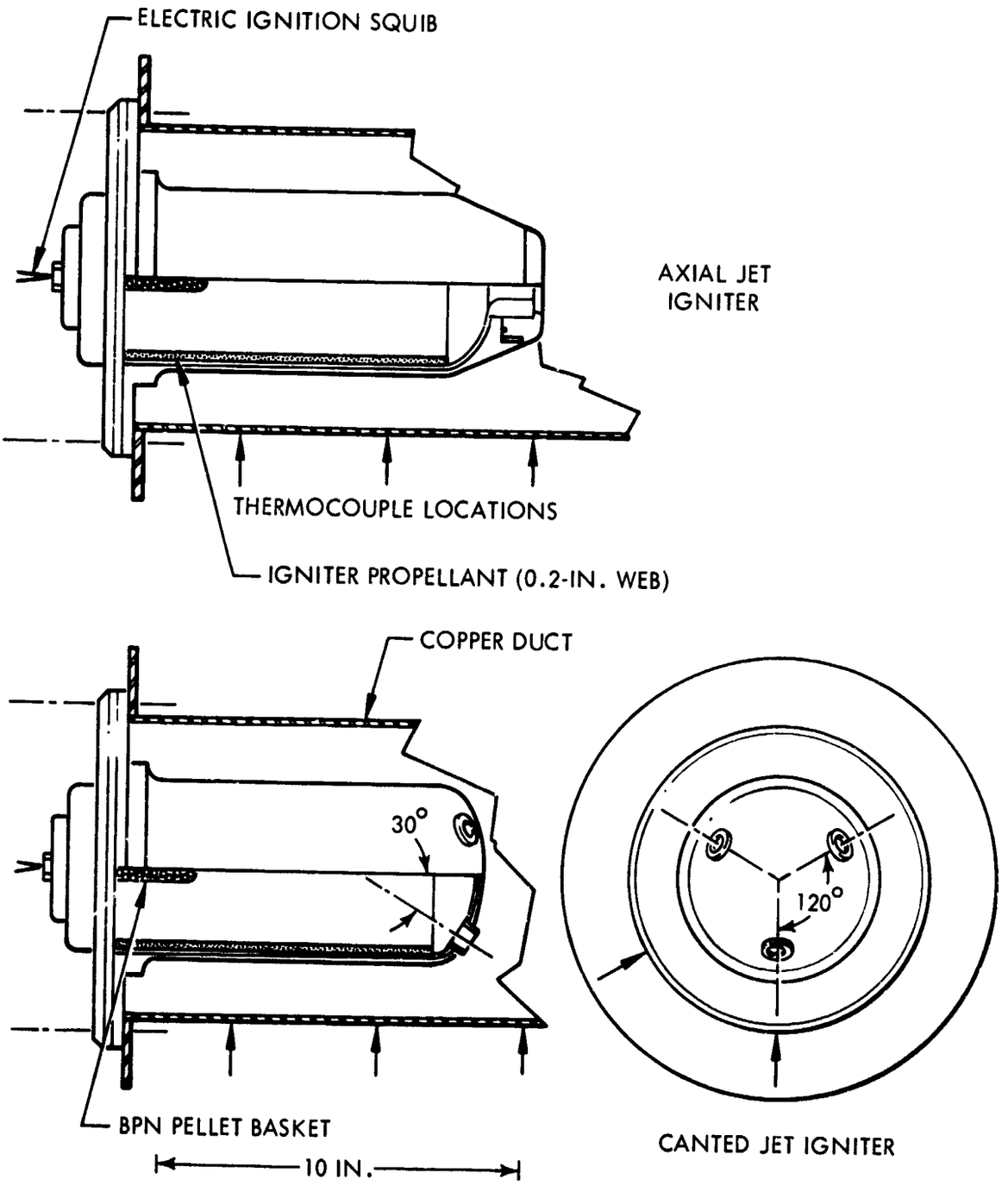

Figure 7. Head-End Igniter Configurations

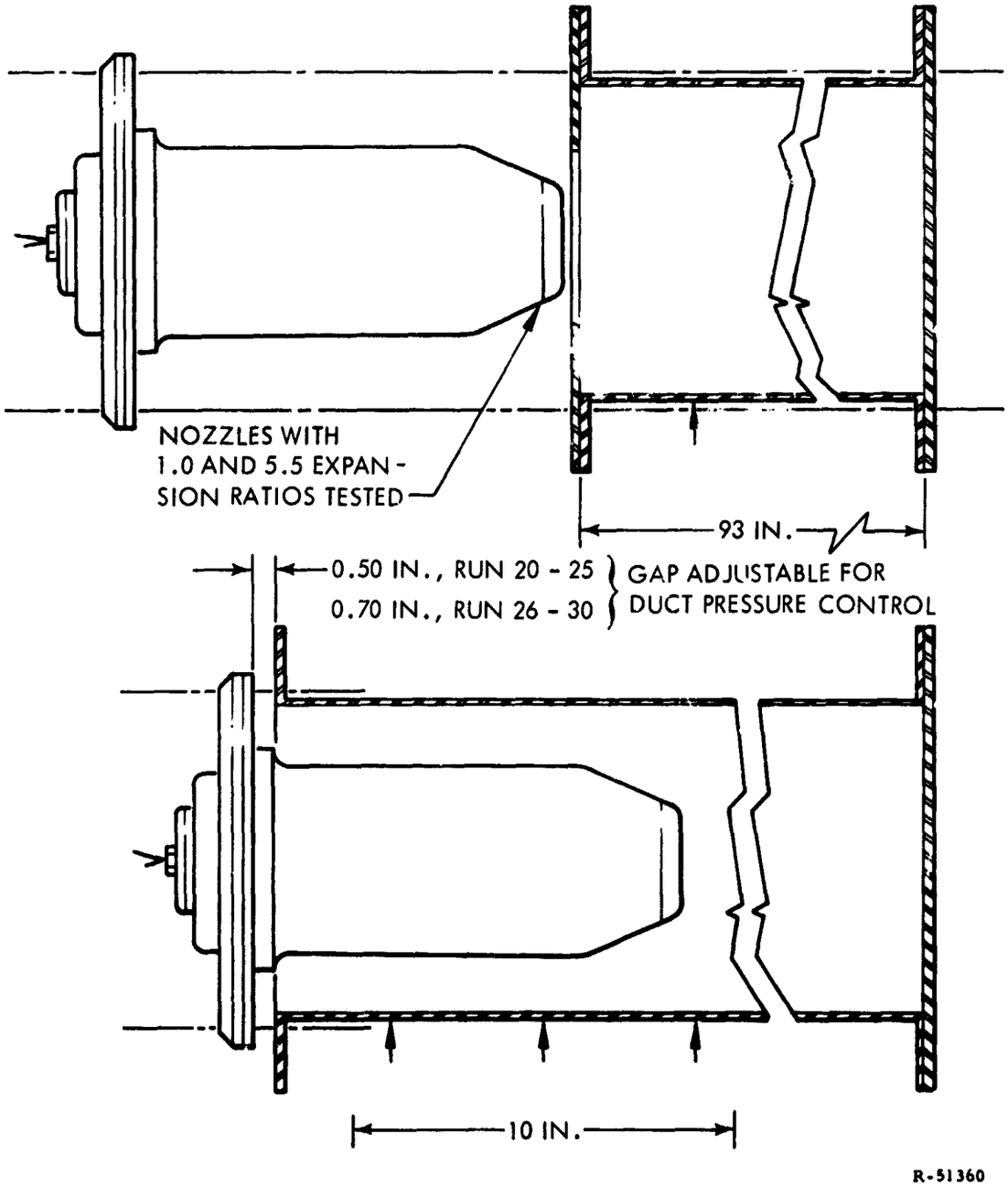

Figure 8. Aft-End Igniter Configurations

Analytical and theoretical work on the program included the development of data reduction techniques and analysis and some correlation of steady-state data with existing heat transfer theory. Significant information obtained included determination of the average wall heat flux as a function of wall location for the various igniters tested. Correlations with classical convective heat transfer theory were found for axial head-end igniters at duct locations greater than 4 port diameters downstream of the igniter nozzle exit plane. Measured radiative data were in qualitative agreement with theoretical prediction; however, the quantitative value of the data was suspect because of buildup of a film of igniter products on the quartz view-window during each test. Theoretical heat transfer correlations for the canted head-end and aft-end igniter data were not completed during the program because of time limitations.

4.0 TECHNICAL ACTIVITY

The technical activity of this program was the reduction, analysis, and correlation of the experimental igniter heat transfer data obtained under Contract No. NAS 7-309. To properly correlate the experimental observations and their analysis, the basic experimental data were examined in relationship to applicable data reduction methods. These methods and correlation techniques used in this program are discussed in this section with the results of the analysis studies.

4.1 DATA REDUCTION

4.1.1 Total Heat Flux

The total heat flux incident upon the propellant surface results primarily from two heat transfer mechanisms: convection and radiation. In the case of aluminized igniter propellant the possibility exists that a third mechanism, that of hot particle impingement of Al_2O_3, will contribute significantly to the total flux. Since the external thermocouples measure the total flux, the convective component can be obtained by subtracting the separately measured radiation flux. Contributions of alumina particle condensation may be determined by comparison of aluminized and nonaluminized igniter propellant tests. The methods used to reduce the total heat flux and radiation fluxes are described in the following paragraphs.

4.1.1.1 Steady-State Heat Flux

Analysis of time-temperature data of the externally located thermocouples indicated that the rate of temperature change was essentially

linear in the igniter action interval from 100 to 300 msec. This constant rate of change implies a constant heat flux input to the inner surface during that time period. Consequently the steady-state heat flux input to the inner surface can be calculated by the formula:

$$q/A = (\rho_{cu}\, \ell\, C_{cu})\ \frac{\Delta T}{\Delta t} \qquad (9)$$

Steady-state heat fluxes for each thermocouple location on all tests were determined by this equation.

4.1.1.2 Transient Heat Flux

The time-dependent inner surface heat-flux and temperature for a given location are determined by solution of the transient one-dimensional axisymmetric heat conduction equation.

$$\frac{1}{r}\frac{\partial}{\partial r}\left(kr\ \frac{\partial T}{\partial r}\right) = \rho C\ \frac{\partial T}{\partial t} \qquad (10)$$

The heat-flux at the inner surface is determined according to the Fourier equation for heat conduction.

$$q/A = -k\left(\frac{\partial T}{\partial t}\right)_{r=r_o} \qquad (11)$$

A UTC computer code by Henderson[8], which employs a finite difference solution of equation 10 and a trial and iteration technique, was used to calculate the transient heat flux. In the computer code, the motor pressure data is used to estimate the time-dependent heat flux input to the inner

surface (front side), from which the corresponding temperature response on the outside surface (backside) is then computed. The calculated and actual test temperatures are compared and the time-dependent heat flux is modified to correct errors in the calculated outside temperature. The iteration technique is continued until the difference in the measured and calculated temperature converge to within a prescribed limit.

One of the principal difficulties in the reduction of the transient heat flux concerns the rapid decrease in temperature with thickness of the duct wall. Large changes in heat flux on inside surface result in only small temperature changes in the outside wall temperature. Because of this attenuation, small fluctuations in the measured backside temperature result in large fluctuations in the calculated inside heat flux.

This problem is further complicated by the use of discrete values from the oscillograph data as input to the computer data reduction program. In general, discrete values of the measured backside temperatures do not lie on a mathematically smooth curve. Because of the small time values and deflections, the slopes from one time interval to the next are discontinuous and heat transfer data calculated for the corresponding front side indicate extreme oscillations. To overcome this problem a data smoothing routine was employed. Typical computer output from nonsmoothed data is shown in figure 9.

Several data-smoothing techniques were investigated by Mullis.[9] The technique finally selected in the earlier program consisted of fitting the data to a fourth-degree polynominal over the entire temperature-time range using a least squares technique. Computer output data using this technique on a typical run are shown in figures 10 and 11. This technique does smooth

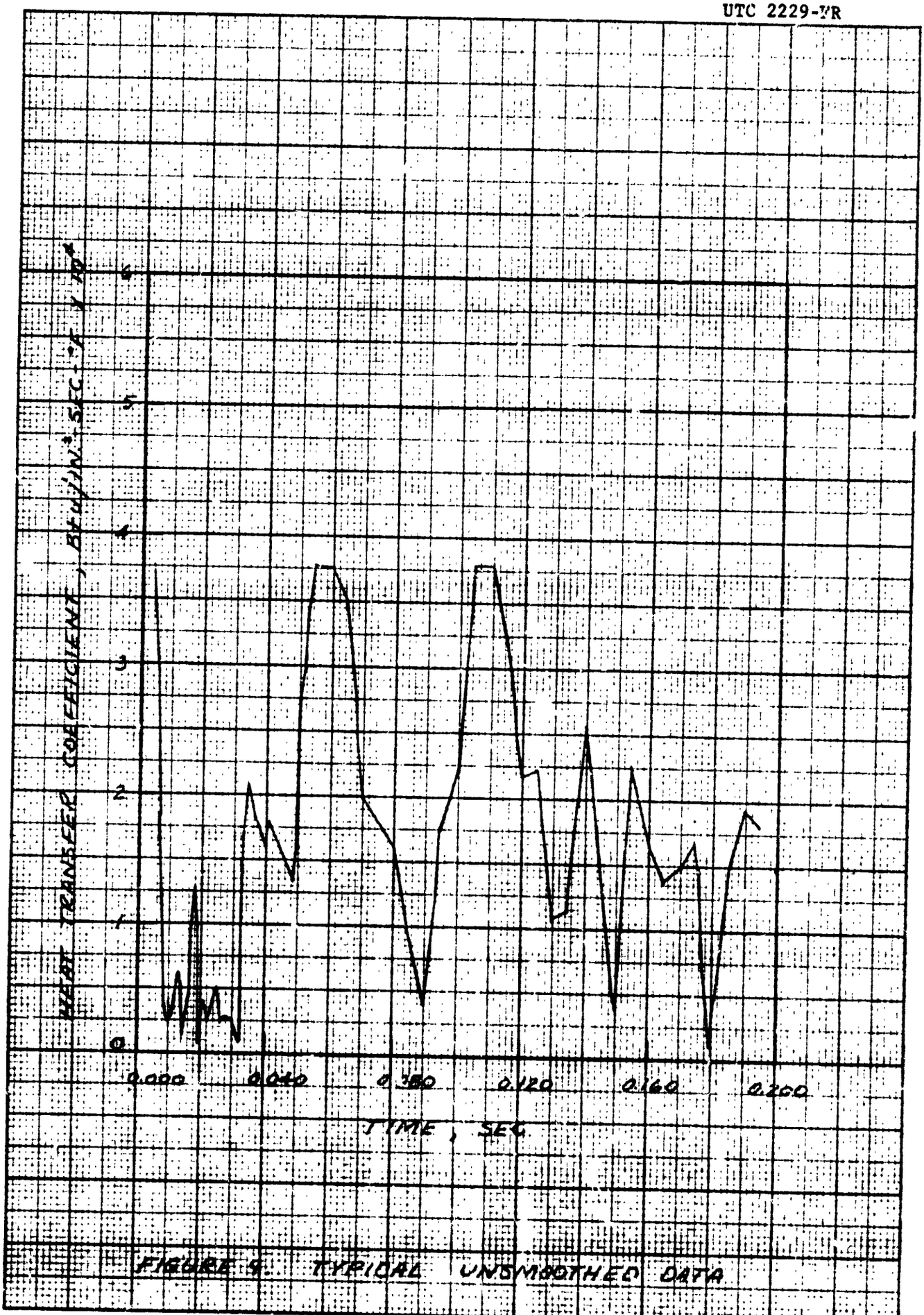

FIGURE 9. TYPICAL UNSMOOTHED DATA

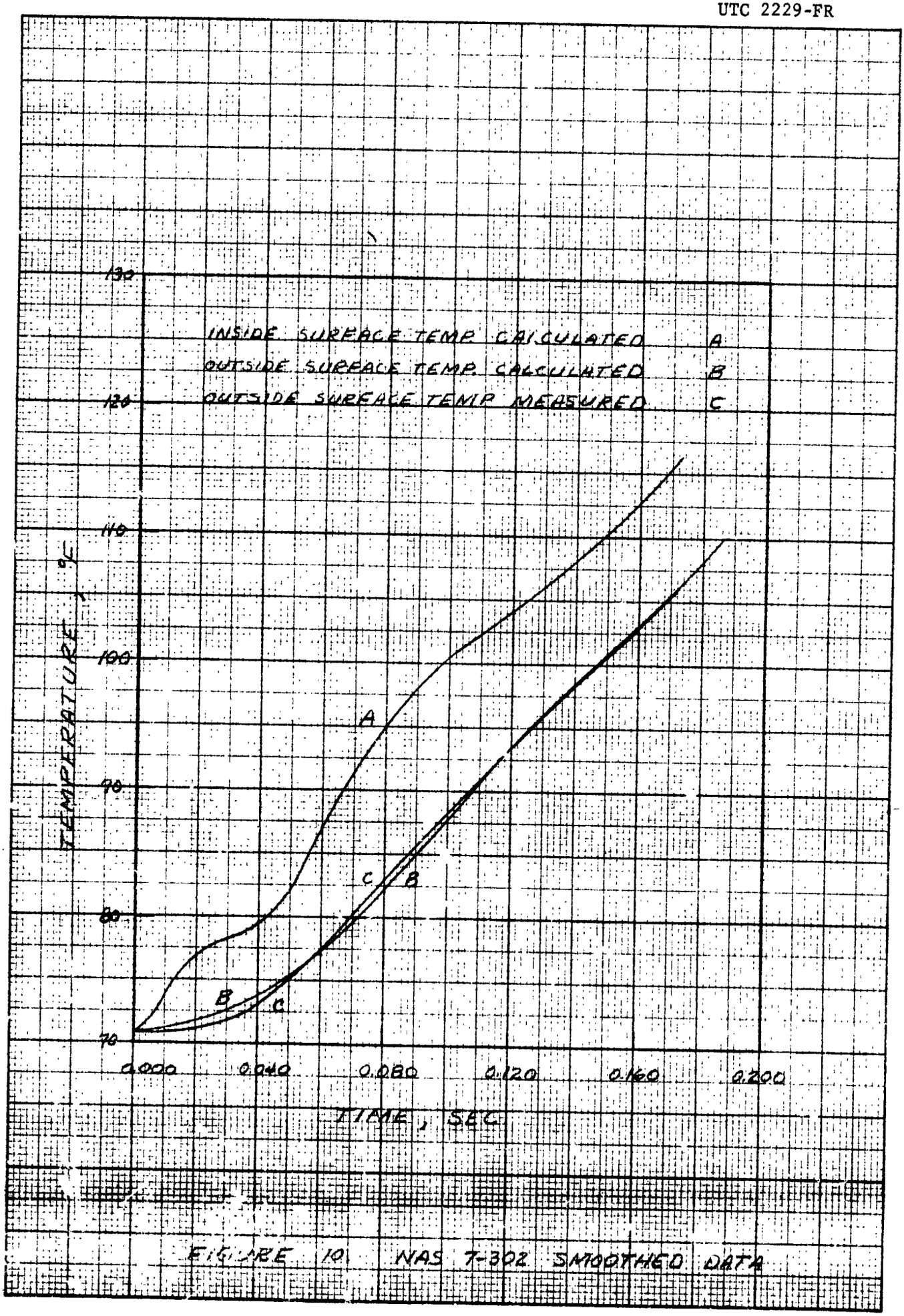

FIGURE 10 NAS 7-302 SMOOTHED DATA

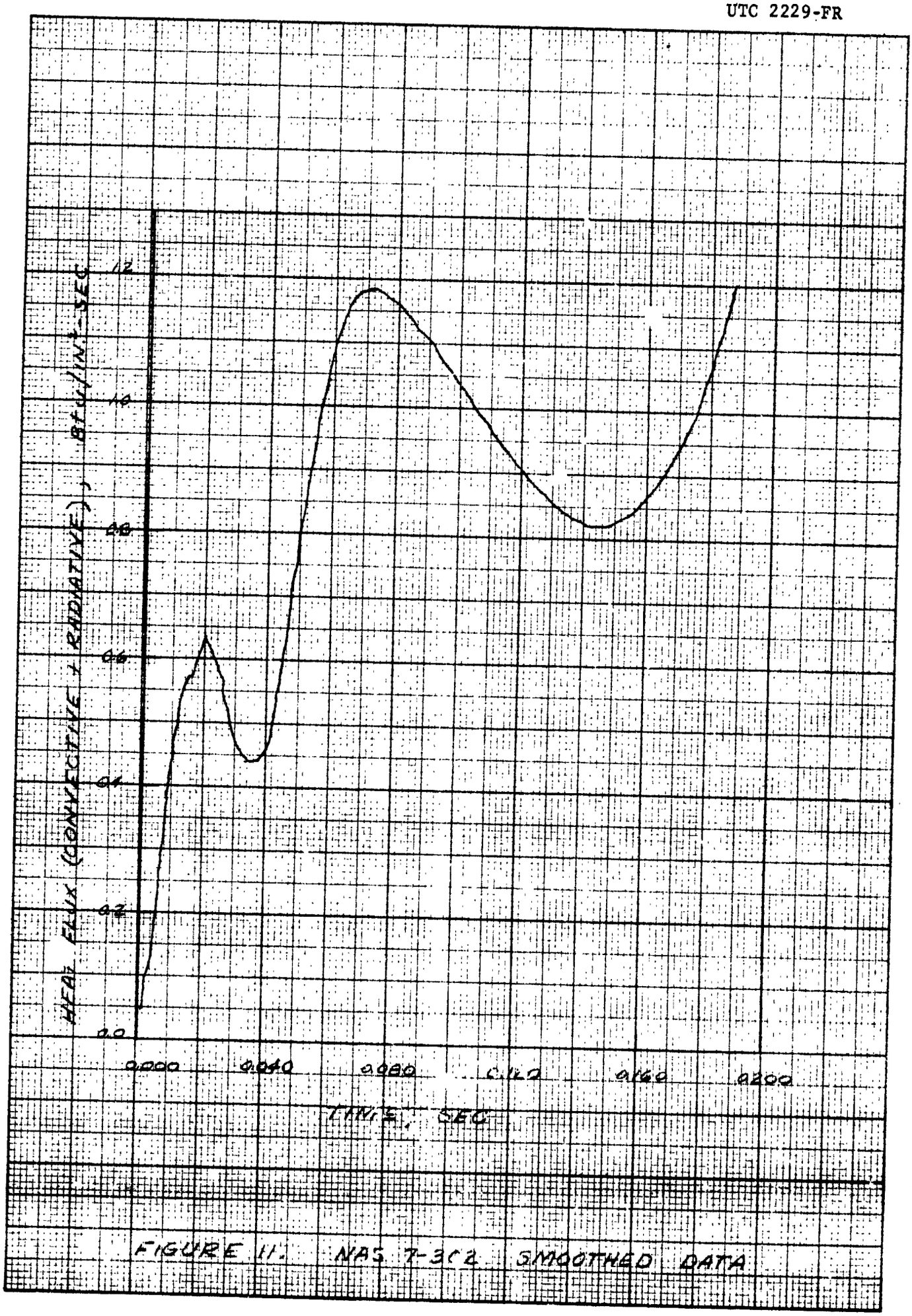

FIGURE 11. NAS 7-362 SMOOTHED DATA

the data but adds an S-shape to the smoothed curves not apparent on the original oscillograph data. To avoid this problem, several improved data smoothing techniques were investigated during the current program. To provide smooth curves which accurately portray the actual test data, a method of dividing the smoothing curve into two segments was selected. The equation selected for the initial segment has the form:

$$T = a + bt^c \qquad (12)$$

where a is the ambient temperature and b and c are constants determined from the oscillograph data. The second portion of the curve is fit by a quadratic equation of the form:

$$T = e + ft + gt^2 \qquad (13)$$

where the constants are also determined from the input data. Constraints placed upon the equations are such that the slope at the origin is zero, the slope of the two equations at their common point is equal, and the system of equations must pass through four different data points, one of which is the ambient temperature at zero time. Introduction of this data-smoothing technique into the inverse heat transfer program produces results which are reasonably smooth. Figures 12 and 13 portray the output of the computer program. The resultant smooth curve from the program, and the calculated outside temperature computed from the calculated inside temperature, are shown in figure 12. Figure 13 shows the resultant heat flux.

Calculations were made in which the calculation time interval, temperature convergence error limit, and number of material nodes were varied to determine the effect of these parameters upon the actual reduced data.

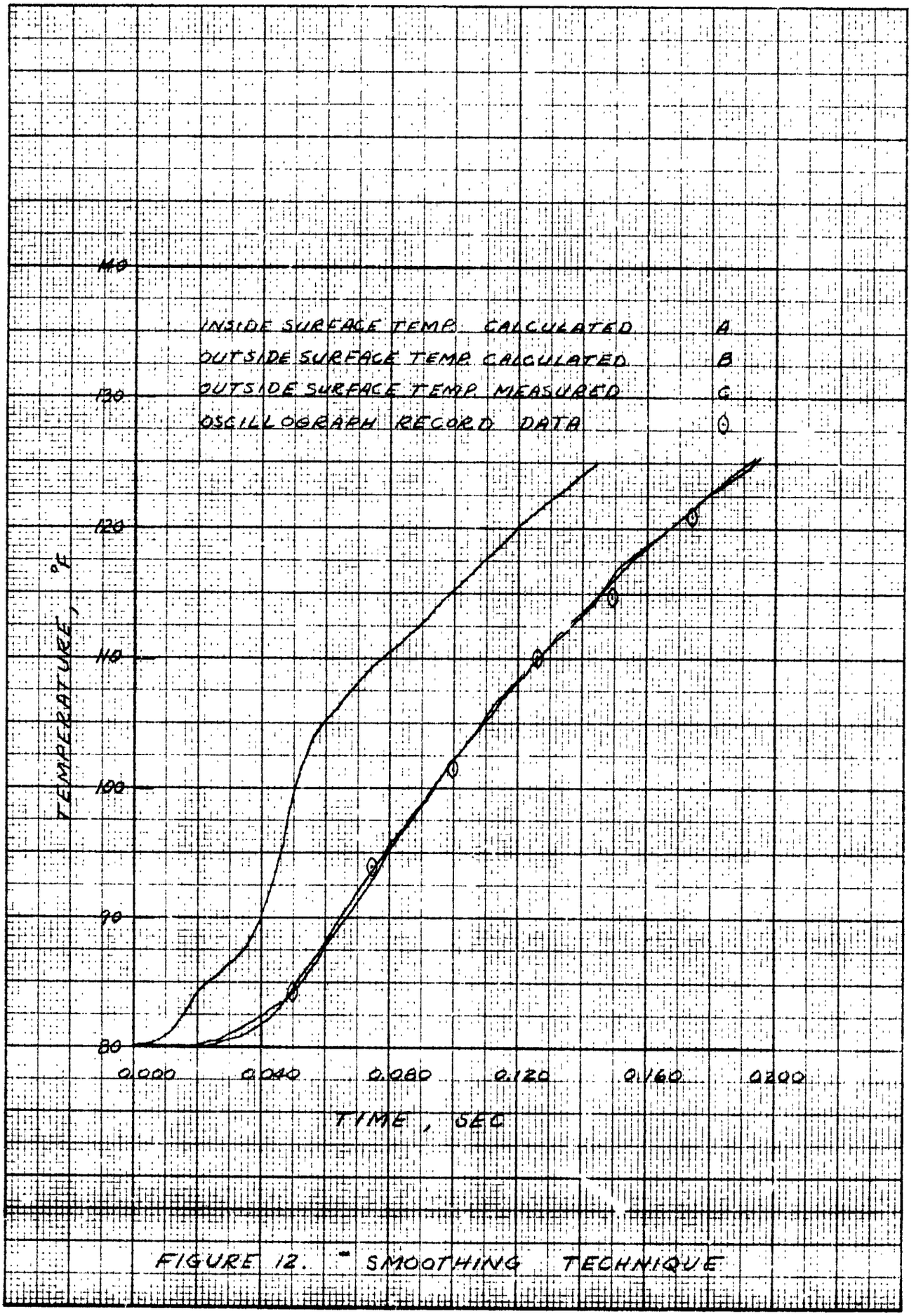

FIGURE 12. - SMOOTHING TECHNIQUE

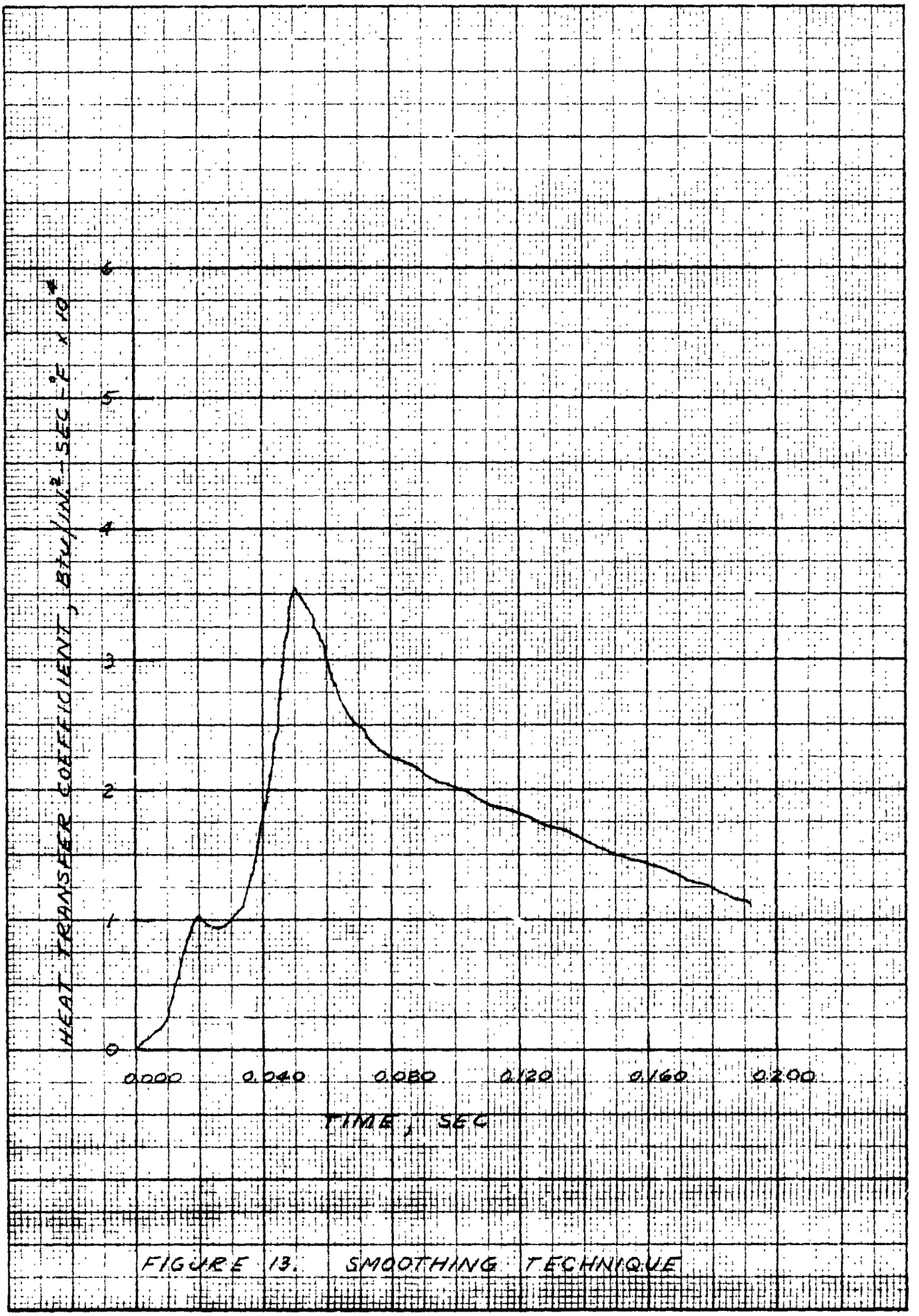

FIGURE 13. SMOOTHING TECHNIQUE

It was found that adequate results were obtained for temperature convergence limits of $\pm^{o}F$, 14 material nodes and calculation interval in the order of 1 msec. A more complete description of the computer data reduction program is given in references 8, 9, and 10.

4.1.1.3 Radiation Heat Flux

Reduction of the incident radiant heat flux from the slug calorimeter thermocouple temperature data involves determination of the heat absorbed by the calorimeter slug and the heat reflected and reradiated. The instantaneous heat absorption rate is given by the equation:

$$q(t) = \frac{MC}{A}\frac{dT}{dt} + K\overline{\Delta T} \qquad (14)$$

where q(t) is the total energy absorption of the slug, $\frac{MC}{A}\frac{dT}{dt}$ is the net rate of storage in the slug, and $K\overline{\Delta T}$ is the rate of heat loss from the slug by radiation, convection, and conduction. The value of $\frac{MC}{A}$, a constant for each calorimeter, was determined by Mullis [9] and is presented in table I. The derivative $\frac{dT}{dt}$ is the instantaneous rate of temperature change determined by the calorimeter thermocouple voltage for each test. The value of $K\overline{\Delta T}$, for a given mean temperature $\overline{\Delta T}$, can be determined experimentally or can be approximated by calculations using known physical properties and calorimeter system geometries. An analysis using typical physical constants and environmental conditions experienced during the test cycles indicates that for measurement durations less than 0.5 sec, an error of less than 5% results if the term $K\overline{\Delta T}$ is neglected. This error is comparable with the experimental and data reduction errors; therefore, the term $K\overline{\Delta T}$ was neglected when calculating the measured radiant heat flux.

Determination of the incident radiant heat flux relative to the measured heat flux requires calibration of the test calorimeters against a known reference source. This calibration was made by Mullis and the results are presented in reference 9. Using the experimentally determined data, the incident heat flux is found by the equation:

$$q_{inc} = q(t) \cdot \frac{1}{F_c} \cdot \frac{1}{\epsilon_{ref}} \qquad (15)$$

where

q_{inc} = incident radiant heat flux

F_c = correction to reference gage = q_{ref}/q_{gage}

ϵ_{ref} = absorptivity (emissivity) of the reference gage.

The total incident radiant heat flux is finally given by the expression:

$$q_{inc} = \frac{MC}{A} \cdot \frac{1}{F_c \cdot \epsilon_{ref}} \cdot \frac{dT}{dt} \qquad (16)$$

4.1.2 Igniter Exhaust Characteristics

Igniter mass flow rates were determined from thermochemical c* calculations, measured igniter chamber pressures, and igniter nozzle dimensions measured on each test nozzle by use of the equation:

$$\dot{w}_{ign} = \frac{P_c A_t g}{c^*} \qquad (17)$$

The stagnation temperature decreases as the hot igniter exhaust transfers heat to the duct wall. Calculations indicate there is a significant

decrease in gas temperature which will influence both the gas physical properties and the heat transfer temperature potential. To calculate temperature loss for the head-end igniters, a heat balance is taken between the duct entrance and any axial location downstream. Temperature losses were thus determined by use of the equation:

$$T_x = T_{ign} - \pi D \int_0^x \frac{(q/A)_x}{\dot{w}_{ign} C_P} \, dx \qquad (18)$$

$$= T_{ign} - \frac{\pi D}{\dot{w}_{ign} \bar{C}_P} \sum_{n=1}^{N} (\bar{q}/A)_x \, \Delta X_n \qquad (19)$$

where $(\bar{q}/A)$ is the average heat flux between the nth axial thermocouple locations, ΔX_n is the distance between thermocouple locations, is the igniter mass flow rate, and $\bar{C}_P$ is the average gas specific heat for the mean duct temperature.

Use of the average specific heat value produces errors in the calculated value in the neighborhood of 5% which is well within the experimental error of heat flux measurements.

Evaluation of the duct Mach number by use of the average duct mass fluxes indicates that the average duct static temperature and stagnation temperature may assume to be equal with little loss in accuracy.

4.1.3 Convective Heat Transfer Coefficient

The convective heat flux is determined by subtracting the radiative heat flux for any given location from the reduced total heat flux. Bastress, et al.,[11] report that the nonradiative heat flux from the exhaust species

of typical pyrogen igniters under conditions of shifting equilibrium is approximately 98% to 100% convective. Therefore,it is deemed justifiable to neglect the small contributions of chemically-induced heat fluxes. The convective transfer coefficient is then determined from the equation

$$h = \dot{q}/(T_x - T_w) \qquad (20)$$

where h is the convective heat transfer coefficient, $\dot{q}$ is the local flux, T_x is the local stagnation temperature determined from equation 19 and T_w is the local average wall temperature.

The wall temperatures data were determined from the transient heat conduction program. Mean wall temperatures corresponding to approximately 200 msec time in the igniter run duration are presented in figure 14 as a function of average steady-state heat flux for various initial ambient copper tube temperature.

4.1.4 Fluid Physical Properties

In order to correlate the heat transfer data in terms of dimensionless parameters,it is necessary to determine the igniter exhaust specie physical properties over a wide range of temperatures. Combustion temperatures and igniter exhaust species composition and concentration were computed for both the aluminized (UTP-1095) and nonaluminized (UTX-6937) igniter propellants. The thermal conductivity (k), specific heat at constant pressure (C_p), and viscosity (μ) for the exhaust species of UTP-1095 were determined by Fullman and Nielsen[12] at an exhaust total temperature of 5,700°R. The thermal

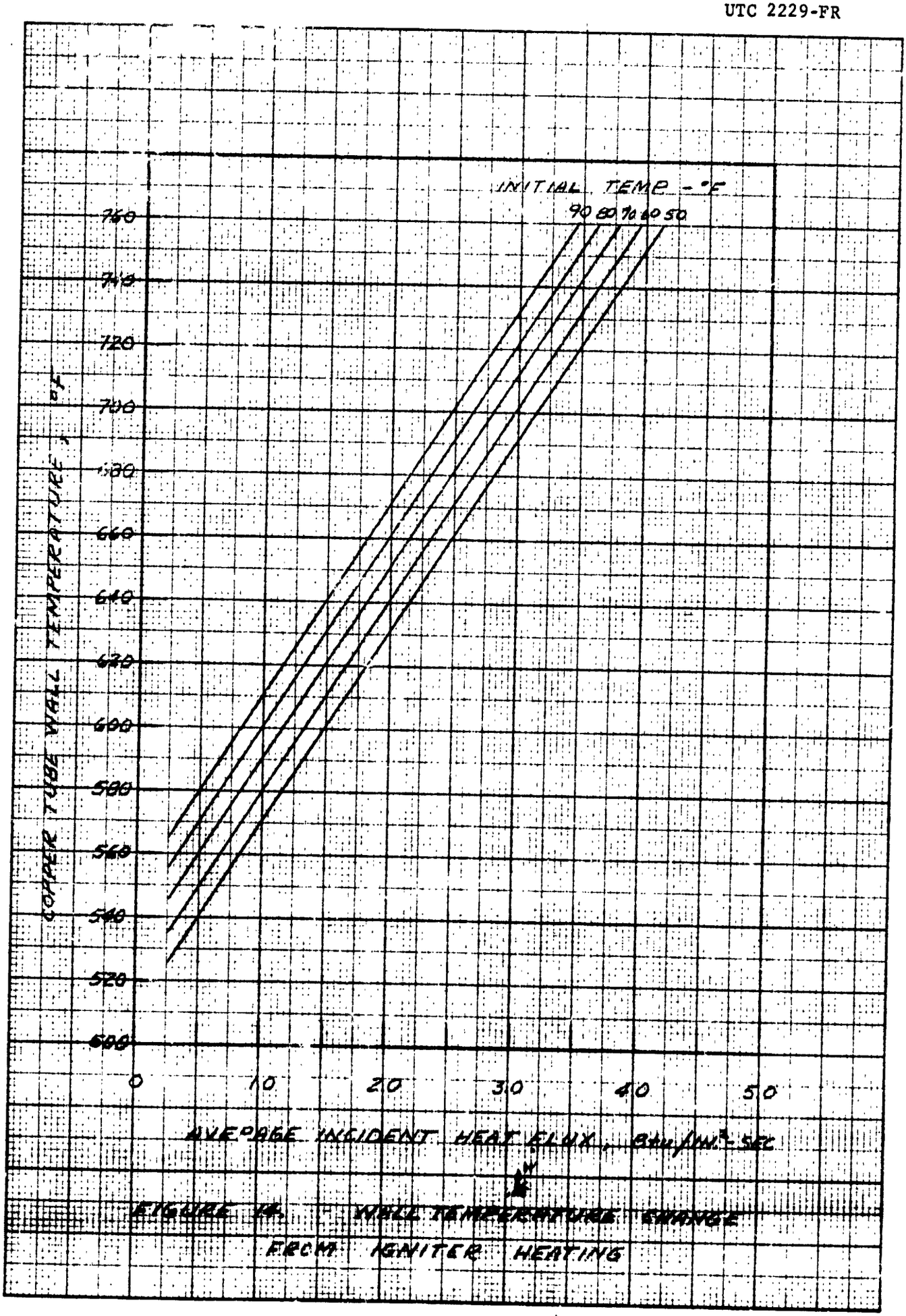

FIGURE 14. WALL TEMPERATURE CHANGE FROM IGNITER HEATING

conductivity and viscosity were assumed to vary about these calculated points according to the relationships

$$k = k_o \left(\frac{T}{T_o}\right)^{0.5} \tag{21}$$

and

$$\mu = \mu_o \left(\frac{T}{T_o}\right)^{0.5} \tag{22}$$

The use of the assumption for temperature variation of the viscosity and thermal conductivity is based upon kinetic theory and the results of experimental investigations reported by Reid and Sherwood.[13] The temperature variation of the specific heat was determined by calculations over the desired temperature range using the combined specific heat of the major constituent species. The temperature-dependent specific heats of the individual species were taken from JANAF thermochemical tables.[14] The variation of the igniter exhaust gas physical properties with temperature as determined by these methods for UTP-1095 is presented in figure 15. The relative percentage of major exhaust gases for both the aluminized and nonaluminized propellants were approximately the same so that the values given in figure 15 were used in the correlation of both aluminized and nonaluminized igniter propellants test data.

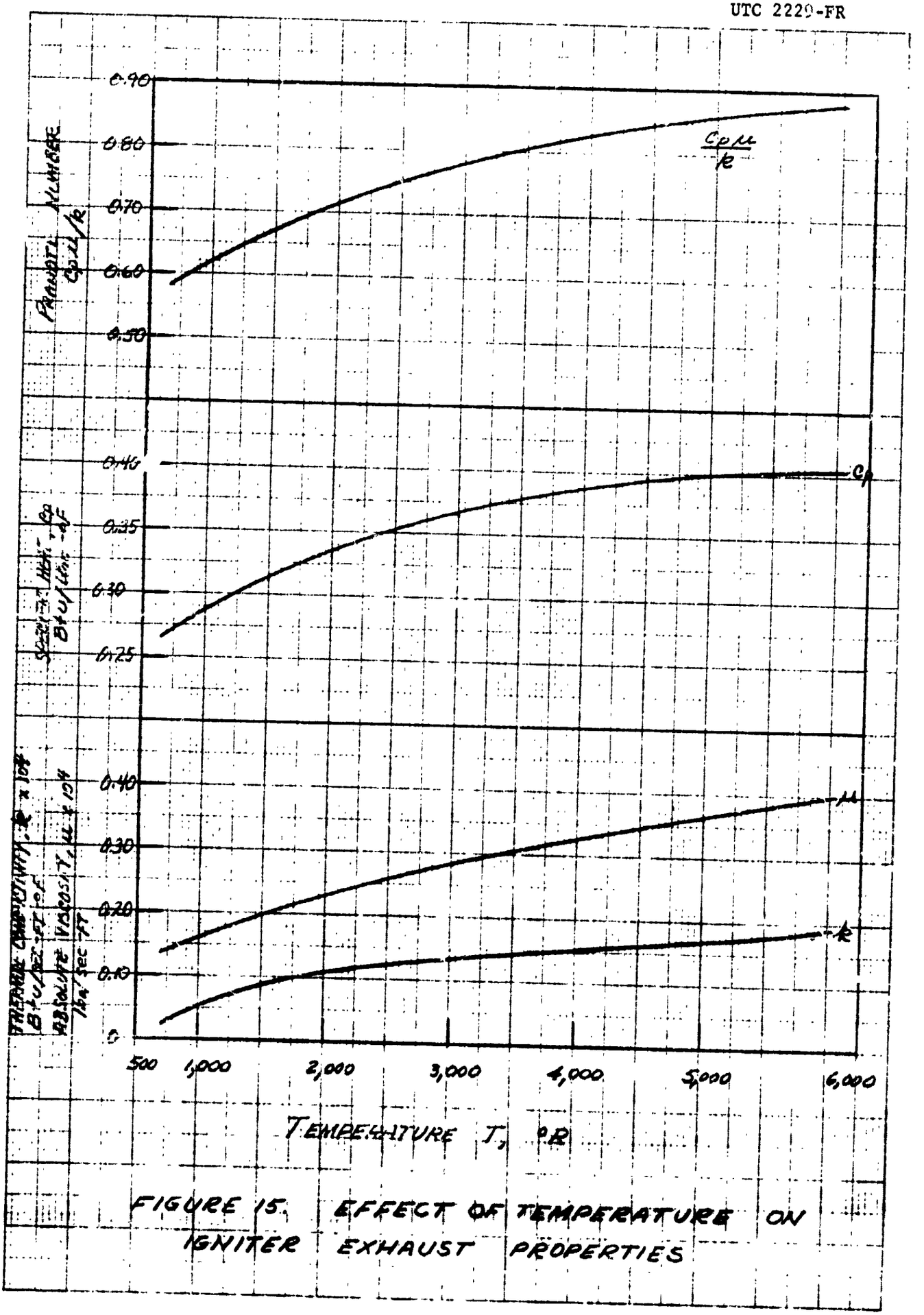

FIGURE 15 EFFECT OF TEMPERATURE ON IGNITER EXHAUST PROPERTIES

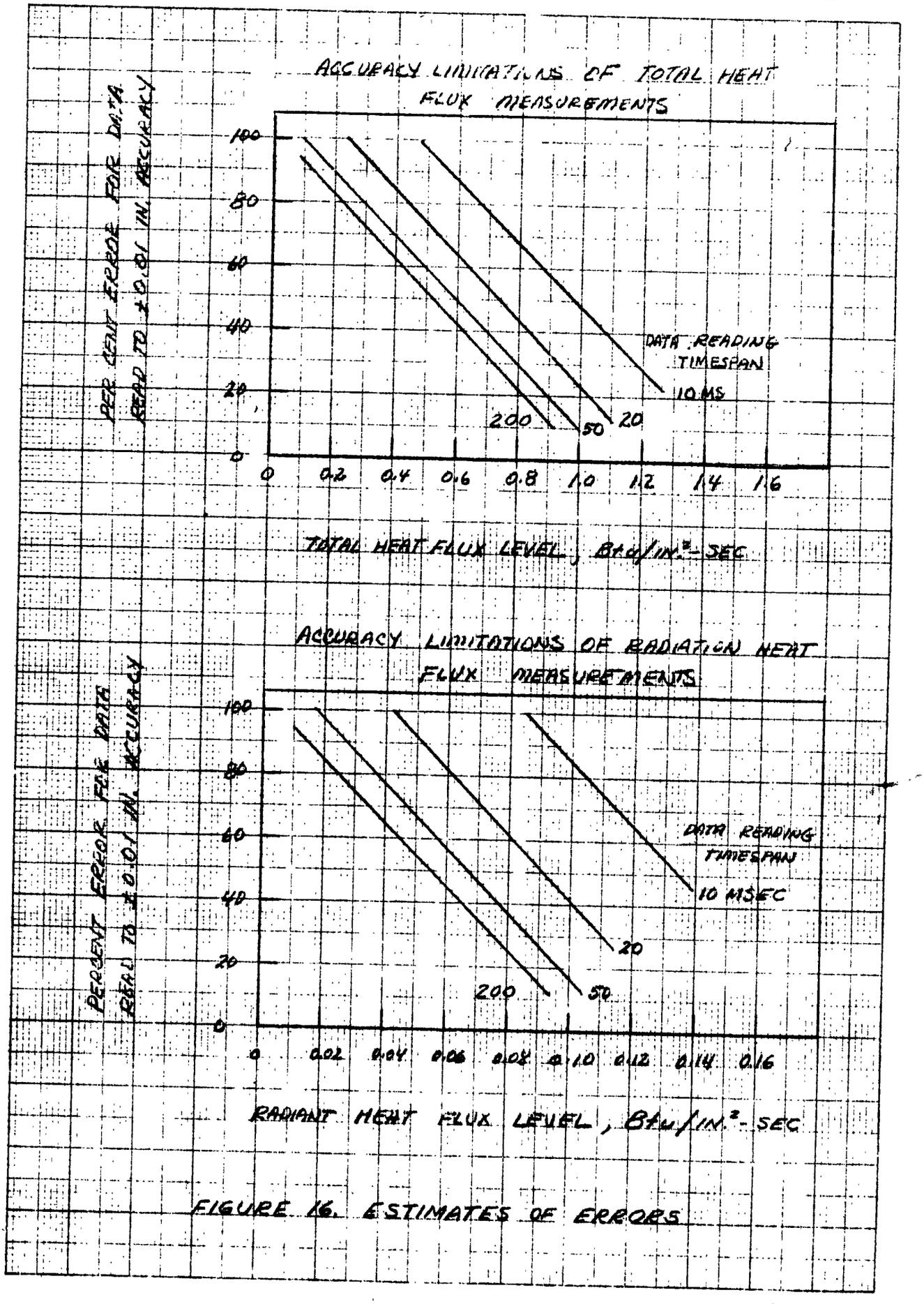

FIGURE 16. ESTIMATES OF ERRORS

4.1.5 Dimensionless Parameters

Convective heat transfer to the walls of tubes is generally correlated using the Reynolds number (Re), Prandtl number (Pr), and Nusselt number (Nu) in an equation of the form:

$$Nu = aRe^{b} Pr^{c} \tag{23}$$

In evaluating these parameters for large wall to free stream temperature differences, Humble, Lowdermilk, and Desmon[15] report that the fluid physical properties should be evaluated at the film temperature, i.e., temperature midway between the bulk temperature and wall temperature. Accordingly, the Nusselt, Prandtl, and Reynolds numbers were evaluated according to the formulae:

$$Nu_x = \frac{h_x D}{k_f} \tag{24}$$

$$Pr = \frac{C_{\rho_f} \mu_f}{k_f} \tag{25}$$

$$Re = \frac{\rho_f V_b D}{\mu_f} = \frac{\rho_f}{\rho_b} \cdot \frac{(\dot{w}/A) D}{\mu_f}$$

$$= \frac{T_b}{T_f} \cdot \frac{(\dot{w}/A) D}{\mu_f} \tag{26}$$

4.2 ERROR ANALYSES

Accuracy of total heat flux measurements was extremely limited because of the low instrumentation scale factors and the thickness of the copper duct. This is evident from a simple error analysis using equation

$$q/A = \left(\rho_{cu}\, \ell\, C_{cu}\right) \frac{\Delta T}{\Delta t} = 0.16 \frac{\Delta Y}{\Delta T} \cdot SF = 0.48 \frac{\Delta Y}{\Delta T} \qquad (27)$$

where $\Delta Y/\Delta T$ is the deflection of the oscillograph traces over a given timespan and SF is the instrumentation thermocouple scale factor. The oscillograph data can be determined, at best to an accuracy of ± 0.01 in. Applying this data reading limitation to equation 27 for various data reading timespans, the accuracy limitations of the total heat flux data are obtained (see figure 16).

If a steady-state timespan of 200 msec is used, an error of less than 10% is obtained for flux levels over 0.9 Btu/in.^{2}-sec. However, for flux levels less than 0.2 Btu/in.^{2}-sec, the error is increased to over $\pm 80\%$. These errors become increasingly large as the data reading timespan is reduced. For timespans of 10 msec, errors in the order of $\pm 100\%$ are noted at flux levels of approximately 0.60 Btu/in.^{2}-sec which is a typical value reading for a large percentage of the test data.

From this analysis it is evident that calculations based upon these transient test data have a high level of uncertainty for any given time. Therefore, transient data determined by the computer program were used primarily to obtain copper tube inside wall temperature for the various steady-state flux levels.

A similar error analysis was made on the radiation heat transfer data and the results are also presented in figure 16. Reasonable accuracies are obtained only for the steady-state values as in the case of the total heat flux measurements. Steady-state radiation heat flux level was approximately 0.06 Btu/in.^{2}-sec which corresponds to errors in the neighborhood of $\pm$40%

It is concluded on the basis of these simple error analyses that the correlated data are accurate to approximately $\pm$50%. These accuracies increase at the higher flux levels and are decreased with decreasing flux.

4.3 REVIEW OF CONTRACT NO. NAS 7-302 TEST DATA

The tests which were conducted on the previous program for various igniter configurations using the copper duct test apparatus are summarized in table III. The first 15 tests (runs 0 through 14) employed head-end igniter configurations. The remaining 14 (runs 17 through 30) were conducted with aft-end igniter configurations. Tests with run numbers of 15, 16, and 23 were unsuccessful and were repeated.

Three variations of igniter mass flow rates are made in each configuration with aluminized and nonaluminized propellants. Exceptions were made in the runs utilizing canted nozzles and aluminized propellants because of possible thermal damage to the duct at the high flow rates and with sonic aft-end igniters.

4.3.1 Total Heat Flux

4.3.1.1 Head-End Igniter

Figures 17 and 18 show the axial variation of total heat flux for the axial flow igniter for which thermocouple data were obtained in two longitudinal planes. Since the flow is symmetrical about the duct centerline

TABLE III

COPPER DUCT TESTS

Run No.	Igniter Location	Igniter Type	Propellant Type	Nominal Flow Rate lb/sec	Nominal Duct Pressure psig	Radiation Calorimeters	Spectral Radiometer	External Thermocouples	Internal Surface Thermocouples	Duct Pressures
0	Head end	Axial	Nonaluminized	1.60	17	6	–	16	–	2
1	Head end	Axial	Nonaluminized	1.60	17	6	–	16	–	4
2	Head end	Axial	Nonaluminized	2.52	30	6	–	16	–	4
3	Head end	Axial	Nonaluminized	3.55	50	6	–	16	–	4
4	Head end	Axial	Nonaluminized	2.52	17	6	–	16	–	4
5	Head end	Canted	Nonaluminized	1.60	17	6	–	16	–	4
6	Head end	Canted	Nonaluminized	2.52	30	6	–	16	–	4
7	Head end	Canted	Nonaluminized	3.55	50	6	–	16	–	4
8	Head end	Canted	Nonaluminized	2.52	17	6	–	16	–	4
9	Head end	Axial	Aluminized	1.60	17	6	–	16	–	4
10	Head end	Axial	Aluminized	2.52	30	6	–	16	–	4
11	Head end	Axial	Aluminized	3.55	50	6	–	16	–	4
12	Head end	Axial	Aluminized	2.52	17	6	–	16	–	4
13	Head end	Canted	Aluminized	1.60	17	6	–	16	–	4
14	Head end	Canted	Aluminized	2.52	30	6	–	16	–	4
17	Aft end External	Axial-Supersonic	Nonaluminized	1.60	17	5	–	16	–	5
18	Aft end External	Axial-Supersonic	Nonaluminized	2.57	30	6	–	16	–	5
19	Aft end External	Axial-Supersonic	Nonaluminized	3.55	50	5		16	–	5
20	Aft end Internal (11/in.)	Axial-Supersonic	Nonaluminized	1.60	17	5		16	–	5
21	Aft end Internal (11/in.)	Axial-Supersonic	Nonaluminized	2.52	30	5		16	–	5
22	Aft end Internal (11/in.)	Axial-Supersonic	Nonaluminized	3.55	50	6	–	16	–	5
24	Aft end Internal (11/in.)	Axial-Sonic	Nonaluminized	2.52	30	6	–	16	–	5
25	Aft end Internal (11/in.)	Axial-Sonic	Nonaluminized	3.55	50	6	–	16	–	5
26	Aft end Internal (11/in.)	Axial-Supersonic	Aluminized	1.60	17	5		16	–	5
27	Aft end Internal (11/in.)	Axial-Supersonic	Aluminized	2.52	30	5		16	–	5
28	Aft end Internal (11/in.)	Axial-Supersonic	Aluminized	3.55	50	5		16	–	5
29	Aft end Internal (11/in.)	Axial-Sonic	Aluminized	1.60	17	5		16	3	5
30	Aft end Internal (11/in.)	Axial-Sonic	Aluminized	2.52	30	5		15	3	5

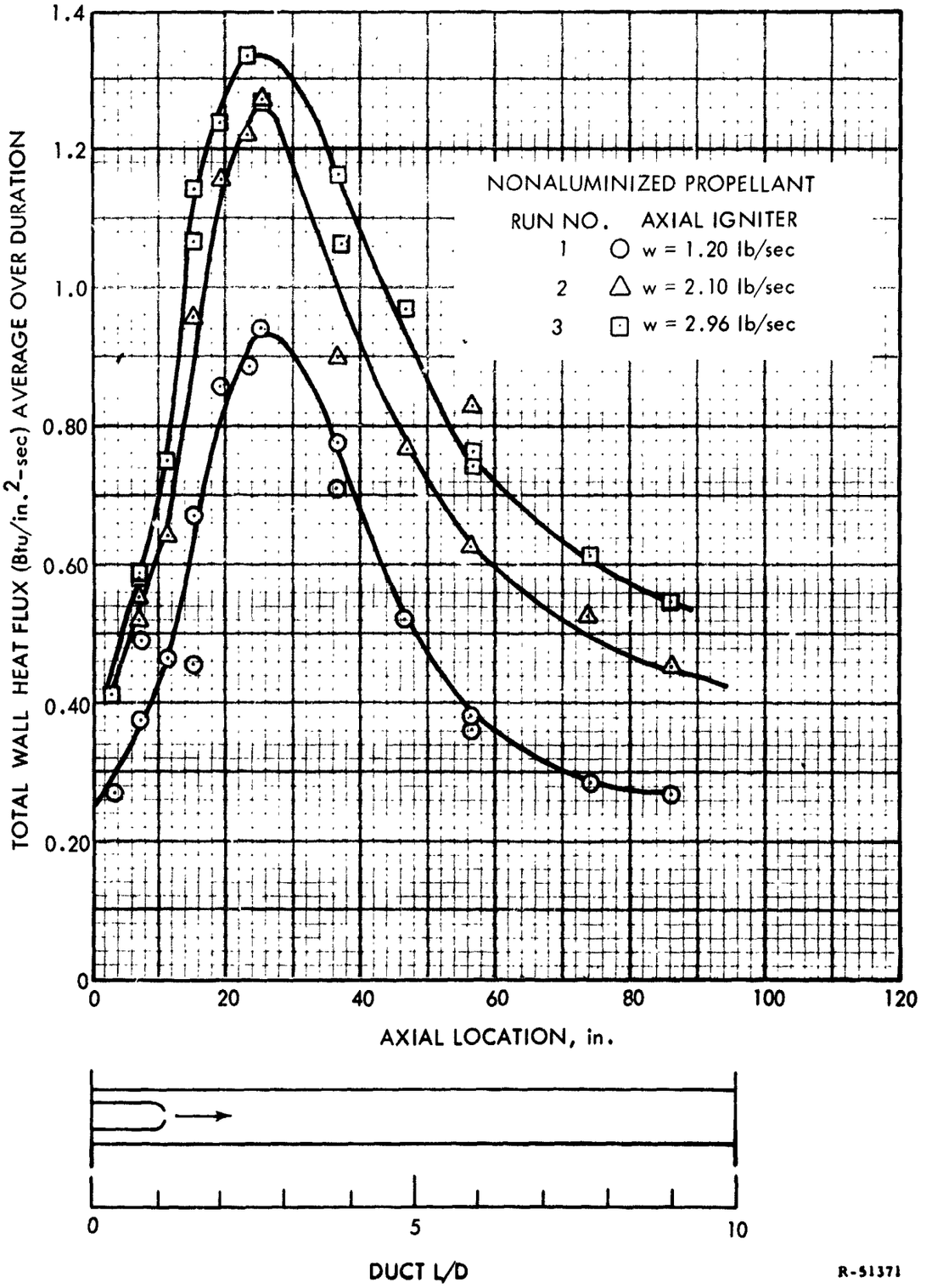

Figure 17. Average Wall Temperature in Copper Tube

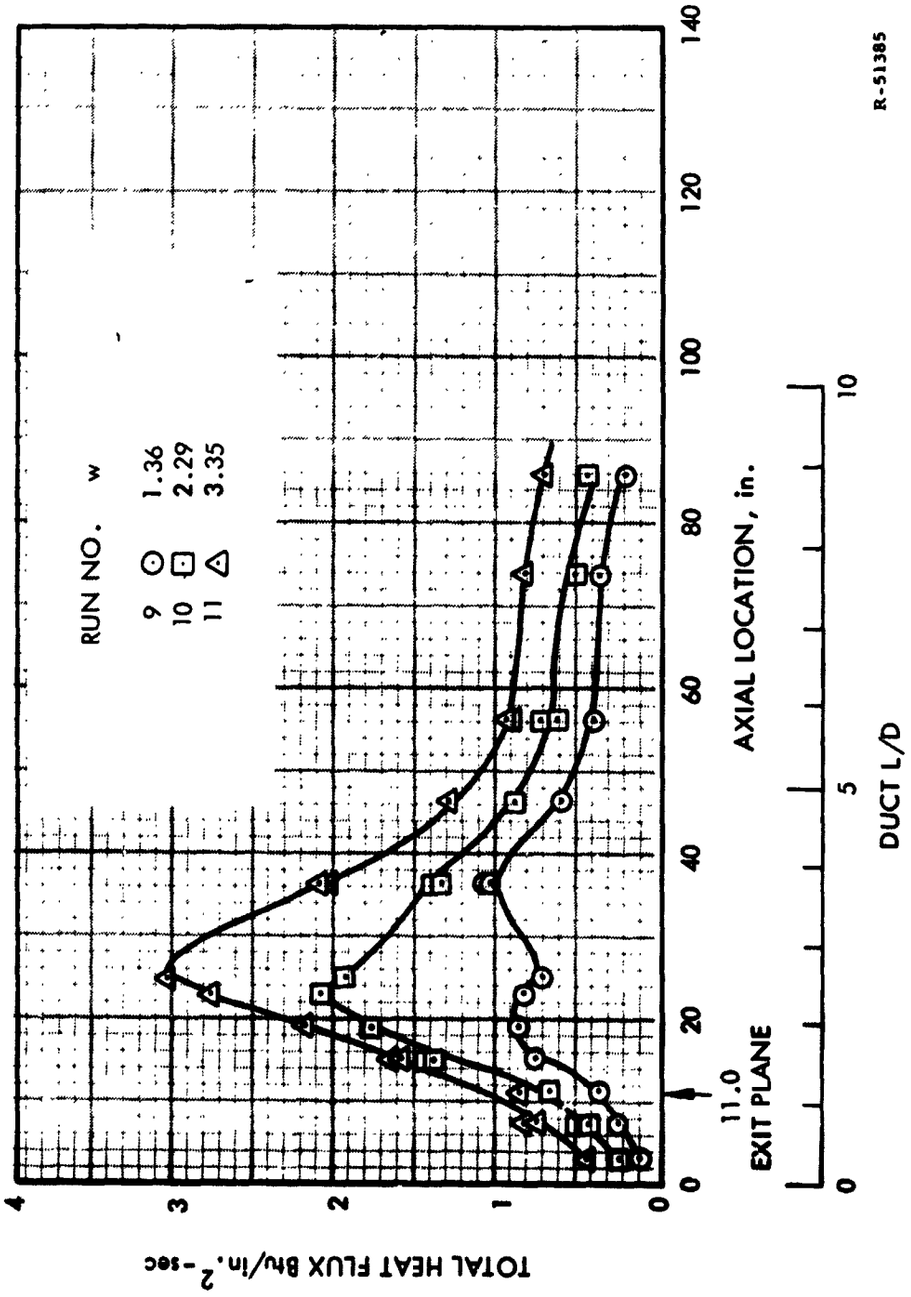

Figure 18. Axial Igniter, Aluminized Propellant

for the axial igniter, no variations are expected around the duct periphery. Variations which do occur are attributed to data scatter.

The axial variation in heat flux from the multiple-port canted igniters is shown in figures 19 and 20 for aluminized and nonaluminized propellants at several mass flow rates. These data are jet centerline data only. While peripheral variations in total heat flux are expected with this igniter nozzle configuration in the regions near the stagnation point, these variations should disappear as the jets spread and coalesce. Figure 21 shows this variation for a nonaluminized multiple-port igniter and figure 22 represents the variation for typical aluminized multiple-port canted igniters.

4.3.1.2 Aft-End Igniters

The heat flux data for the aft-end igniters are presented in figures 23 and 24. The variations due to igniter mass flow, as shown in figure 23, are for aluminized propellant products exhausting into the duct from internally-mounted near-optimum expansion ratio supersonic nozzles. Figure 24 shows a comparison of total heat flux for nonaluminized propellants. Tests 17, 18, and 19 were conducted with the aft-end igniters in an externally-mounted position (as shown in figure 8) and the remaining tests were conducted with the igniters mounted internally (as shown also in figure 8). Figure 25 presents steady-state heat flux data comparing three separate tests, two for externally-mounted and one for internally-mounted igniters. In all cases, a stagnation zone in the duct head-end is clearly in evidence. The higher heat flux produced by the higher mass flow igniter also is as expected. The differences in peak heat flux for the internally and externally-mounted igniters which have approximately the same igniter flow rate are a result, in part, of the higher flow rate and duct pressure recorded for the external

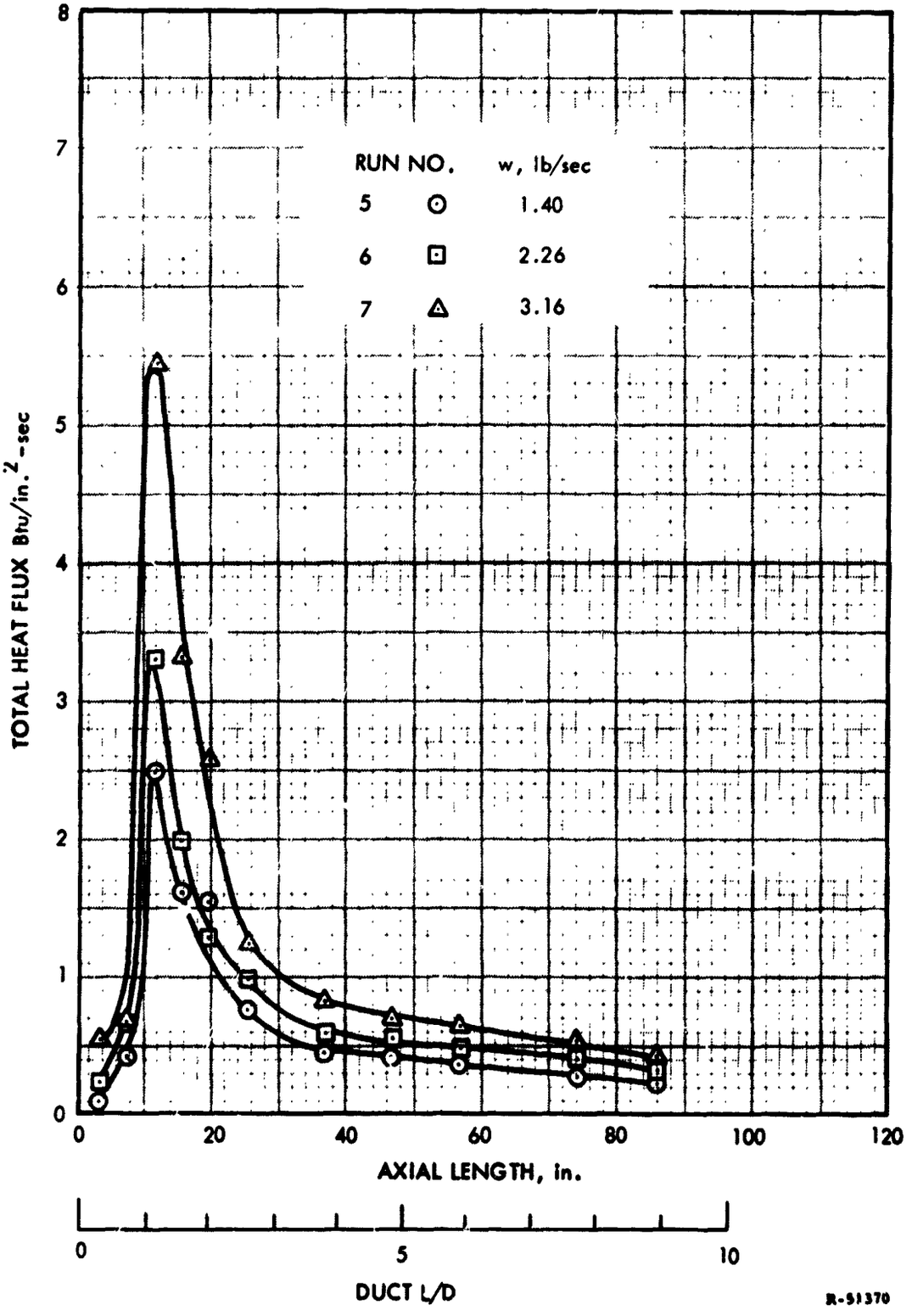

Figure 19. Canted Igniter Nonaluminized Products Jet Centerline Flux Only

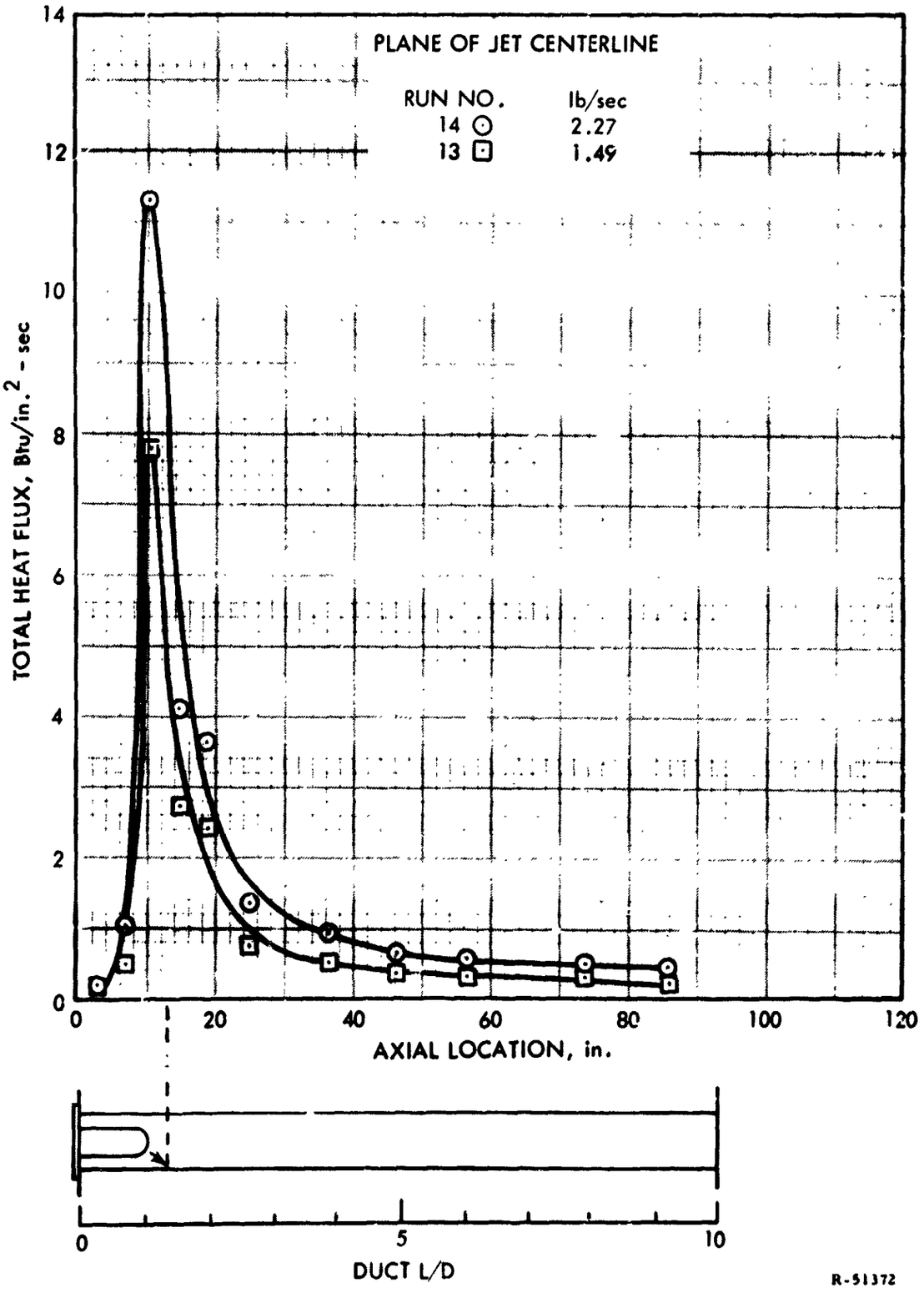

Figure 20. Multiple-Port Canted Igniter, Aluminized Exhaust (18.9% Al_2O_3), Total Flux vs Length

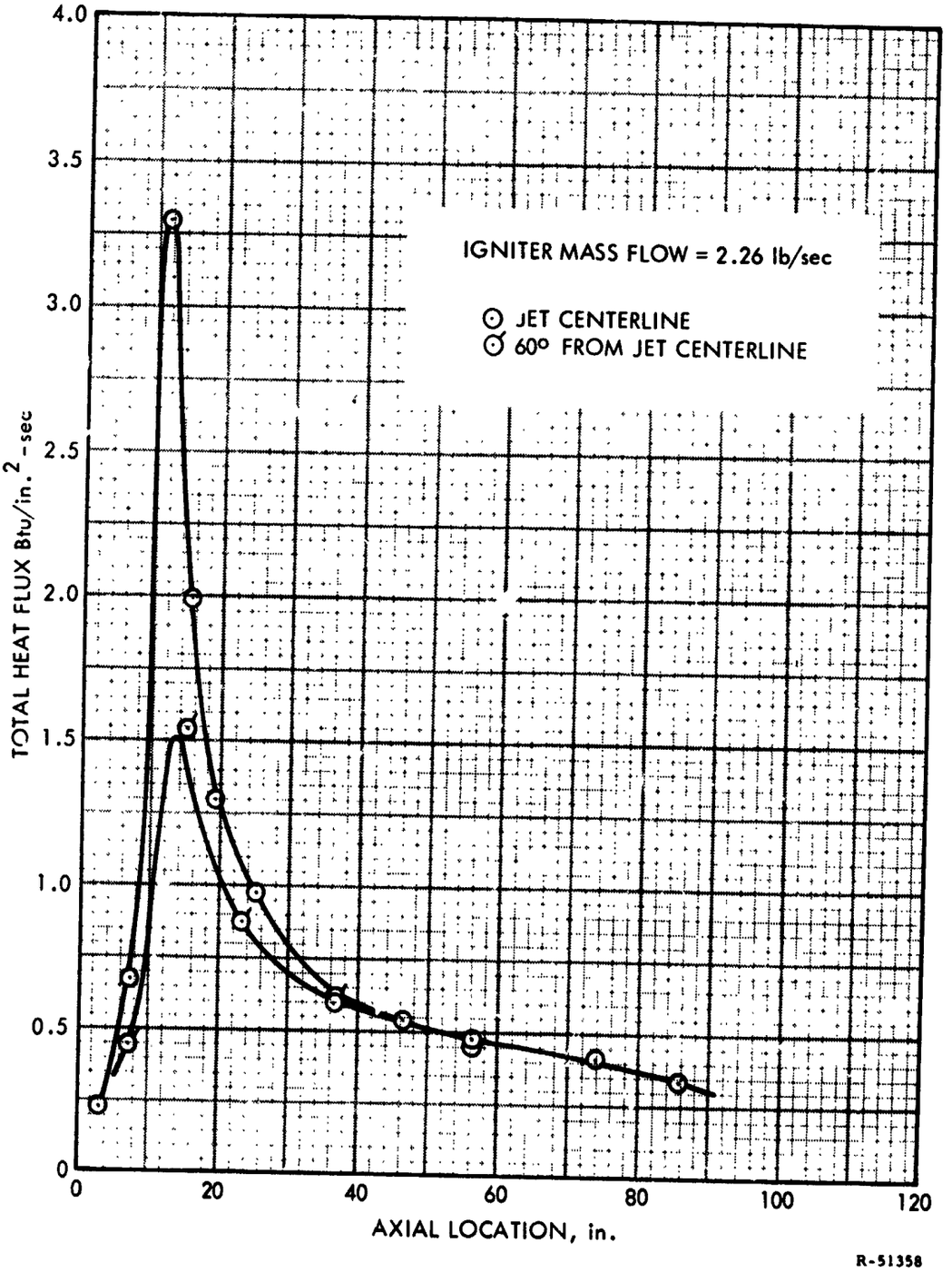

Figure 21. Multiple-Port Canted Igniter, Non-Aluminized Propellant, Heat Flux vs Length

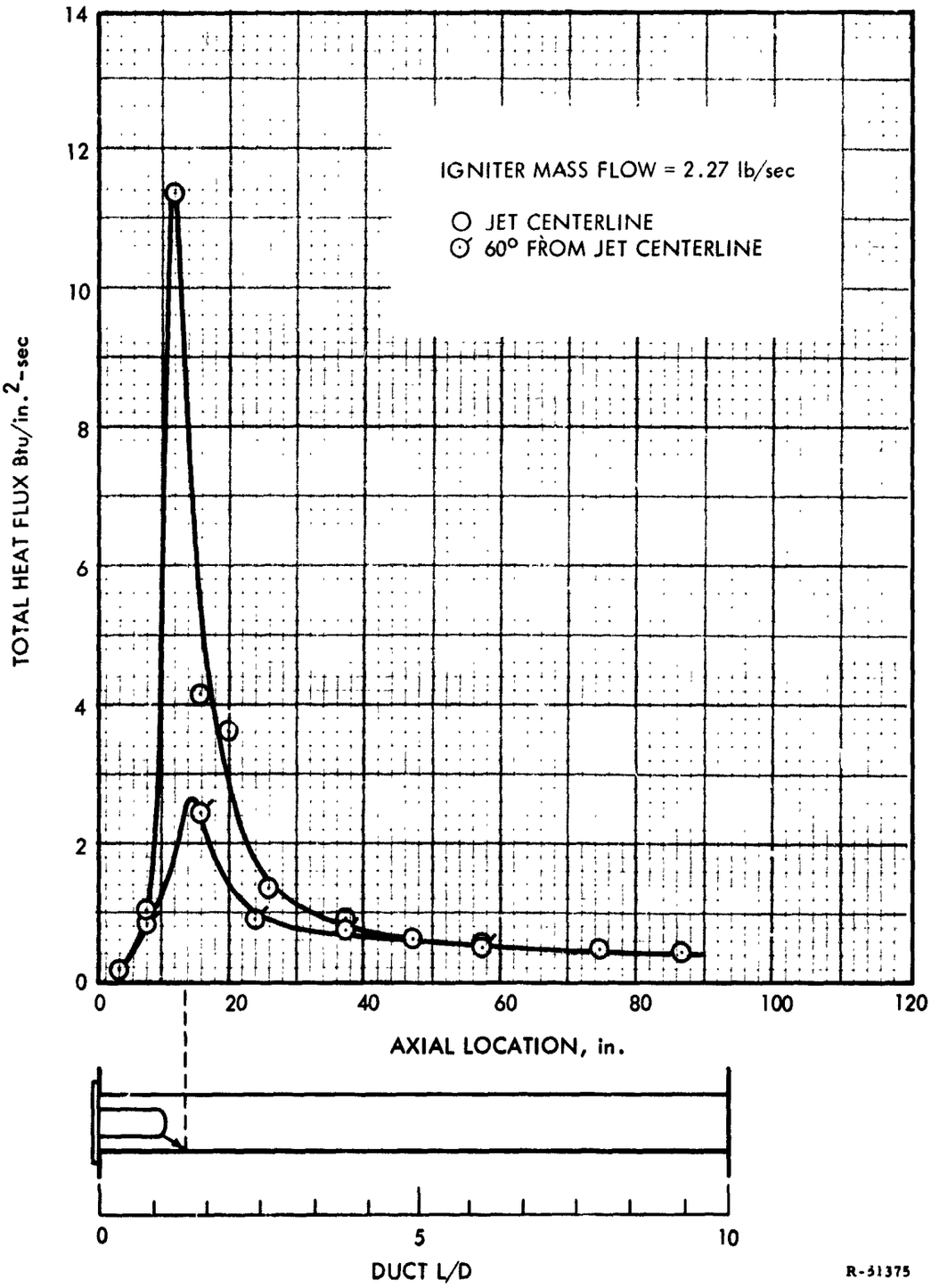

Figure 22. Multiple-Port Canted Igniter, Aluminized Products (18.9% Al_2O_3), Total Heat Flux vs Length

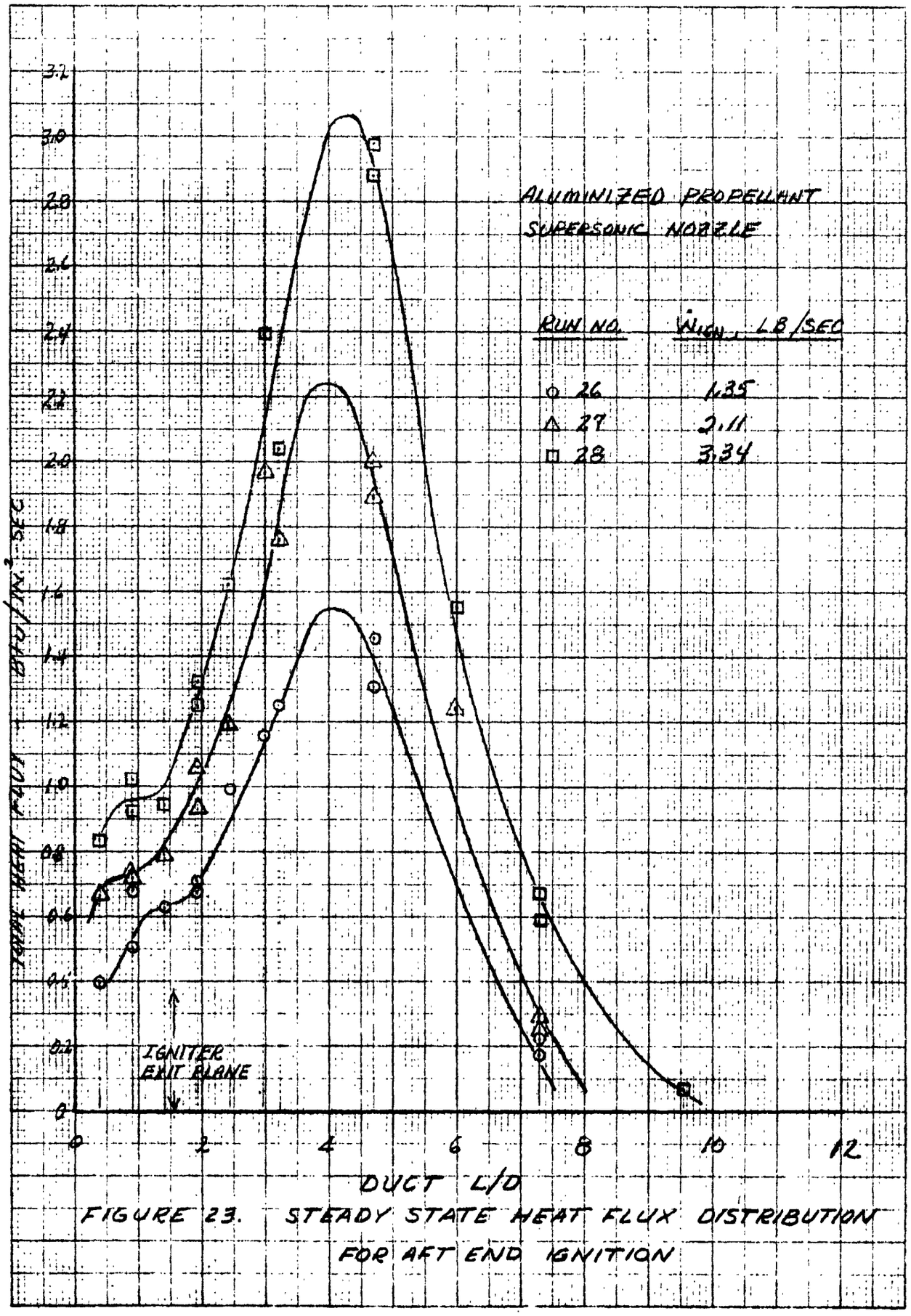

FIGURE 23. STEADY STATE HEAT FLUX DISTRIBUTION FOR AFT END IGNITION

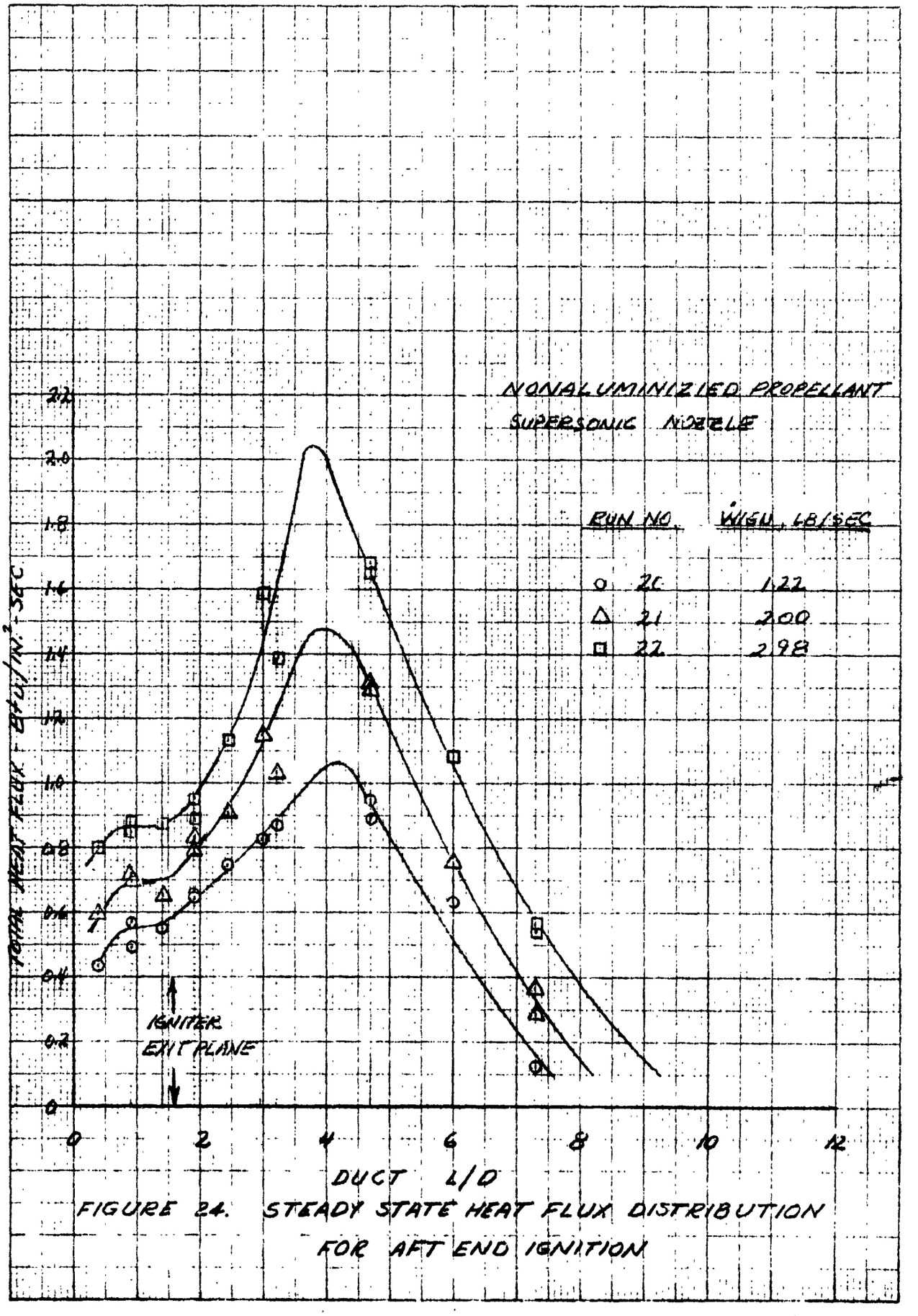

FIGURE 24. STEADY STATE HEAT FLUX DISTRIBUTION FOR AFT END IGNITION

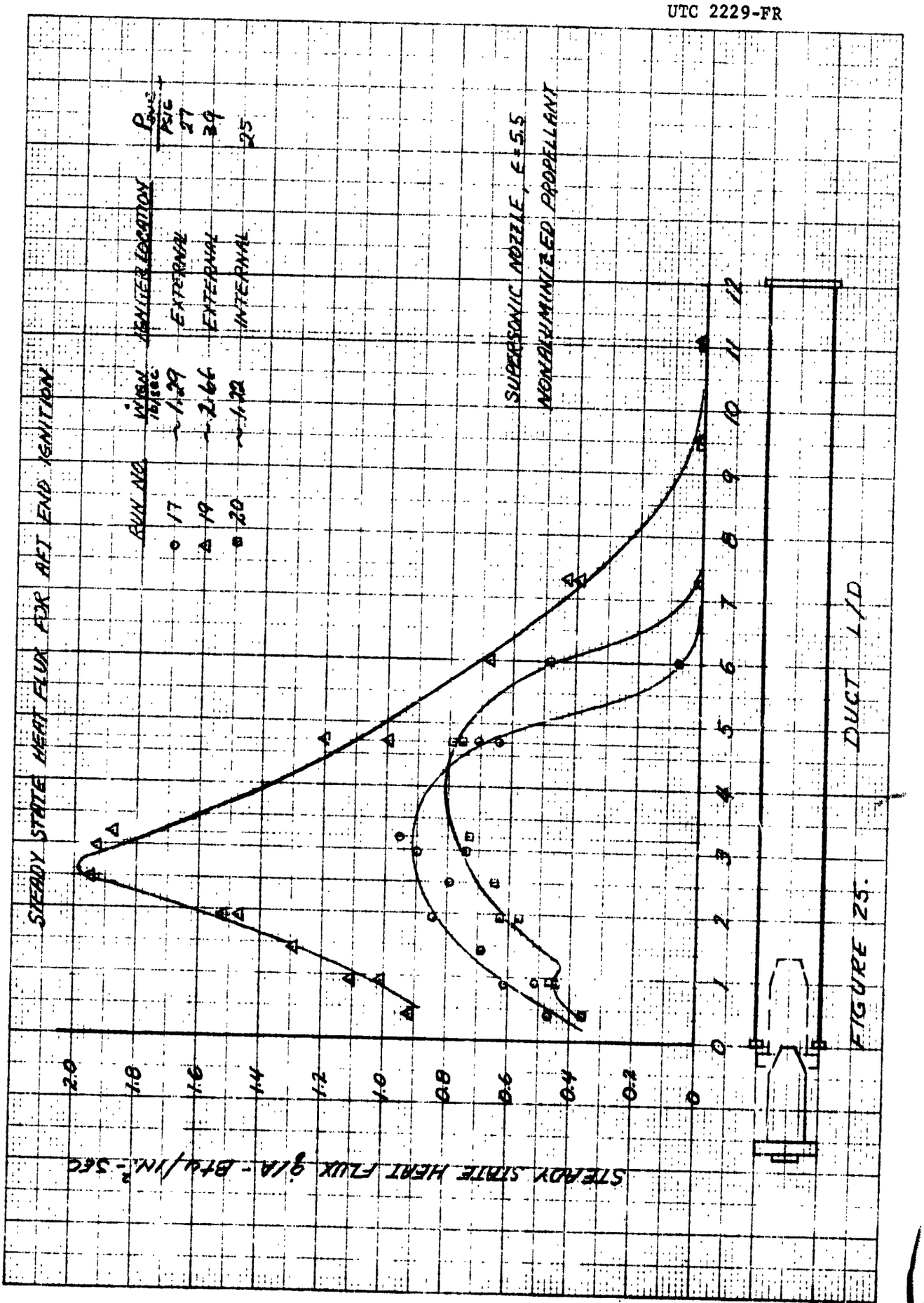
STEADY STATE HEAT FLUX FOR AFT END IGNITION
SUPERSONIC NOZZLE, ε = 5.5
NONALUMINIZED PROPELLANT
RUN NO. ẇ lb/sec GAUGE LOCATION P_ave/P_ic
17 ~1.29 EXTERNAL 27
19 ~1.26 EXTERNAL 29
20 ~1.22 INTERNAL 25
STEADY STATE HEAT FLUX q/A - Btu/in.²-sec
DUCT L/D
FIGURE 25.

configuration. The shift in peak heat flux down the duct length for the internal configuration in test 20 corresponds well with the change downstream in the position of the igniter exit plane. A similarity in curve shape is also preserved. This indicates that the internal configuration should produce data which agree reasonably well with the externally-mounted igniters.

The effect of sonic and supersonic nozzles on igniter heat flux is shown by comparison of figures 26 through 28. The peak heat fluxes for comparable igniter flow rates are equivalent, but location of the stagnation zone and peak heat flux is displaced forward for the supersonic nozzle igniters.

4.3.1.3 Radiation Data

Radiation data for head-end axial flow igniter and canted igniters with nonaluminized propellant are shown in figure 29. The axial variation is as expected for a radiating cloud within a cylindrical duct. Figure 30 shows equivalent radiation data for the aluminized propellant. The relationship of data from figures 29 and 30 is within the proper ratio for the temperature differences in exhaust products of aluminized and nonaluminized propellants.

The axial radiation heat flux for the aft-end igniter tests is presented in figures 31 through 33. The abrupt dropoff in flux in the stagnation end of the duct is strong evidence that little or no mixing occurs between the igniter exhaust and entrapped air.

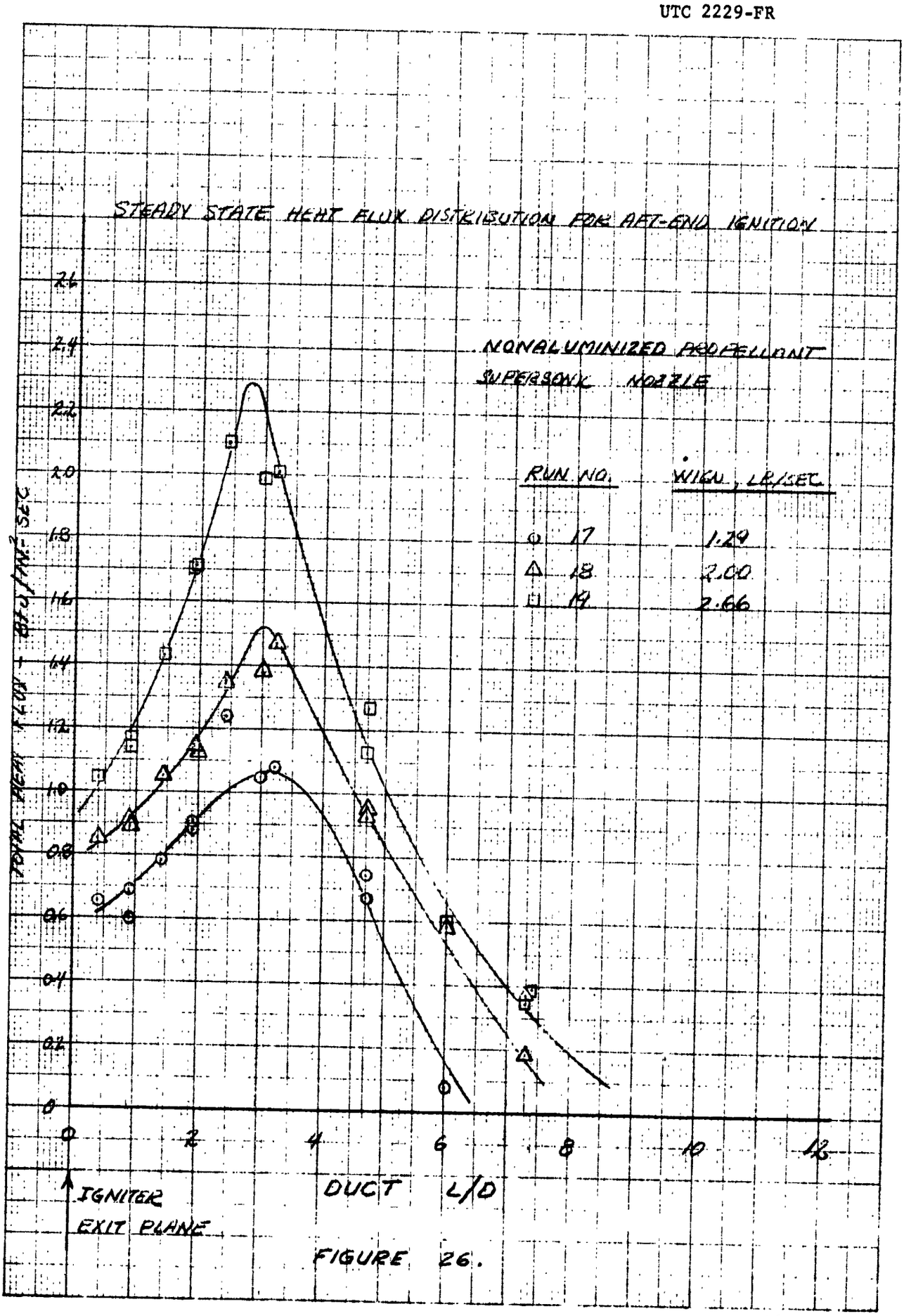
STEADY STATE HEAT FLUX DISTRIBUTION FOR AFT-END IGNITION
NONALUMINIZED PROPELLANT
SUPERSONIC NOZZLE
RUN NO.
WIGN. LB/SEC.
17
1.29
18
2.00
19
2.66
TOTAL HEAT FLUX - BTU/IN.² SEC
2.6
2.4
2.2
2.0
1.8
1.6
1.4
1.2
1.0
0.8
0.6
0.4
0.2
0
0
2
4
6
8
10
12
IGNITER EXIT PLANE
DUCT L/D

FIGURE 26.

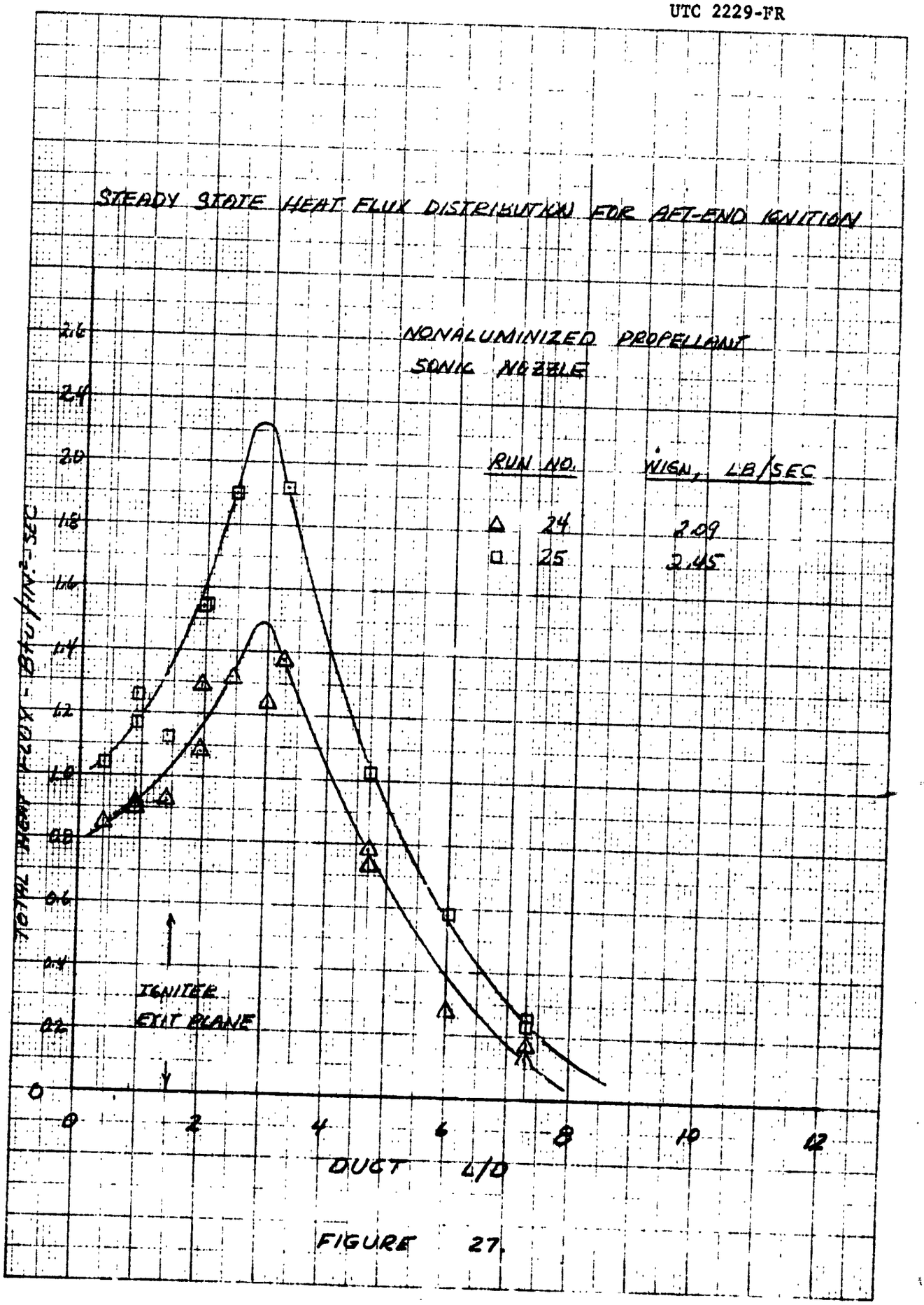
STEADY STATE HEAT FLUX DISTRIBUTION FOR AFT-END IGNITION
NONALUMINIZED PROPELLANT
SONIC NOZZLE
RUN NO.
WIGN, LB/SEC
24
2.09
25
2.45
IGNITER EXIT PLANE
DUCT L/D

FIGURE 27.

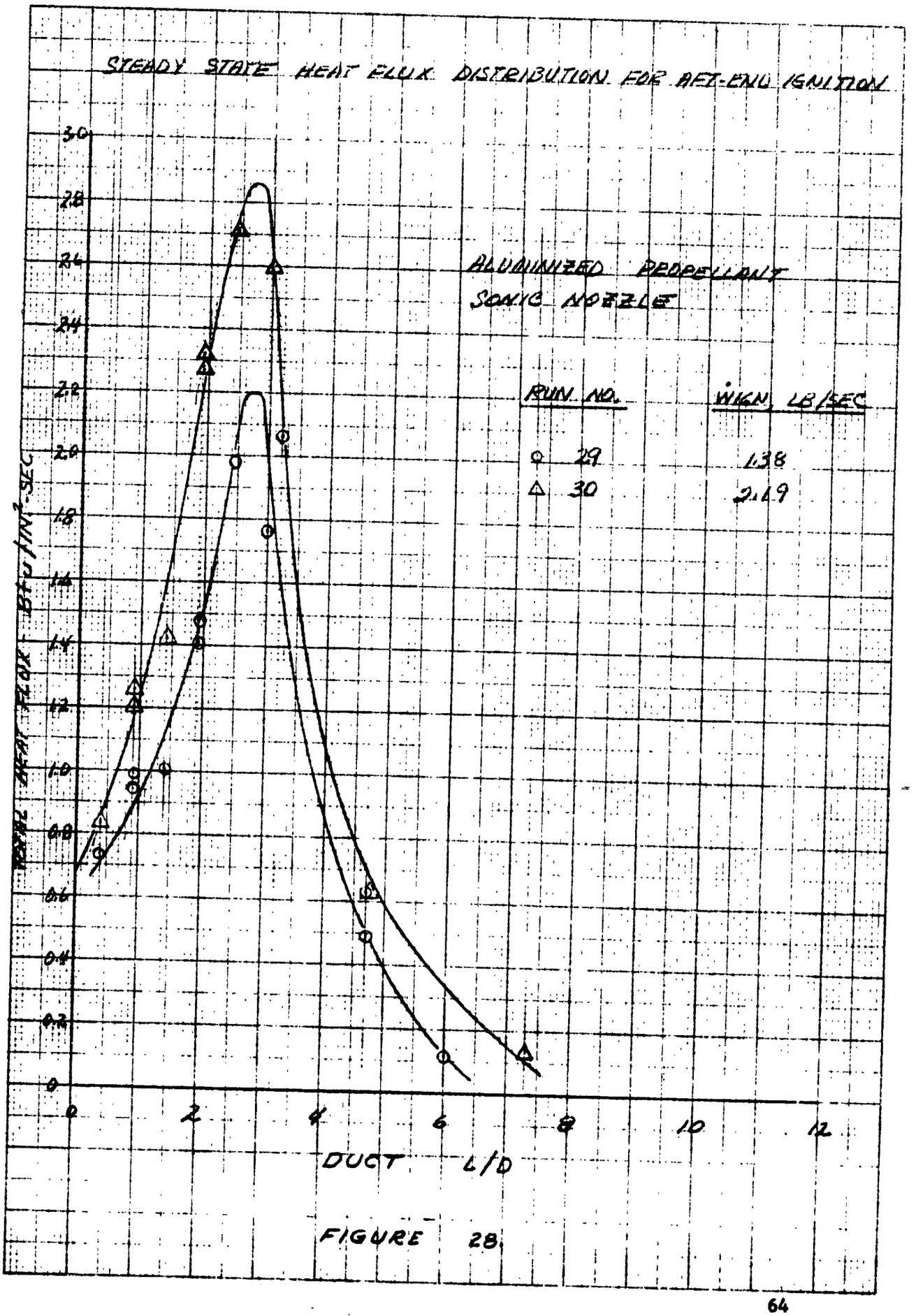
STEADY STATE HEAT FLUX DISTRIBUTION FOR AFI-ENU IGNITION
ALUMINIZED PROPELLANT
SONIC NOZZLE
RUN NO.
WIGN, LB/SEC
29
1.38
30
2.19
HEAT FLUX - BTU/IN²-SEC
DUCT L/D
0
0.2
0.4
0.6
0.8
1.0
1.2
1.4
1.6
1.8
2.0
2.2
2.4
2.6
2.8
3.0
2
4
6
8
10
12

FIGURE 28.

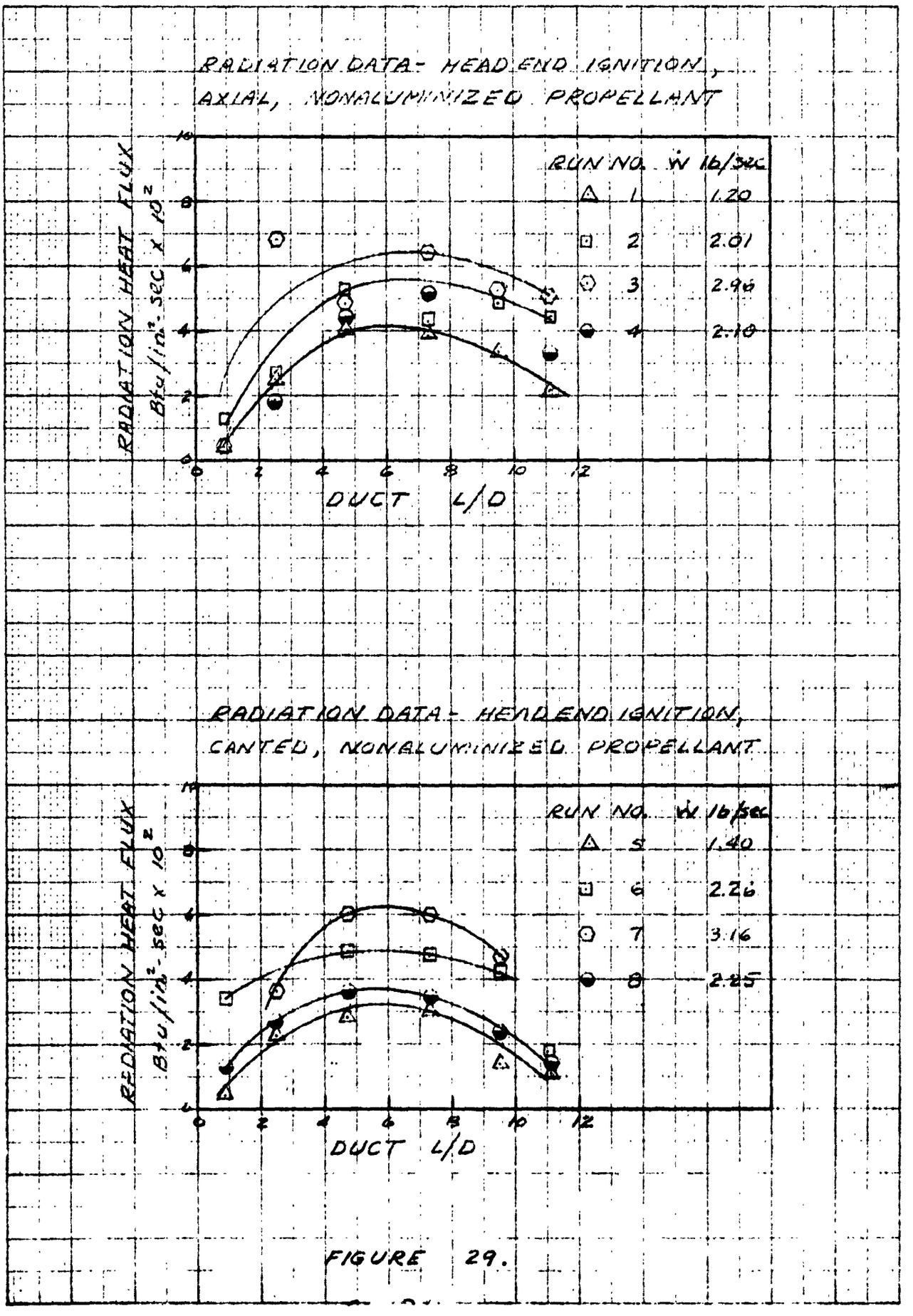
RADIATION DATA - HEAD END IGNITION, AXIAL, NONALUMINIZED PROPELLANT
RADIATION HEAT FLUX Btu/in²-sec x 10²
DUCT L/D
RUN NO. Ẇ lb/sec
1 1.20
2 2.01
3 2.96
4 2.10
RADIATION DATA - HEAD END IGNITION, CANTED, NONALUMINIZED PROPELLANT
RADIATION HEAT FLUX Btu/in²-sec x 10²
DUCT L/D
RUN NO. Ẇ lb/sec
5 1.40
6 2.26
7 3.16
8 2.25

FIGURE 29.

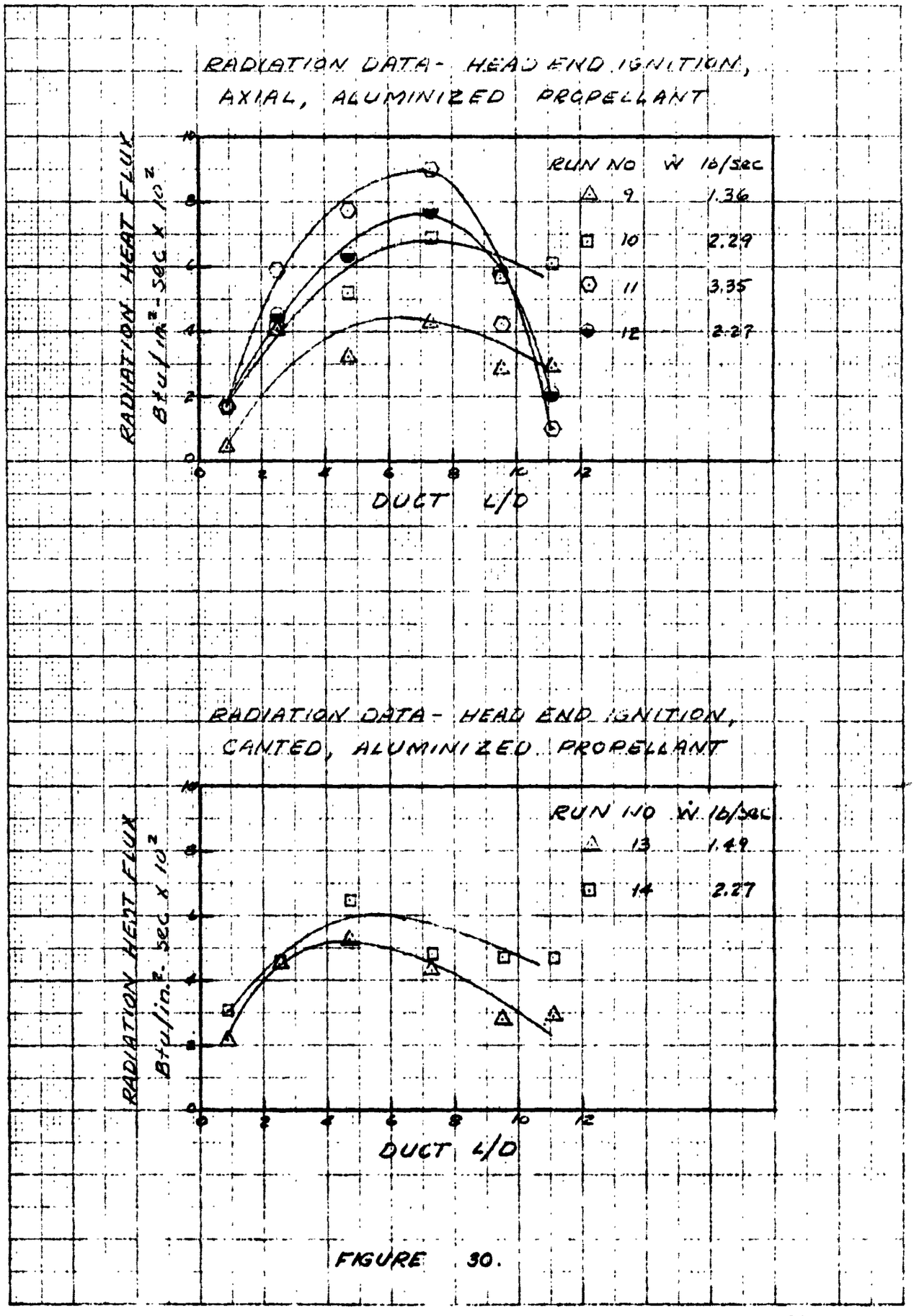
RADIATION DATA - HEAD END IGNITION, AXIAL, ALUMINIZED PROPELLANT
RADIATION HEAT FLUX
Btu/in.² - sec x 10²
RUN NO
Ẇ lb/sec
9 1.36
10 2.29
11 3.35
12 2.27
DUCT L/D
RADIATION DATA - HEAD END IGNITION, CANTED, ALUMINIZED PROPELLANT
RADIATION HEAT FLUX
Btu/in.² - sec x 10²
RUN NO
Ẇ lb/sec
13 1.49
14 2.27
DUCT L/D

FIGURE 30.

RADIATION DATA - AFT END IGNITION
SUPERSONIC NOZZLE, NONALUMINIZED PROPELLANT

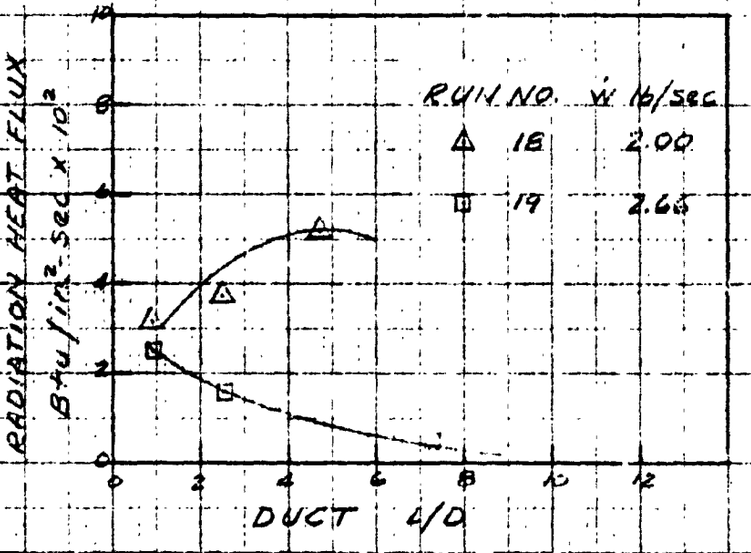

RADIATION DATA - AFT END IGNITION
SUPERSONIC NOZZLE, NONALUMINIZED PROPELLANT

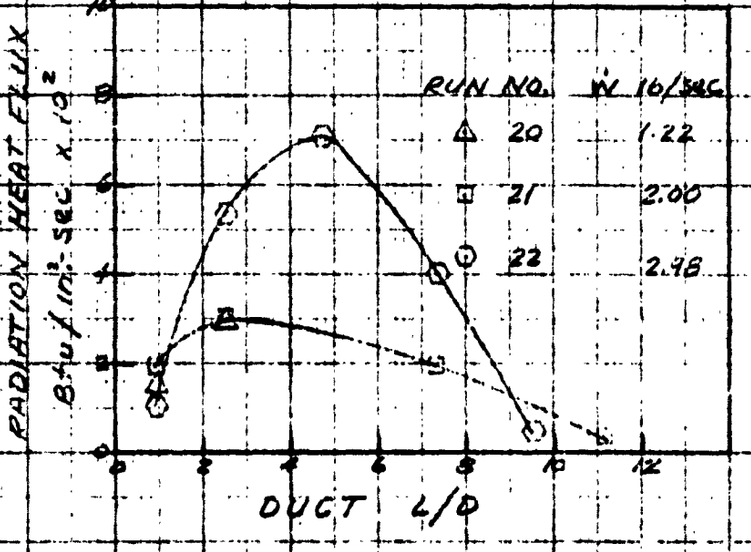

FIGURE 31.

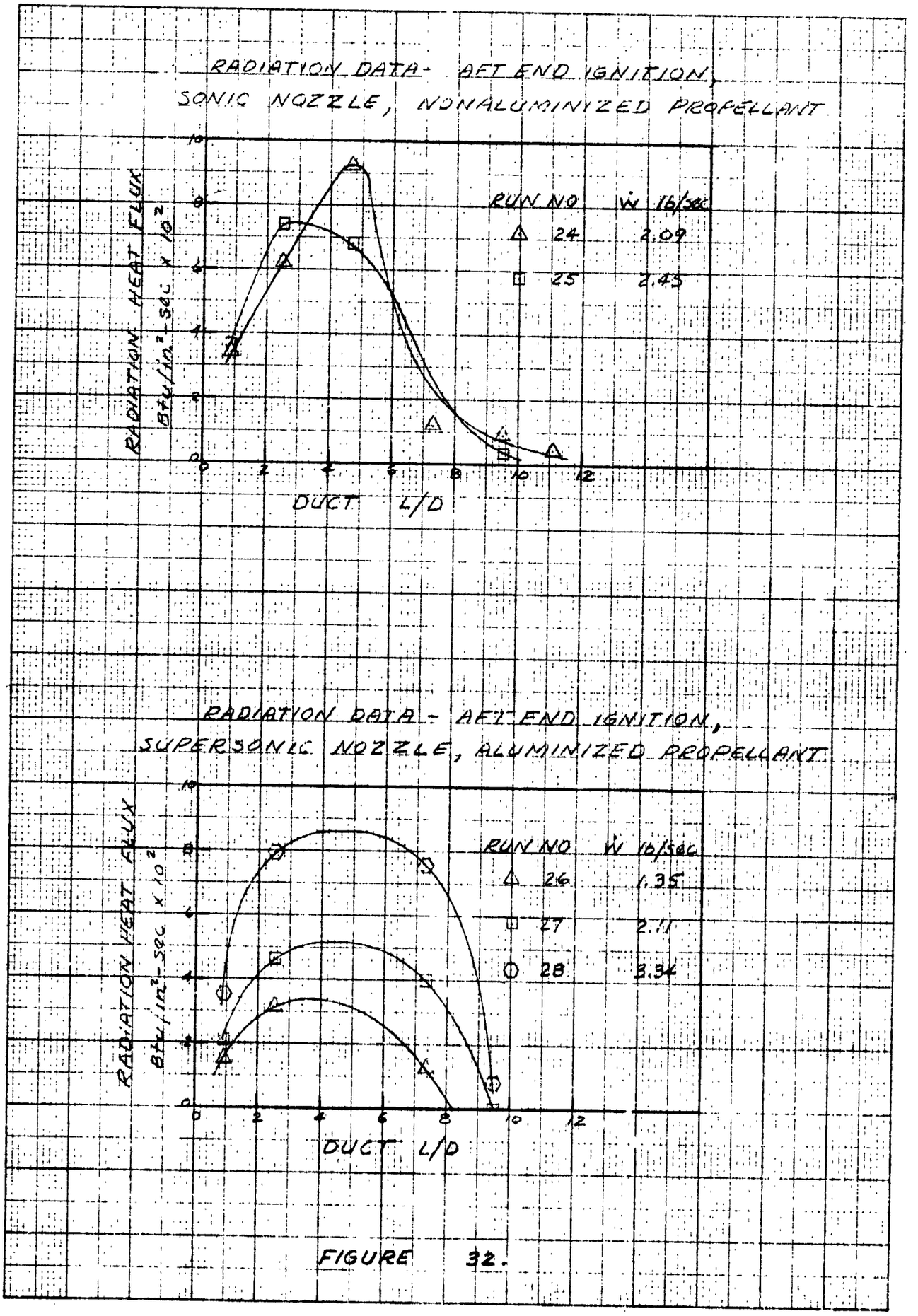
RADIATION DATA- AFT END IGNITION, SONIC NOZZLE, NONALUMINIZED PROPELLANT
RADIATION HEAT FLUX BTU/in²-sec x 10²
RUN NO ẇ lb/sec
24 2.09
25 2.45
DUCT L/D
RADIATION DATA - AFT END IGNITION, SUPERSONIC NOZZLE, ALUMINIZED PROPELLANT
RADIATION HEAT FLUX BTU/in²-sec x 10²
RUN NO ẇ lb/sec
26 1.35
27 2.11
28 3.34
DUCT L/D

FIGURE 32.

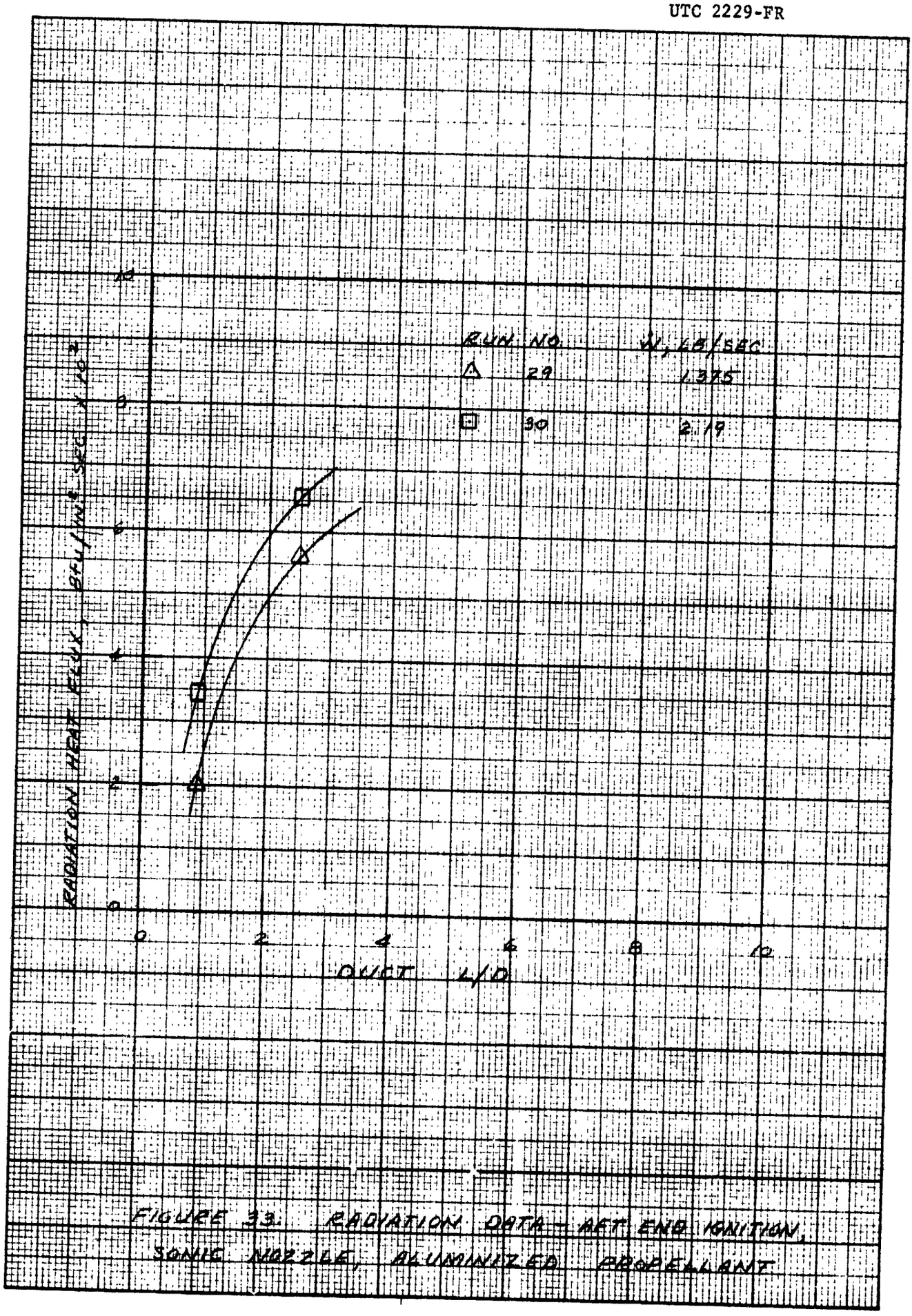

FIGURE 33. RADIATION DATA - AFT END IGNITION, SONIC NOZZLE, ALUMINIZED PROPELLANT

4.3.1.4 Duct Pressure Data

Steady duct pressure data for a typical head-end igniter test are shown in figure 34. Pressure dropoff at the duct ends corresponding to aspiration effects in the head-end and velocity effects at the aft end are apparent. Typical transient pressure data for an aft-end ignition test is shown in figure 35. The tailoff in aft-end duct pressure probably corresponds to a loss in igniter chamber pressure and reduction in mass flow. Measurements at the duct head-end reflect the duct total pressures in the stagnation region while the two measurements at the aft end show the effects of igniter gas velocity on the static pressure. Figure 36 shows the variation of duct steady-state pressure and total heat flux for a typical aft-end ignition test. The correspondence of the duct pressure and heat flux in definition of the stagnation region is noted.

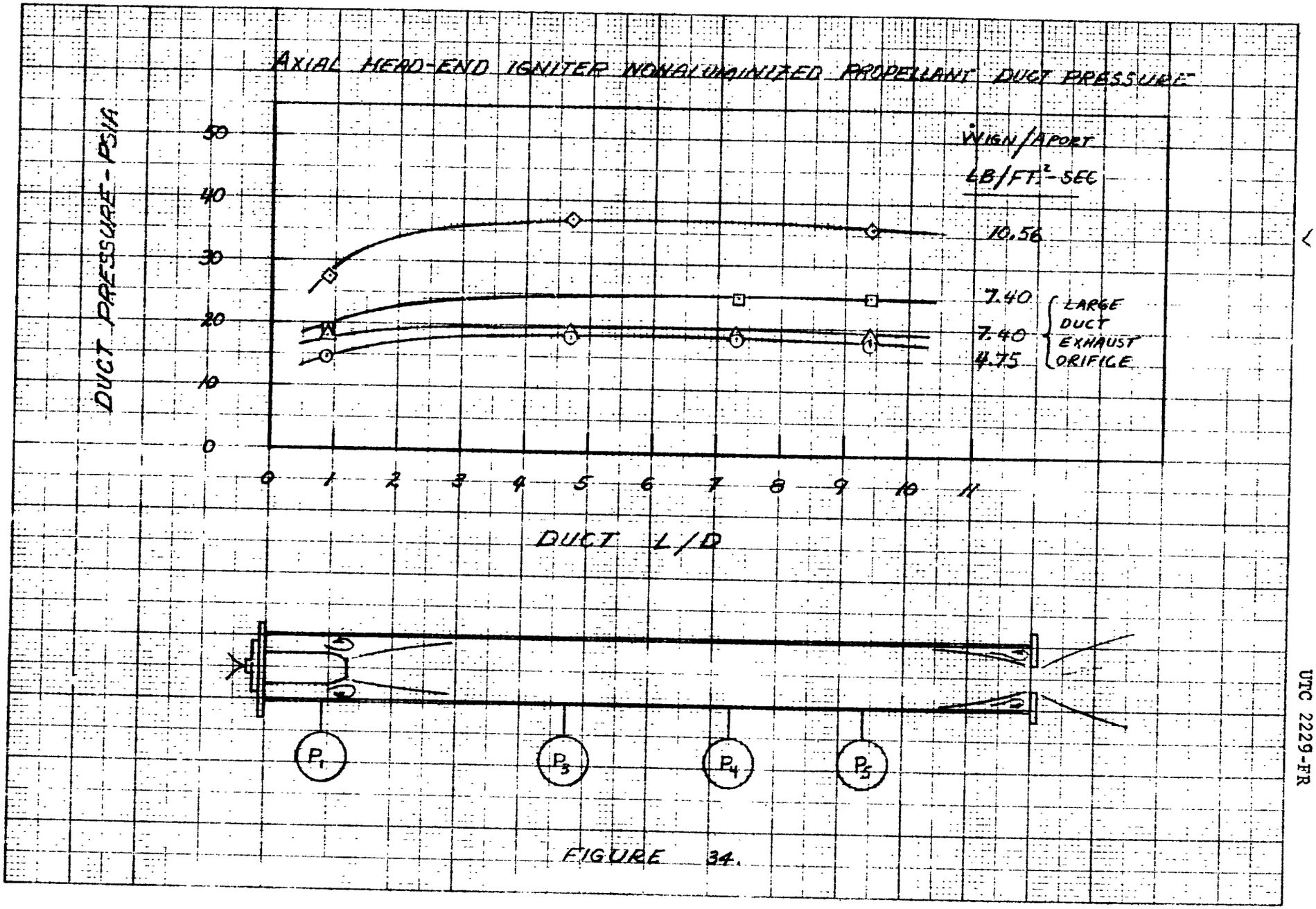
AXIAL HEAD-END IGNITER NONALUMINIZED PROPELLANT DUCT PRESSURE
DUCT PRESSURE - PSIA
50
40
30
20
10
0
0 1 2 3 4 5 6 7 8 9 10 11
DUCT L/D
ẆIGN/APORT
LB/FT²-SEC
10.56
7.40
7.40
4.75
LARGE DUCT EXHAUST ORIFICE
P1
P3
P4
P5

FIGURE 34.

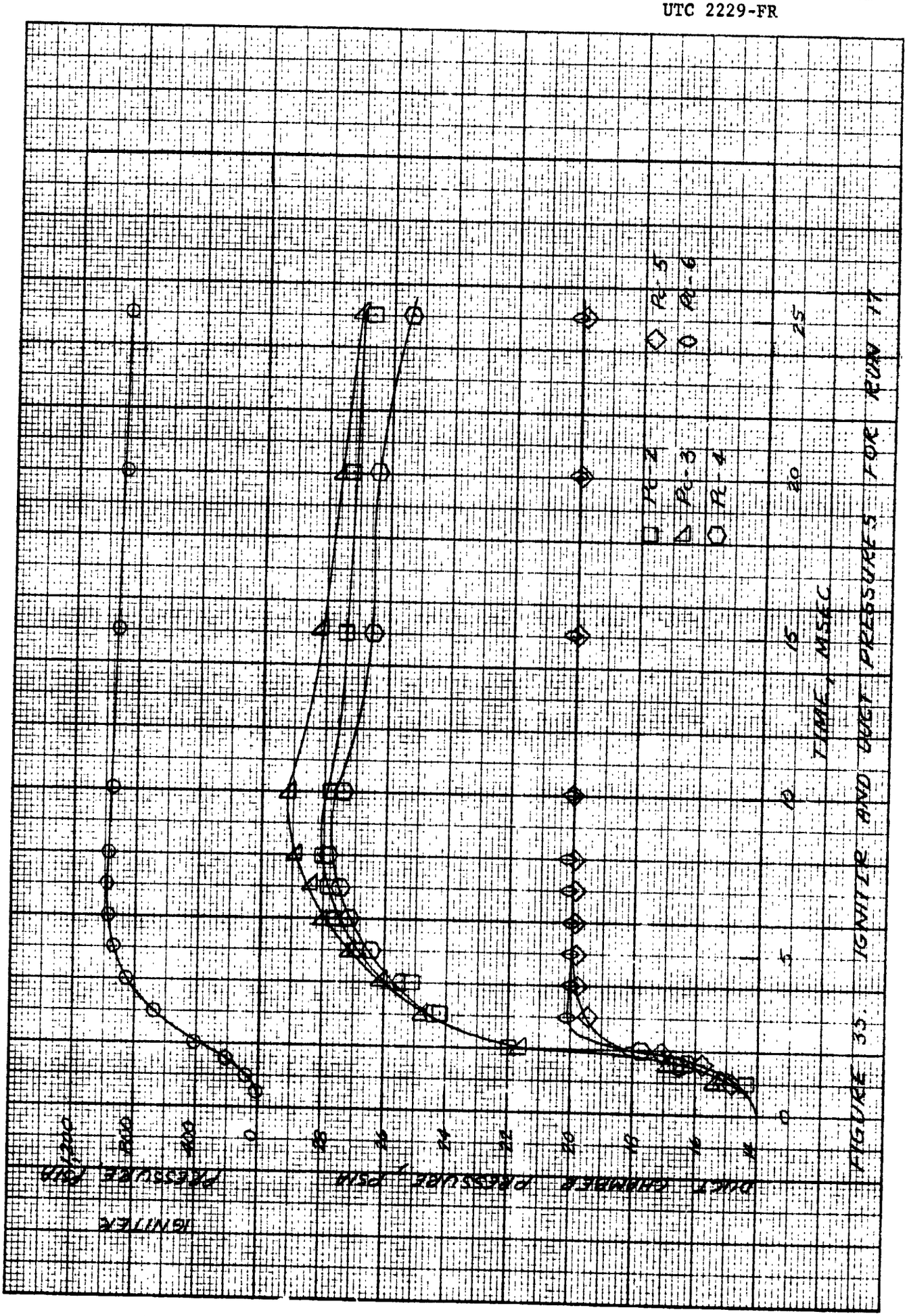

FIGURE 35. IGNITER AND DUCT PRESSURES FOR RUN 11

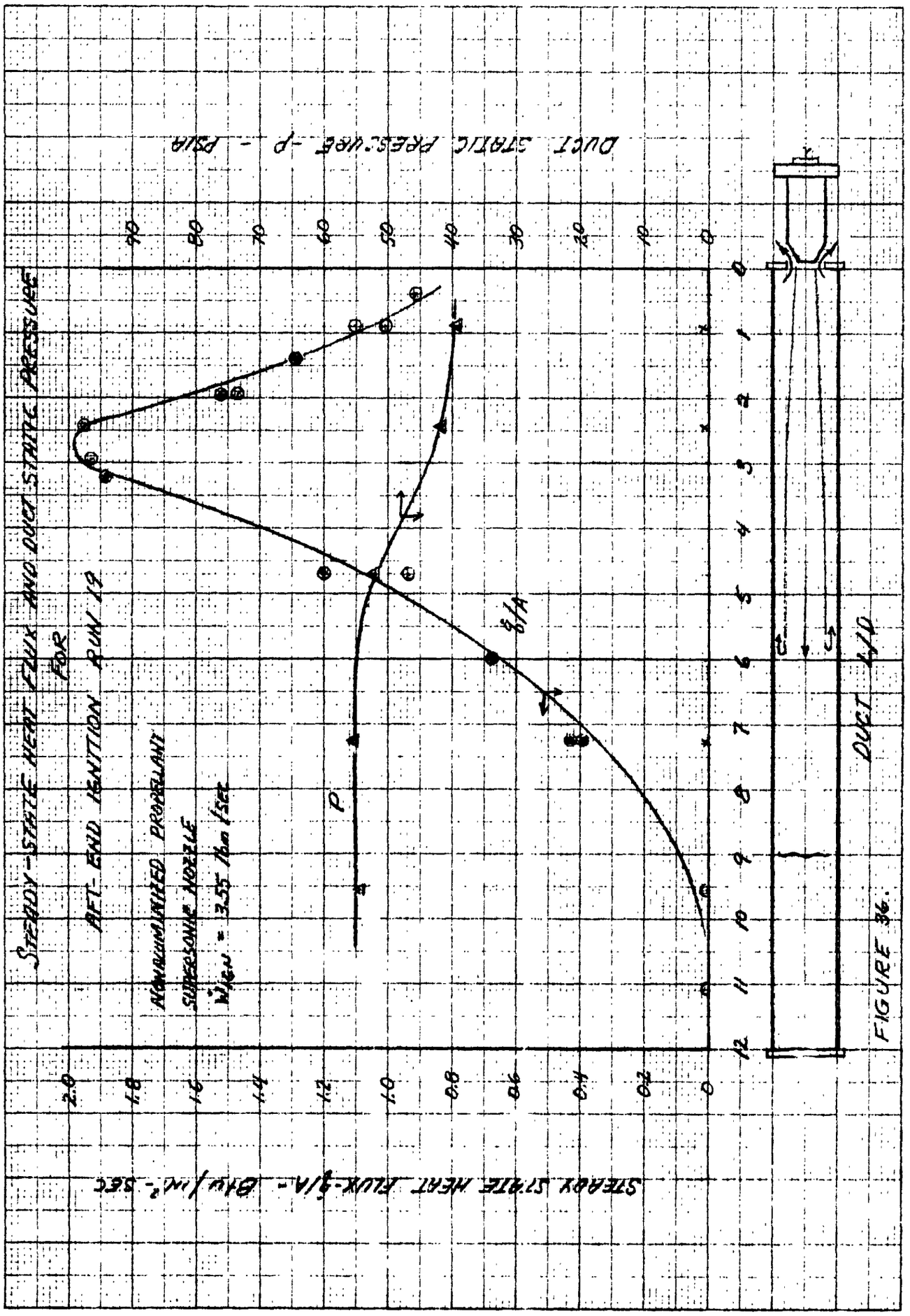
STEADY-STATE HEAT FLUX AND DUCT STATIC PRESSURE
FOR
AFT END IGNITION RUN 19
NONALUMINIZED PROPELLANT
SUBSONIC NOZZLE
$\dot{W}_{GW}$ = 3.55 lbm/sec
STEADY STATE HEAT FLUX-$\dot{q}/A$ - Btu/in^2-sec
DUCT STATIC PRESSURE -P - PSIA
P
$\dot{q}/A$
DUCT L/D

FIGURE 36.

4.4 DATA CORRELATION

The development of generalized data correlations from model tests depends upon expression of data in terms of parameters which preserve similarity between the modeling and modeled systems. For the igniter and copper duct model under consideration, the parameters of interest are those which preserve:

A. Fluid physical property similarity (Prandtl number)

B. System dynamic similarity (Reynolds number and geometrical correspondence determined by igniter and duct design parameters)

C. Temperature field similarity (implied in heat transfer coefficient and Nusselt number)

D. Surface heat transfer properties similarity (thermal conductivity, surface roughness, absorptivity, and emissivity)

For the model under study, only the physical properties affecting surface heat transfer pose a problem. The primary properties of interest in correlation of the convective heat transfer data are the surface roughness and thermal conductivity. Surface roughness primarily affects the velocity profile near the wall and will be neglected in this study. Differences in wall thermal properties result in an expansion or contraction of the timespan between the modeling and modeled systems for equivalent wall temperature changes. Calculations indicate that surface temperature changes in the copper duct model, which occur over a timespan of 100 to 300 msec correspond to a timespan from 8 to 25 msec for a system with the thermal conductivity of typical solid propellants. This indicates that correlations which are based upon the model wall temperature distributions

correspond to wall temperatures which occur very early in the igniter action interval in real motors. The question then arises as to whether the correlations based upon the low wall temperature levels of the modeling system can be extrapolated to the autoignition temperature ranges of the solid propellant. Wrubel[16] reports that the heat transfer coefficient remains constant in time for systems with high temperature potentials. If this is the case, then the correlations developed from the copper duct model will be valid over the range of solid propellant surface temperatures of interest.

A second question arises which concerns the applicability of using steady-state heat flux correlations in determination of transient ignition phenomena. For typical peak heat flux levels experienced with pyrogen igniters, propellant ignitibility data [5] indicate that ignitions will occur in less than 50 msec. In the test data analyzed here, the duct pressure transient during the ignition phase corresponds well with data obtained with actual motors, e.g., in the neighborhood of 60 to 80 msec. Therefore, the timespan in the solid propellant motor to which the steady-state duct correlations must be applied corresponds to a period of developing hydrodynamic and thermal flow fields. During a portion of this program, the transient motor phenomena were investigated but due to accuracy limitations of the basic experiment, no conclusions could be reached as to the interaction of the developing hydrodynamic flow field with heat transfer. However, the free shear velocities are relatively high (over 100 ft/sec) and hence, the characteristic time for the transient boundary layer development (α/V^2) is of the order of milliseconds.

Therefore, the development of the boundary layer will follow the changes in igniter mass flow reasonably closely. On this basis, then the steady-state correlations heat transfer can be applied to the ignition transient period by assuming a series of quasi-steady-state processes. It is recognized that this is an oversimplification of the phenomena and that the postulated correspondence between hydrodynamic and thermal flow fields may be invalid above a certain critical rate, but available information does not permit a detailed study of these mechanisms.

Qualitatively, steady-state igniter heat transfer may be characterized by analogy to developing pipe flow phenomena. For the head-end igniter tests, the flow of igniter exhausts into the duct head-end breaks up and is attached to the duct at some distance downstream of the igniter exhaust nozzle (see figure 37). At the point of attachment, boundary layer growth begins and all regions downstream correspond to the developing boundary layers in pipes. Regions upstream of the attachment (or impingement region for canted igniters) are characterized by stagnation zones and areas of recirculation. Data correlations discussed in the following sections are based on these preceding observations.

4.4.1 Axial Head-End Igniters

Head-end igniter heat transfer studies show many similarities to heat transfer in circular pipes. For distances sufficiently downstream of the igniter exit plane, the heat transfer should correspond to fully developed pipe flow and should be correlated by classical boundary layer heat transfer methods. This, in fact, has been the case as demonstrated by Bastress, et al.,[11] Carlson and Seader,[17] and Mullis.[9] Locations

Flow Pattern in Motor for Head-End Igniter

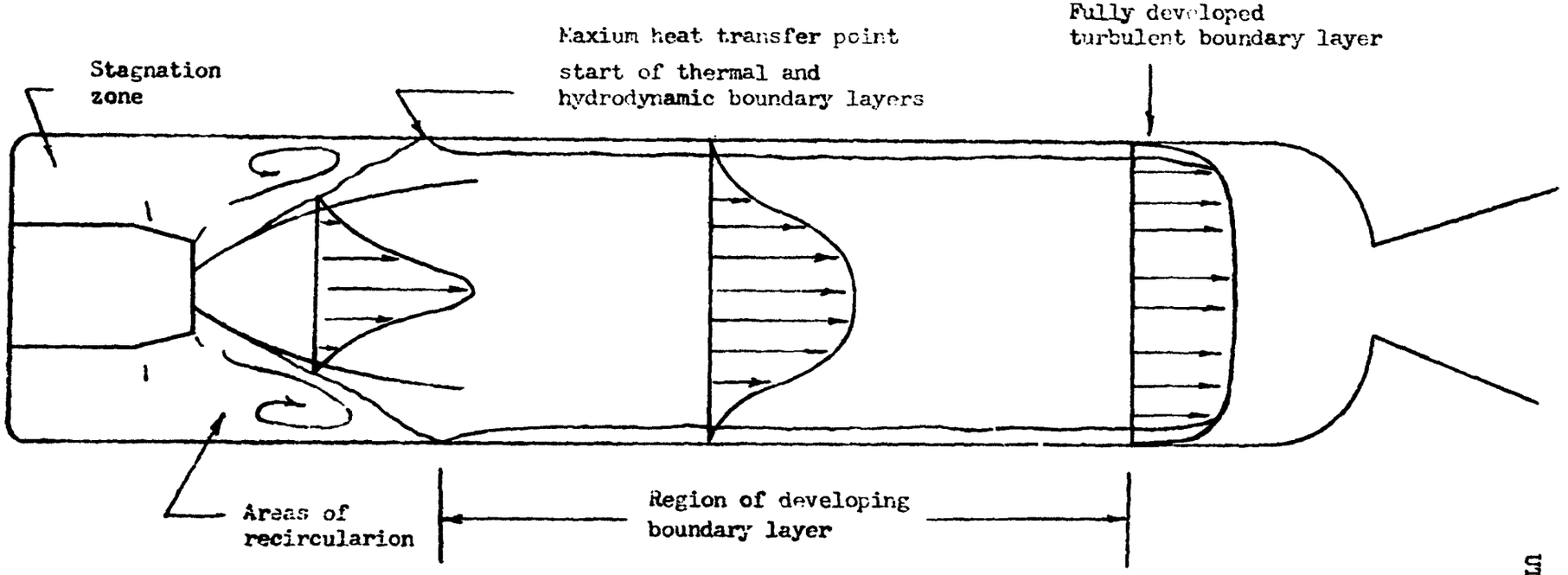

FIGURE - 37

upstream of the fully developed flow region and downstream of the boundary layer starting point (impingement point) display qualitatively the same heat transfer characteristics observed in the entry regions of pipes which are characterized by developing hydrodynamic and thermal boundary layers. Existing pipe entry correlations, however, are not applicable to axial head-end igniter heat transfer because of the more complicated flow patterns introduced by the igniter jet. Canted jet igniters produce further perturbations because of the direct jet impingement upon the wall with associated high localized heat transfer rates.

The region upstream of the boundary layer starting point is characterized by stagnation and recirculation. Heat transfer in this region is highly dependent upon the igniter and motor configuration and mass flow variables. Fortunately, this region is generally small with respect to total area available for heat transfer; therefore, estimation of the heat transfer in the head-end region should produce only small errors in calculation of the total solid propellant motor ignition transient.

In view of these uncertainties, correlation of the data within the framework of existing correlations was restricted to the points near the region of maximum heat transfer and the development of additional empirical methods which apply to the transition to fully developed flow. The point of maximum flux was considered to be best correlated based on hydrodynamic considerations. The combined correlations would then provide a basis for predicting the point of maximum heat flux, the magnitude of the maximum, and the distribution of flux along the propellant surface. These correlations could then be combined with other reported results[5,18,19] to

permit prediction of solid propellant motor ignition pressure transients.

Boelter,[20] Humble,[15] and others have experimentally investigated turbulent convective heat transfer in pipes and have found that convective heat transfer in fully developed turbulent flow can generally be calculated by use of the relationship

$$Nu_{\infty} = a\, Re^{b}\, Pr^{c} \qquad (28)$$

which is composed of empirically determined constants and similarity parameters. The Prandtl number is a function only of the physical properties of the heat transfer fluid and represents the rates of momentum diffusivity to thermal diffusivity of the fluid. If the Prandtl number is greater than 1.0, then heat and momentum are diffused through the fluid at the same rate. In the case of gases for which Pr = 0.7, heat is propagated through the fluid at a higher rate than momentum. The Reynolds number may be interpreted as the ratio of the inertia to viscous forces in a fluid. Two fluids are dynamically similar, i.e., the velocity fields are similar if the Reynolds numbers are equal. Implied in the Nusselt number is the similarity of temperature profiles through the boundary layer and, hence, heat transfer. Thus, equation 28 indicates that for a similarity of physical properties, a defined similarity between velocity profiles and temperature profiles exists and the heat transfer may be determined. This relationship applies only to fully developed velocity and thermal profiles.

In the entrance regions of pipes for igniter heat transfer, an

empirical equation of the form of 28 is no longer valid because the heat transfer depends upon the developing thermal and hydrodynamic boundary layers. However, if the length effects of the developing thermal and hydrodynamic layers can be determined, one would expect an empirical relationship of the following form to apply

$$Nu_x = a\eta_n (x') \; Re_D^b \; Pr^c \qquad (29)$$

Theoretically, the function $\eta_n(x')$ would be quite complex because of the number of degrees of freedom added to the equation. The function $\eta_n(x')$, where the integer n corresponds to a given set of similarity parameters, would depend upon parameters affecting the entering thermal and hydrodynamic profiles as well as variables influencing either the thermal or hydrodynamic profile at any downstream axial location until fully developed flow conditions are established. For a solid propellant igniter exhausting into a motor port, the additional similarity parameters for which a given $\eta_n(x')$ function would be defined would include the igniter jet and motor configuration parameters as determined by (1) the jet exit Mach number (M_e), (2) the nozzle exit half angle (e_n), (3) the duct-to-igniter throat diameter (D_p/D_i), and (4) the igniter jet-to-duct back-pressure (P_j/P_d). The time and spatial temperature distributions would also affect the development of the thermal boundary layer as would physical irregularities in the port surface, such as slots, which would tend to disrupt the developing hydrodynamic boundary layer. The latter effects, hopefully, would be small and could be neglected. The other important variables, including igniter mass flow rate and igniter exhaust specie

physical properties, are accounted for in Reynolds and Prandtl numbers. The perturbing effects of two-phase flow are a further complication which is beyond the scope of this study.

Experimentally, Boelter, et al.[20] found the length-dependence of the heat transfer coefficient to be similar to those found in the solid propellant igniter application under study. Boelter reported that the magnitudes and length variations in the localized and average heat transfer coefficient depended greatly upon the entering fluid conditions, i.e., the thermal and velocity profiles. The implication of these observations is that an empirical heat transfer correlation for each entrance or igniter configuration which does not correspond to a known, completely similar case must be determined individually.

In igniter heat transfer studies with hot gas igniters, Carlson and Seader[17] presented generalized head-end igniter heat transfer correlations in terms of the normalized local diameter Nusselt number and length-to-diameter location for various igniter motor (test chamber) design variables. The normalizing Nusselt number was calculated by the Dittus-Boelter equations for fully developed turbulent pipe flow

$$Nu_{\infty} = 0.023\ Re^{0.8}\ Pr^{0.4} \qquad (30)$$

Typical generalized heat transfer data generated by Carlson and Seader[17] are given in figures 38 and 39, respectively. Figure 38 indicates the length-dependent Nusselt number at zero time (initiation of the igniter) for a duct port-to-throat area ratio of 2 with duct-to-igniter nozzle

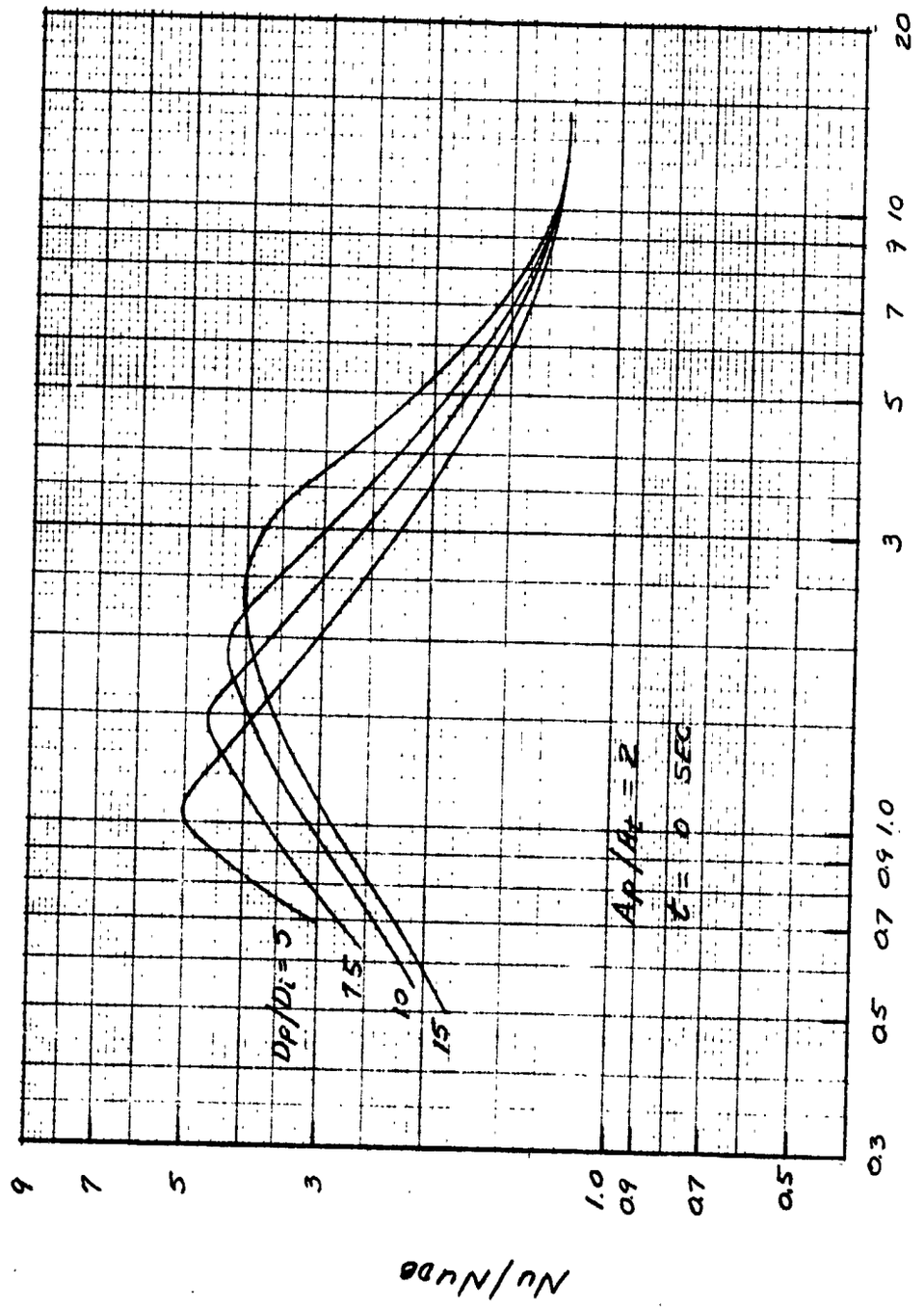

(FROM REFERENCE 17)

FIGURE 38. GENERALIZED HEAD-END HEAT TRANSFER CORRELATION

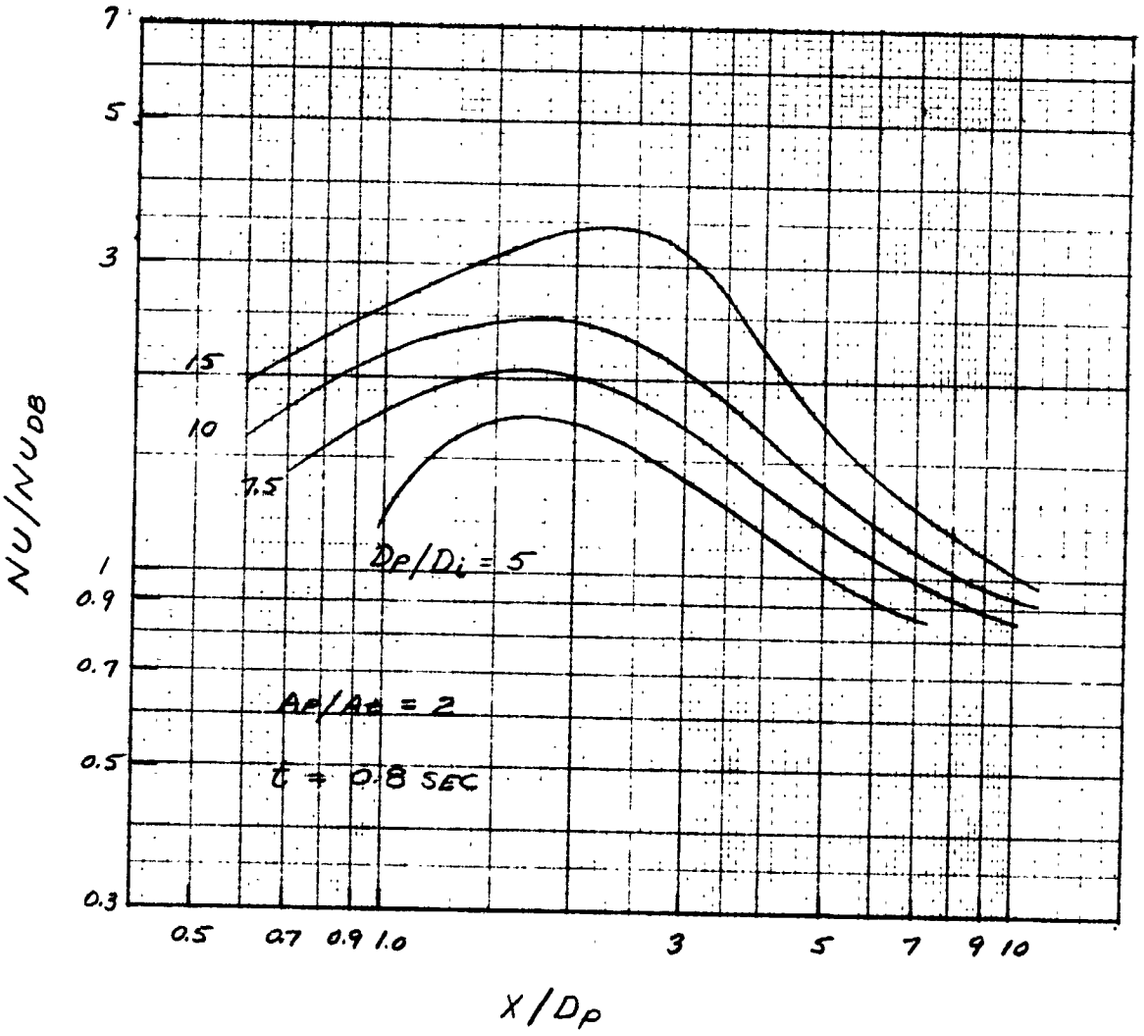

(FROM REFERENCE 17)

FIGURE 39. GENERALIZED HEAD-END HEAT TRANSFER CORRELATION

throat diameter ratio as a parameter. Figure 39 indicates the same information at a time of 0.8 sec. A significant fact indicated by these figures is the shifting and changing magnitudes of the normalized Nusselt number with time. The changing maximum points and asymptotic values for high length-to-diameter ratio are of particular interest. Carlson[17] reports that the large time-dependent changes noted are associated with the transient thermal boundary layer mechanisms brought about by the changing wall temperature. He indicates these transient changes should not be as severe in actual rocket motor application as a result of the greater fluid-to-wall temperature difference experienced in the short interval prior to ignition. In later studies, Wrubel[16] reported that the heat transfer coefficient remained constant as a function of time when a high gas temperature driving potential was preserved. The results of this program substantiate their results.

4.4.1.1 Correlation of Downstream Heat Flux and Length Effect

Mullis[9] reported a correlation by Kays[21] for which the head-end axial igniter data showed good agreement for distances greater than 4 port diameters downstream of the igniter exit plane. The correlation used was of the form

$$\frac{Nu_x}{Nu_\infty} = \left(\frac{Nu_x}{Nu}\right)_{thermal} \left[1 + \frac{c}{X'/D}\right] \quad (31)$$

where the thermal entry Nusselt number was determined from a series solution for the entry length by Kays,[22]* and the asymptotic solution Nu_∞ was determined from the Colburn equation for fully developed turbulent pipe flow. Distances were referenced to the point of maximum heat transfer where $X' = 0$. A basic failing of equation 20 is that it predicts an infinite heat transfer rate at locations of X' approaching zero. This is physically unrealistic and does not provide a means of determining the maximum heat transfer rate which is of the utmost importance since it determines the point and time of first ignition.

In the current studies, data correlation followed an empirical engineering approach. The review of previous work, the complexity of the problem, and the limited quantity and accuracy of the data dictated this empirical solution.

The head-end igniter test data were reduced to dimensionless parameter form as indicated in section 4.1. The igniter gas temperature drop along the duct length was determined by use of equation 19 using the average values of the steady-state heat flux determined by equation 9. The dimensionless parameters were then determined using the fluid physical properties evaluated at the local film temperature, the local average heat transfer rate, the duct mass flux, and the local wall temperature and duct bulk temperatures.

*Kays' thermal entry length solution was based upon the assumption of a fully developed hydrodynamic profile entering the tube, a constant initial gas temperature, and a constant wall temperature along the tube length. These assumptions deviate considerably from reality in the igniter tests and his solution should not be expected to provide close agreement for locations near the maximum heat transfer point.

The Nusselt numbers for each axial head-end igniter test were plotted versus L/D to determine the approximate asymptotic Nusselt number (Nu_∞). The Nusselt numbers were then normalized by the derived values of Nu_∞ and were plotted versus x'/D as shown in figure 40 for nonaluminized igniter propellants, and in figure 41 for aluminized igniter propellants. For positive values of x'/D, the normalized Nusselt number can be approximated by an exponential function of the form

$$\phi_{x'} = \frac{Nu_x}{Nu_\infty} = 1 + k_1 e^{-k_2 \frac{x'}{D}} \qquad (32)$$

For negative values of x'/D, i.e., locations upstream of the point of maximum heat flux, normalized Nusselt numbers can be approximated by a straight line in the case of the nonaluminized propellant and a parabolic or exponential curve in the case of the aluminized propellant. In the latter case, the normalized Nusselt number can also be approximated by a straight line with little loss in accuracy.

Since the Nusselt number is dependent upon length for only the first 6 to 10 diameters downstream of the point of maximum heat flux, it is desirable to correlate the data in terms of the diameter-based Nusselt and Reynolds numbers. By noting that

$$Nu_x = \phi_{x'} \quad N_\infty = \phi_{x'} \left(\frac{hD}{k}\right) \qquad (33)$$

or

$$Nu_\infty = \frac{Nu_x}{\phi_{x'}} \qquad (34)$$

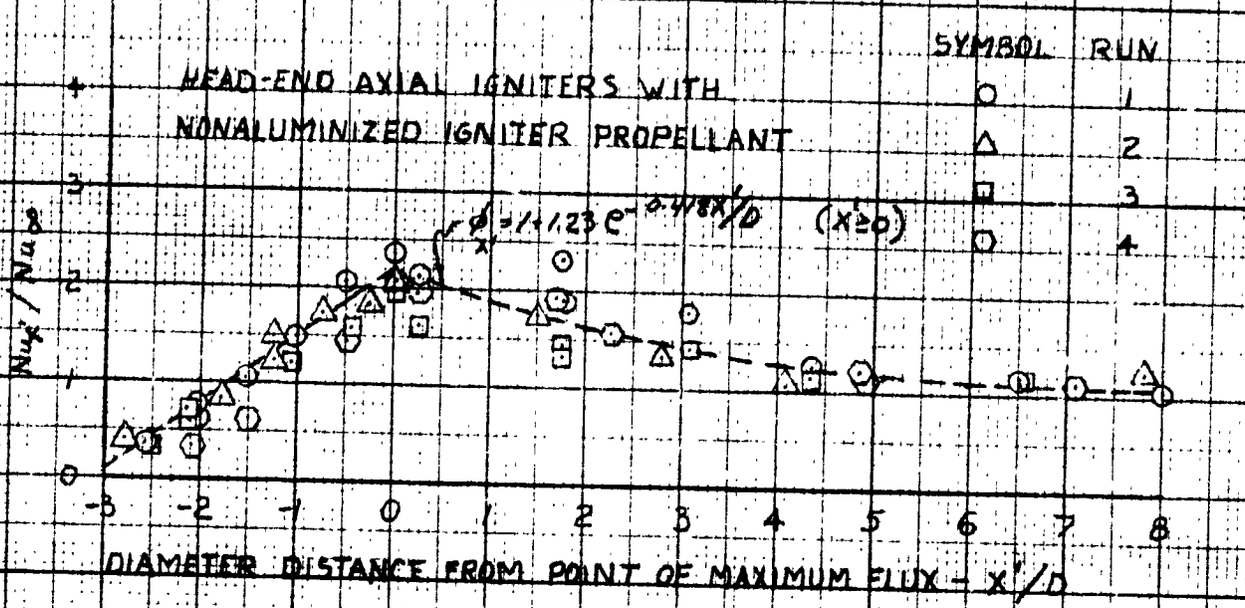

FIGURE -40

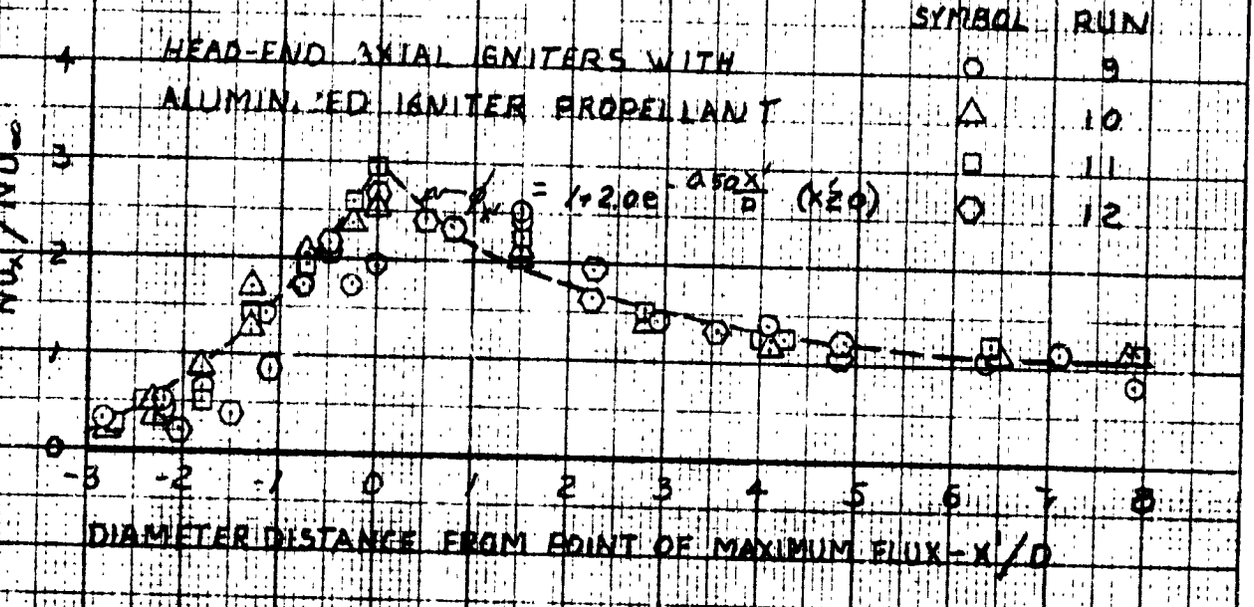

FIGURE -41

it is apparent that the function $\phi_{x'}$ converts the length-dependent Nusselt numbers characteristic of the entrance region to corresponding diameter-based Nusselt numbers for sufficiently large distances.

The data were then plotted as suggested by equation 34. The results for the nonaluminized propellant are presented in figure 42 and the aluminized propellant in figure 43. In both figures 42 and 43, a line with slope of 0.8 was drawn through the data points. Although separate lines of differing slopes for each figure could be used to represent each set, a composite of data points shows that an 0.8 slope gives an adequate representation of the data.

The equation of the line is

$$Nu_D = 0.033\ Re_D^{0.8} Pr^{0.3} \qquad (35)$$

It should be noted that the diameter-based Nusselt and the Reynolds numbers, as well as the Prandtl numbers used above, were corrected for physical property changes induced by the temperature variation along the duct length. This accounts for the variation in Reynolds number for each specific test and some of the variations in the product of $Nu_x Pr^{-0.3}/\phi_{x'}$. For the tests involved, these changes were on the order of 10%. In reconstructing the length-dependent heat flux for a given igniter design, in most cases, the length-dependency of thermal properties could be ignored since their influence is slight compared with the $\phi_{x'}$ function and is less than the experimental error, i.e., accuracy of determination of $\phi_{x'}$ for a given configuration.

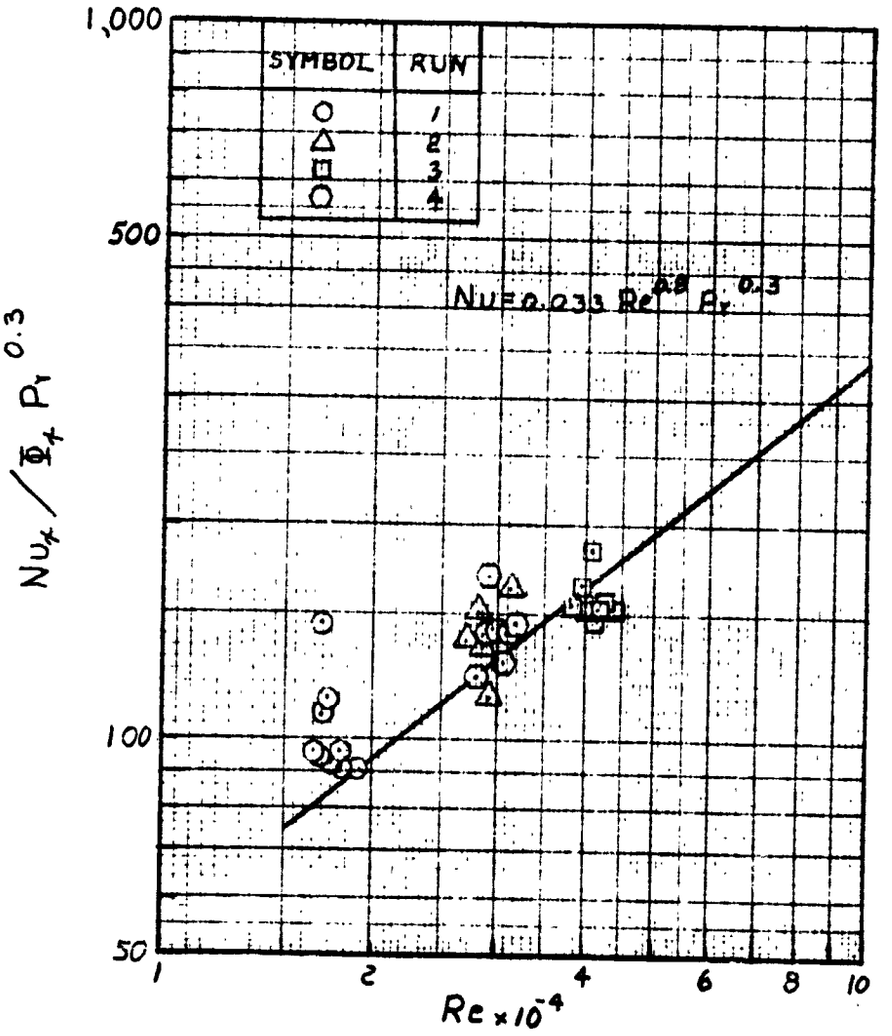

FIGURE-42. DATA CORRELATION FOR NONALUMINIZED PROPELLANT HEAD-END IGNITION

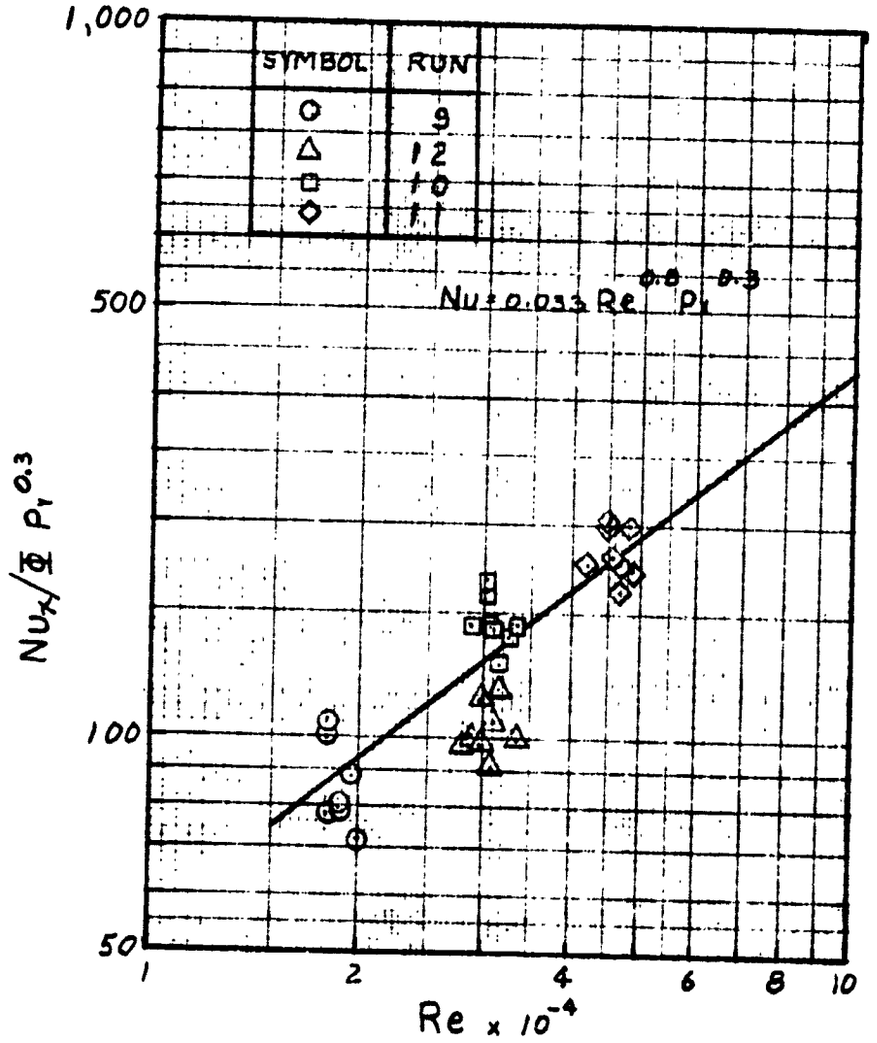

FIGURE - 43 DATA CORRELATION FOR ALUMINIZED PROPELLANT HEAD-END IGNITION

To determine the igniter heat flux distribution for a given design with known equivalent pipe flow conditions, it is necessary to define the corresponding $\phi_{x'}$ function for that design. Since the maximum point of heat flux must correspond to the value of $\phi_{x'}(0)$ and the value of $\phi_{x'}$ is seen to be approximately 1.1 at an x'/D of 6 (i.e., 110% of the pipe flow equivalent), the coefficients in the $\phi_{x'}$ function may be determined by the relationships

$$k_1 = \left(\frac{Nu_x}{Nu_\infty}\right)_{max} - 1 \qquad (36)$$

and

$$k_2 = -\frac{1}{6} \ln \left(\frac{0.1}{k_1}\right) \qquad (37)$$

A review of data by Carlson and Seader[17] and by Mullis[9] indicates that the decay of the Nusselt number with length is such that $Nu_x = 1.1\ Nu$ at x/D = 6 for all tests. It is apparent from equations 36 and 37 that when the magnitude of the maximum Nusselt number is established, the coefficients k_1 and k_2 can be established.

4.4.1.2 Correlation of Maximum Heat Flux

The maximum heat flux for both aluminized and nonaluminized igniter propellant was correlated by plotting the diameter-based Reynolds number against the product $Nu_x Pr^{-0.3}$ taken at the maximum value of the length-dependent Nusselt number for each test. The results are shown in figure 44. An approximate correlation of the data for the nonaluminized propellant can be represented by the equation

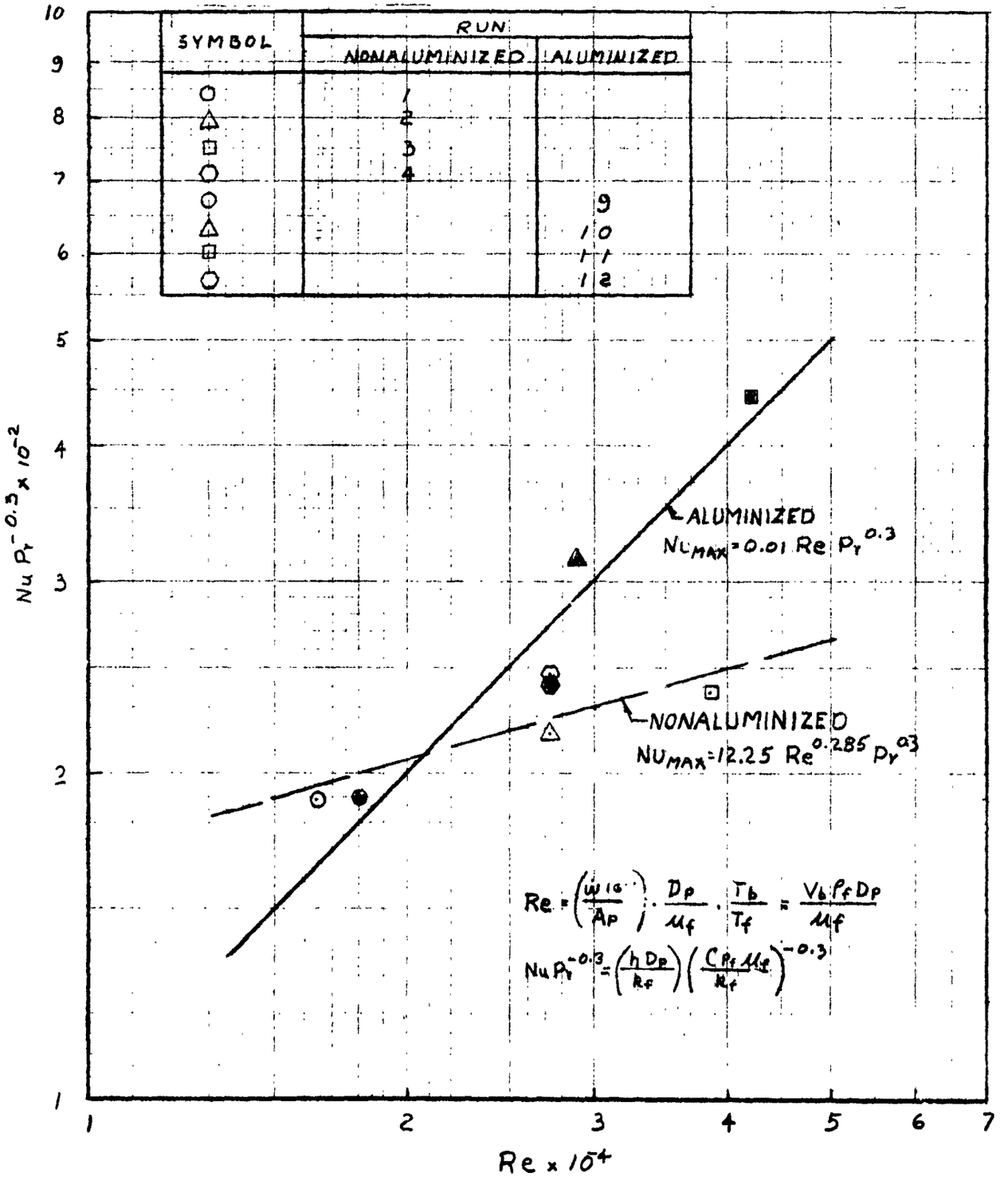

FIGURE-44. CORRELATION OF MAXIMUM HEAT FLUX LEVEL FOR HEAD END IGNITION (AXIAL)

$$Nu_{max} = 12.25\ Re^{0.285} Pr^{0.3} \qquad (38)$$

The data for the aluminized igniter propellant can be represented by

$$Nu_{max} = 0.01\ Re\ Pr^{0.3} \qquad (39)$$

While the basis for this correlation is empirical and the coefficients are not those which are normally observed, it indicates that the aluminized igniter propellant maxima show a greater dependency on mass flux as reflected in the Reynolds number power dependency. The reason for this trend is not clear; it may arise in part from the effects of two-phase flow upon the boundary layer development and heat transfer mechanisms associated with solid particle condensation upon the walls of the duct.

Comparing equations 38 and 39 with equation 30, it is seen that the value Nu_{max}/Nu_{∞} is dependent upon Reynolds number. By determination of Nu_{max}/Nu_{∞}, we may determine the ϕ_x, function by use of equations 36 and 37. Alternately, by referring to figures 40 and 41, it can be seen that the length-dependent Nusselt numbers for the aluminized and nonaluminized propellants may be approximated by the ϕ_x, curves whose maximum values are 2.23 and 3.0, respectively. A high percentage of the scattering of the data points at the maxima is accounted for by the fact that the data does not lie on a true exponential near the maximum point. This trend away from the exponential is accentuated as the igniter mass flow is decreased. However, for distances in the neighborhood of 2 diameters downstream, best agreement between the actual data and exponential approximations is obtained. This suggests that the exponential may be used to

determine the heat flux for distances greater than 2 diameters downstream and that a second order correction which is a function of the igniter mass flux and dimensional characteristics may be used to adjust the data upstream to the maximum.

Although the current data establish a few quantitative data points and indicate qualitative trends, insufficient information exists at points of constant hydrodynamic and thermal similarity to determine the quanitative behavior of the maximum heat for a wide range of interest.

4.4.1.3 Location of Maximum Heat Flux

The location of the region of maximum heat transfer in the duct headend is highly dependent upon igniter jet dynamics and interaction of the jet with the constraining duct walls. Stagnation zones, areas of recirculation and vortexing, and regions of jet impingement are all possible.

Love, et al.[23] conducted extensive experimental and theoretical studies into the flow field characteristics of axisymmetric free jets. The effects of jet Mach number, the rates of specific heat, nozzle divergence angle and jet static-pressure ratio upon jet structure, jet wave length, and the shape and curvature of the jet boundary were investigated. For constant specific heat, exit Mach number, and nozzle divergence angle, the jet boundary was found to be dependent only upon the ratio of jet exit static pressure to free stream or back pressure (P_j/P_b).

An increase in jet pressure ratio (P_j/P_b) was found to increase the

maximum jet diameter and shift its location downstream. The effect of an increase in the ratio of specific heats, considering the other variables constant, was to likewise increase the maximum jet diameter and displace the axial location of the maximum downstream. Two analytical methods for predicting the jet boundary, the method of characteristics, and the circular arc method were presented. Figure 45 presents a typical sonic jet expansion envelope for various jet total to back pressure ratios (P_o/P_b) as constructed by Carlson and Seader[17] from the data of Love, et al.[23]

For cases where the igniter jet impinges upon the wall, the point of impingement can be used as the maximum point of heat transfer. This point may be found by determining the point of intersection of the free jet boundary with cylindrical boundary radius by application of methods presented by Love. Although the referenced methods apply to the shape of free axisymmetric jets, Zumwalt[24] reports that Love's methods adequately represent the case of jets discharging into a duct provided the jet base pressure is used to determine the jet boundary.

For cases where the jet does not intersect the walls, the problem is more complex and depends to a large extent upon the relative igniter and motor configurations. Using figure 45 with a correction for specific heats, the location of the maximum jet expansion for each of the axial head-end igniter tests was approximated. The region of the jet expansion and its position relative to the igniter and points of maximum heat flux are depicted in figure 46. The pertinent data for each of these tests are presented in table IV. Although there is data scatter in the thermocouple readings at the locations recording the maximum heat flux, it is apparent

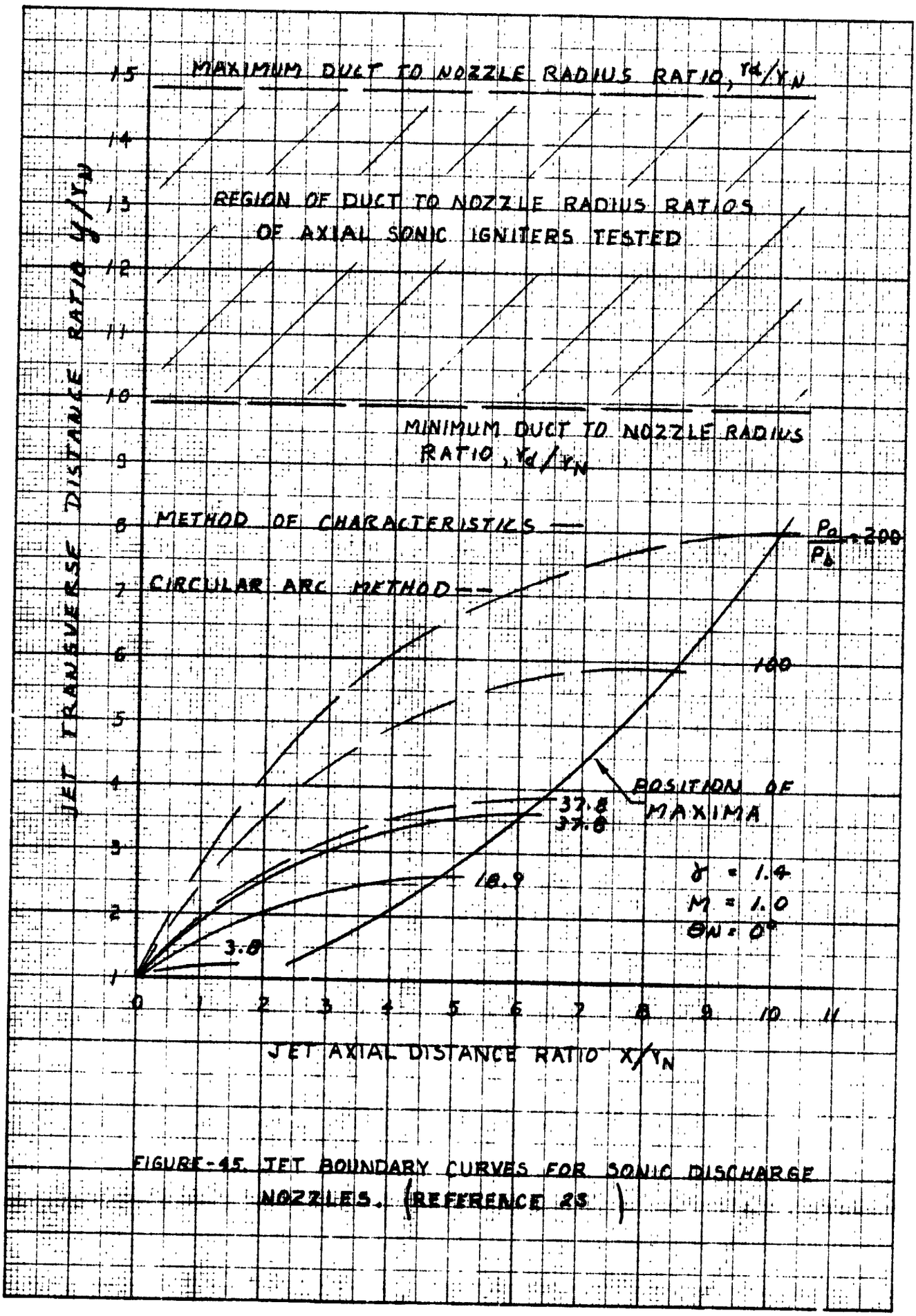

FIGURE-45. JET BOUNDARY CURVES FOR SONIC DISCHARGE NOZZLES. (REFERENCE 25)

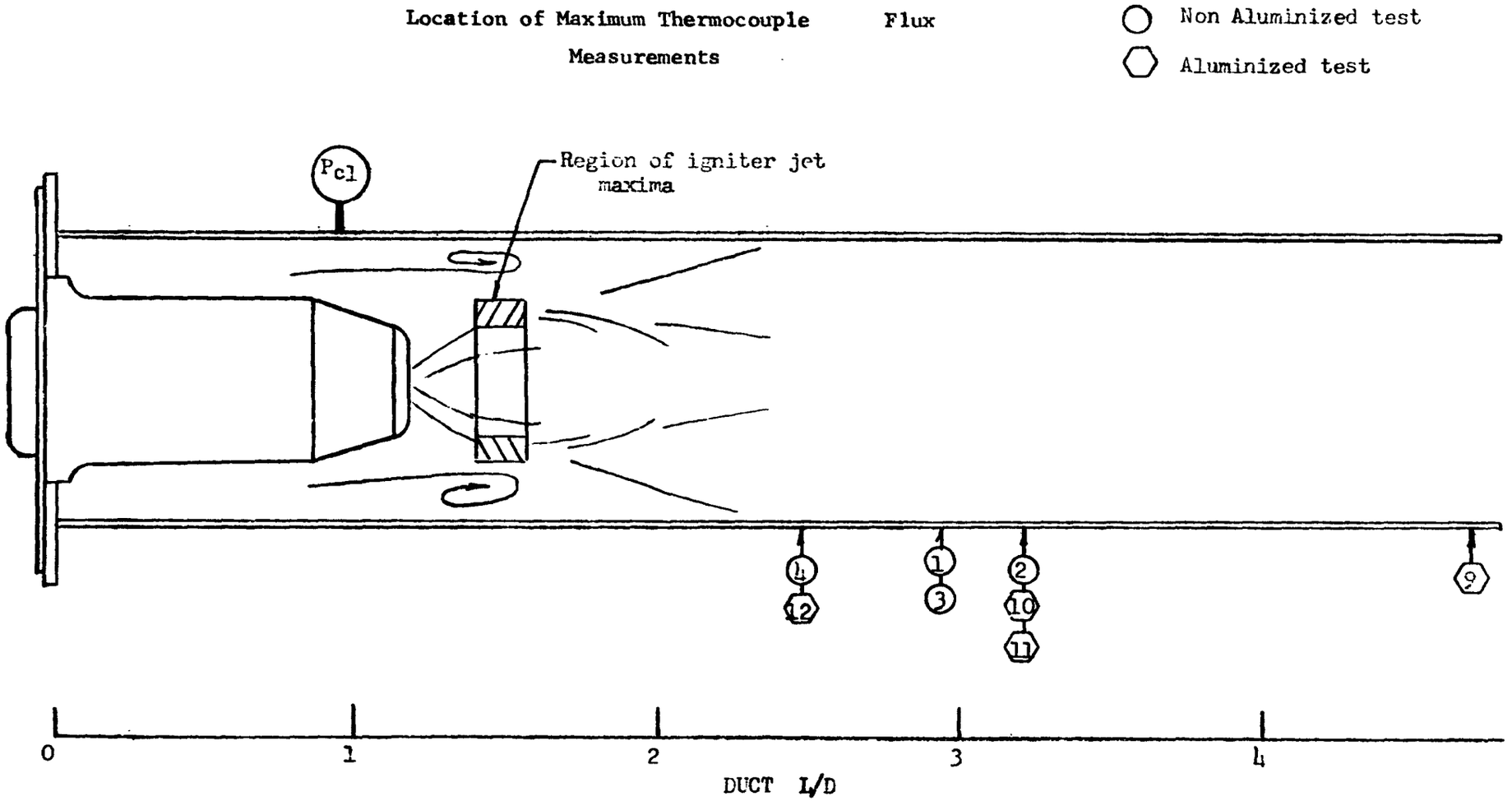
Location of Maximum Thermocouple Flux Measurements
Non Aluminized test
Aluminized test
Pcl
Region of igniter jet maxima
4
12
1
3
2
10
11
9
0
1
2
3
4
DUCT L/D

FIGURE - 46

TABLE IV

AXIAL IGNITER MAXIMA

Run	$\dot{w}_{ign}$	P_{ign}/Pc_1	Nu_{max}/Nu	$(x/D)_{max}$	Propellant	D_d/D_i	d_j	Y_m/r_j	x_m/r_j
1	1.20	60.5	2.39	2.97	Nonaluminum	14.85	0.522	5.75	8.7
2	2.01	47.6	2.04	3.22	Nonaluminum	11.85	0.658	5.3	8.05
3	2.96	34.0	1.98	2.97	Nonaluminum	9.85	0.786	4.2	6.95
4	2.1	74.5	2.04	2.45	Nonaluminum	11.80	0.657	6.25	9.1
9	1.36	63.5	2.53	4.70	Aluminum	14.80	0.523	5.98	8.88
10	2.29	50.5	2.52	3.22	Aluminum	11.90	0.659	5.4	8.27
11	3.35	36.8	2.97	3.22	Aluminum	9.95	0.779	4.32	7.07
12	2.27	76.0	2.34	2.45	Aluminum	11.80	0.68	6.30	9.20

that the maxima for tests 4 and 12 definitely are upstream of the maxima of the other tests. In tests 4 and 12, a large duct orifice was used to produce low duct chamber pressures, while maintaining comparable mass fluxes to tests 2 and 10.

In referring to table IV, it is seen that the locations of the maximum jet diameter for tests 4 and 12 are downstream of the maximum for tests 2 and 10. However, this is in the reverse order of the maxima obtained for the heat transfer data. On review of the test data, it was found that the jet pressure ratios for tests 4 and 12 were higher than those for the other tests and, based on jet expansion data from Love, et al.,[23] which indicates that the initial jet turning angles are greater. Data from Carlson and Seader[17] indicate the same effect. Therefore, it is concluded that this back pressure has a significant effect upon the location of maximum heat transfer through its effect on the jet plume initial turning angle.

Mullis[9] has shown that the location of the maximum jet diameter does not correspond to the heat flux maximum in those tests where intersection between the jet and the wall does not occur. Instead, the duct back pressure and the turbulent mixing behind the normal shock play more important (but at the present, quantitatively indeterminate) roles in locating the maximum. Fortunately, the variation in maxima location appears to be less than 1 diameter for typical igniter designs under consideration. From review of the data of Mullis[9] and Carlson and Seader,[17] use can be made of the approximation that the point of maximum heat flux will occur from about 1.5 to 3.0 port diameters downstream of the igniter

exit plane. This is valid for igniter throat-to-port diameter ratios from 5 to 15 and jet-to-back pressure ratios of approximately 20 to 50.

4.4.2 Canted Head-End Igniters

Head-end canted igniter data were correlated in the same manner as the head-end axial igniter data. The stagnation temperature drop along the duct was determined and convective heat transfer and flow data for each thermocouple location were converted to their corresponding dimensionless parameters. The length-dependent normalized Nusselt number for each test indicated significant difference in the heat transfer rates between points along the centerline of jet impingement and points 60° from the centerline (midway between the impinging igniter streams). The difference is more significant for the aluminized propellant than for the nonaluminized propellant. This is in contradiction to Carlson and Seader's[17] results which indicated little circumferential difference in the heat transfer rate for canted nozzle igniters. This difference is probably affected by the lower gas temperatures of the igniters used by Carlson and Seader.[17]

On comparison of axial and canted igniter test data, it is apparent that an exponential function similar to equation 32 may be used to approximate the length variation of Nusselt number. Consequently, the data for each test for locations downstream of the maximum were reduced to the equivalent diameter Nusselt number by the application of the ϕ_x, function with constants determined by equations 36 and 37. The results are plotted in figure 47. The reduced flow relationship can be approximated by equation

$$Nu_D = 0.0278\ Re^{0.8}\ Pr^{0.3} \qquad (40)$$

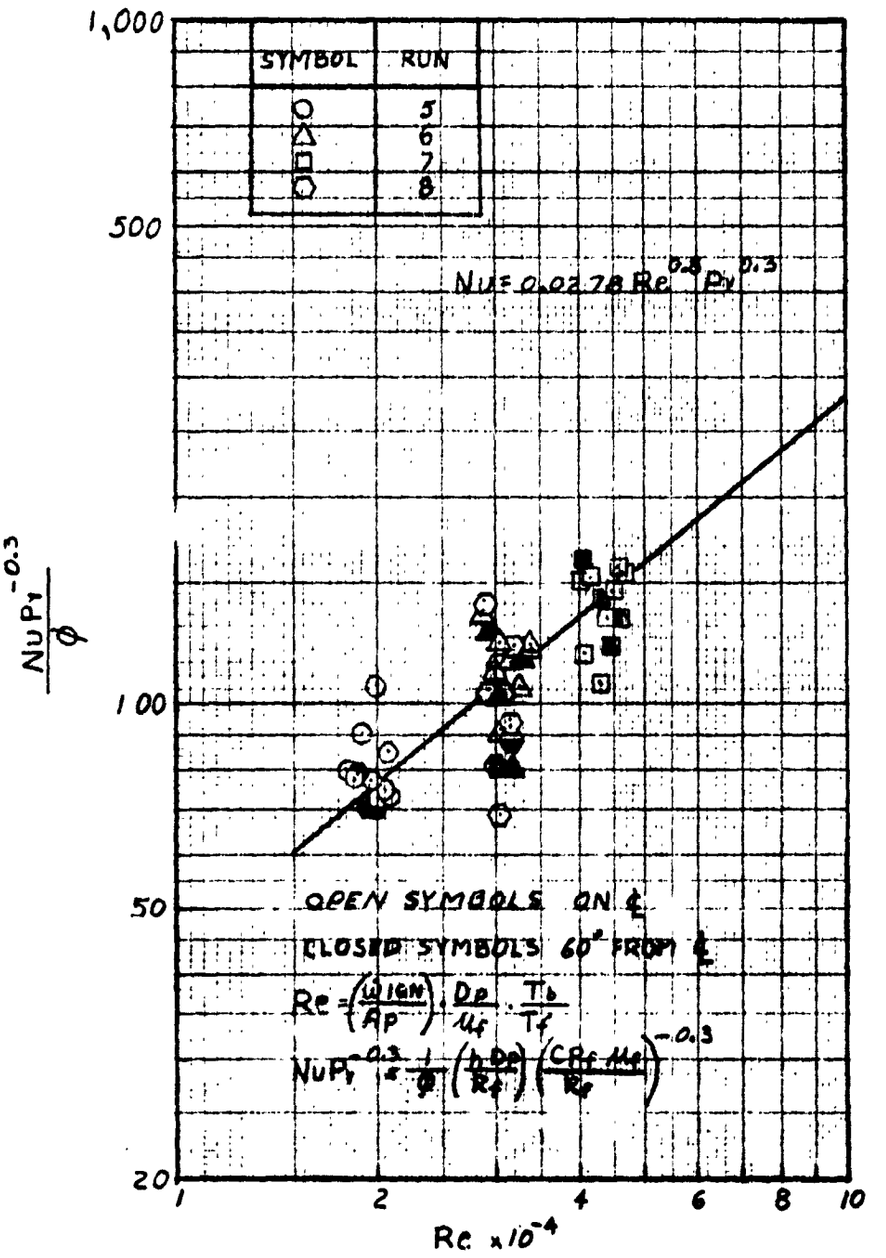

FIGURE -47 HEAD-END IGNITION - CANTED IGNITER NOZZLE

The coefficient in equation 40 is approximately 12% lower than the corresponding coefficient determined for axial head-end ignition. This implies that the fully developed pipe flow heat transfer for the canted igniter is approximately 12% lower than similar fully developed axial igniter conditions. This approximate 12% variation is well within the accuracy of the experimental data and assumptions on variation of physical properties used in the data correlation. Theoretically, there should be no difference between the fully developed flow heat transfer for the axial and canted igniters.

The location of maximum heat transfer for all tests was the same and corresponded to the area of direct jet impingement. In each case, the maximum along the jet centerline occurred at an approximate duct L/D of 1.4. The maximum heat transfer based on the thermocouples located midway between jet centerlines was at an approximate L/D station of 1.9. The difference in heat flux at the common circumferential stations in general persisted until about 6 to 7 diameters downstream of the impingement point beyond which a circumferentially constant heat flux was noted.

By application of heat flux at the circumferential and axial locations and assuming symmetry, lines of constant heat flux may be constructed and the surface temperature variation of the duct or propellant surface determined.

Significant data relating to the magnitude of maximum heat flux both on and off the jet centerline are presented in figure 48. The locations of the maximum Nusselt number ratios (Nu_{max}/Nu_{∞}) for the nonaluminized igniter propellants varied from 3.5 to 7.0 along the jet centerline and appear to

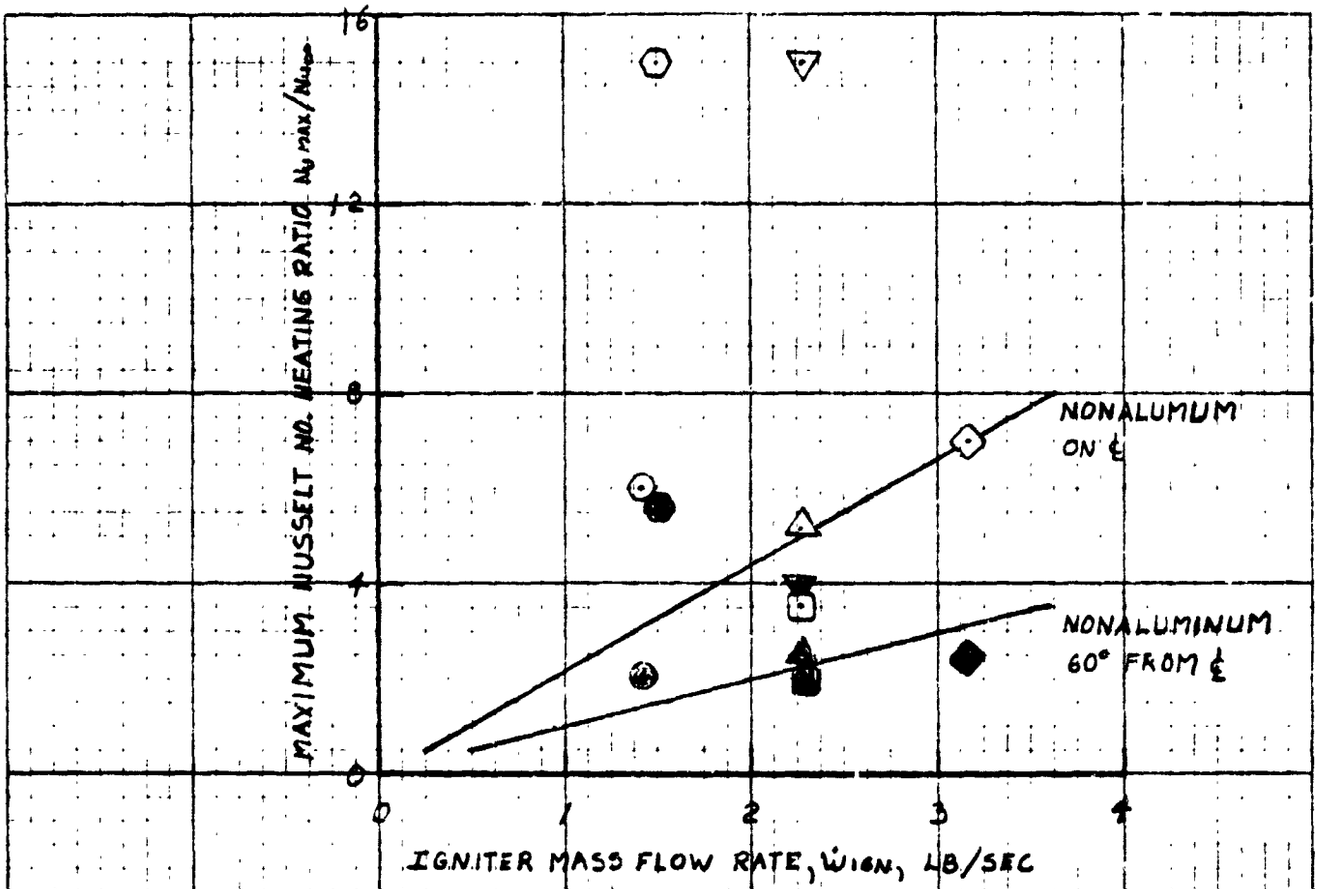

MAXIMUM HEATING RATIO RELATIONSHIP FOR CANTED IGNITER TESTS

RUN	SYMBOL ON-℄	SYMBOL OFF-℄	$\dot{W}_{IGN}$ LB/SEC	$N_{u,max}/N_{u_\infty}$ (ON JET ℄)	$N_{u,max}/N_{u_\infty}$ (60° FROM ℄)	MAX HEATING RATIO ⑤/④	IGNITER PROPELLANT
5	○	○	1.40	6.0	3.0	2.0	NONALUMINUM
6	△	△	2.26	5.0	2.5	2.0	NONALUMINUM
7	◇	◇	3.16	7.0	2.5	2.8	NONALUMINUM
8	□	□	2.25	3.5	2.0	1.75	NONALUMINUM
13	○	○	1.49	15.0	5.5	2.73	ALUMINUM
14	▽	▽	2.27	15.0	4.0	3.75	ALUMINUM

FIGURE-48

be an increasing function of igniter jet mass flow, as does the maximum heat flux off the jet centerline. A significant difference is noted in run 8. The ratio (Nu_{max}/Nu_{∞}) on the jet centerline is lower than that for run 6 which has a comparable igniter mass flow rate. This is also the case for the ratio of the jet centerline to the point of 60° from the centerline. Although test 8 was conducted with the same igniter mass flux, a larger duct orifice was used to reduce the average duct chamber pressure by a factor of approximately two. This decrease in duct pressure ratio would result in an increased jet pressure ratio (P_j/P_b) from approximately 26 to 40 and thereby an increase in the effective jet cross section and drop in igniter mass flux of the impingement point. This in effect would spread the jet over a larger area, reducing the peak flux, and indicates a considerable dependency of maximum heat flux upon igniter jet dynamics as influenced by igniter design and duct or motor configuration.

The maximum heating rates for aluminized propellant are seen to be about twice as high as for the nonaluminized propellant. This is attributed to impingement and condensation of alumina particles in the region of jet impingement. Insufficient test data are available to determine the effects of the igniter design variables on the maximum flux level, but qualitatively it is observed that for the observed flux levels the propellant ignition delay at the point of maximum heat would be of the order of msec for typical solid propellants. For these cases, the initial igniter heat flux would be relatively unimportant in determination of the total ignition transient. Interaction of the igniter with motor combustion products would be controlling in defining flame propagation.

4.4.3 Aft-End Igniters

There are significant differences between the phenomena of head-end and aft-end ignition by pyrogen igniters. These differences result from variations in igniter gas flow patterns and their effect upon heat transfer to the propellant grain. Head-end igniters provide gas flows which may be characterized at distances sufficiently downstream of the igniter exit plane with classical pipe flow correlations. Aft-end igniters yield more complex flow fields because of igniter gas flow reversal and mixing within the main motor cavity. These phenomena are highly dependent upon both igniter and motor design parameters. Although a complete quantitative description of the dynamics of aft-end ignition has not been found, a theoretical model has been derived which qualitatively agrees with observed experimental data.

Early work on the theoretical and experimental aspects of aft-end ignition system was conducted at UTC by Fullman and Nielsen.[12] Experimental work included aft-end ignition of multiple TM-3A test motors of three, six, and 12 segments. Two large-volume simulation tests and two clustered motor tests were also conducted. The igniter employed was an aft-mounted pyrogen (rocket) with a nominal 1,000 psi chamber pressure and a convergent-divergent nozzle designed for optimum expansion.

An aft-end ignition model based on theoretical considerations and the results of UTC's tests and later work by Neilsen and Bretting[25] and by Plumley, et al.,[26] has subsequently been developed. The sequence of events as described by the ignition model is as follows:

A. The pyrogen is ignited and discharges a jet through the nozzle of the motor being ignited.

B. As the igniter jet penetrates into the motor port cavity it begins to break down by the mechanisms of Riemann shocks and viscous turbulent mixing. In this process the jet expands and becomes attached to the port walls. Finally, the expanded jet completely blocks the port and acts as a piston to compress the cold gas in the head end of the motor as shown schematically in figure 49.

C. Equilibrium is established when flow out of the main motor balances the igniter jet mass flow rate. At this time, a stable stagnation plane or region which separates the hot igniter gas from the cold motor port gas is formed within the motor port. The position of this plane is stable as long as the igniter mass flow rate remains constant and no propellant ignition occurs.

D. Aft of the stagnation zone, the igniter gases flow in a core toward the stagnation region are reversed, and flow along the port walls and out the motor nozzle in an annular area around the incoming jet. In the area aft of the stagnation zone the ignition process is similar to that of a head-end igniter.

Flow Patterns in Motor for Aft-End Igniter

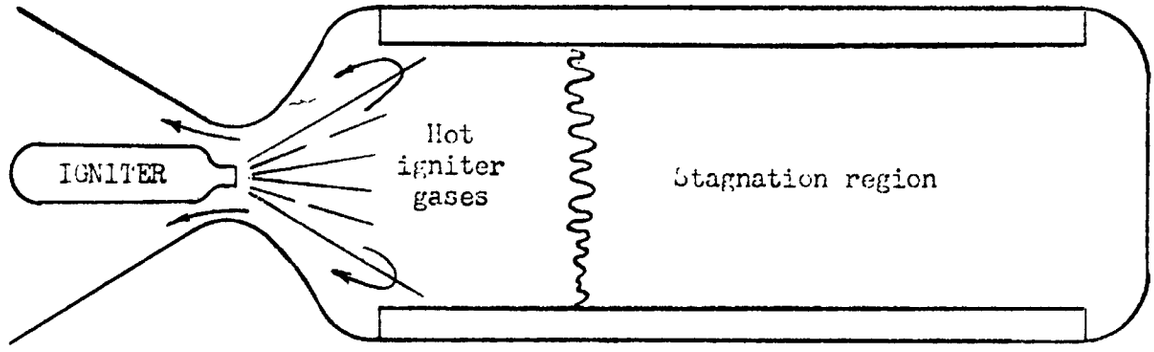

SONIC NOZZLE WITH LOW PENETRATION

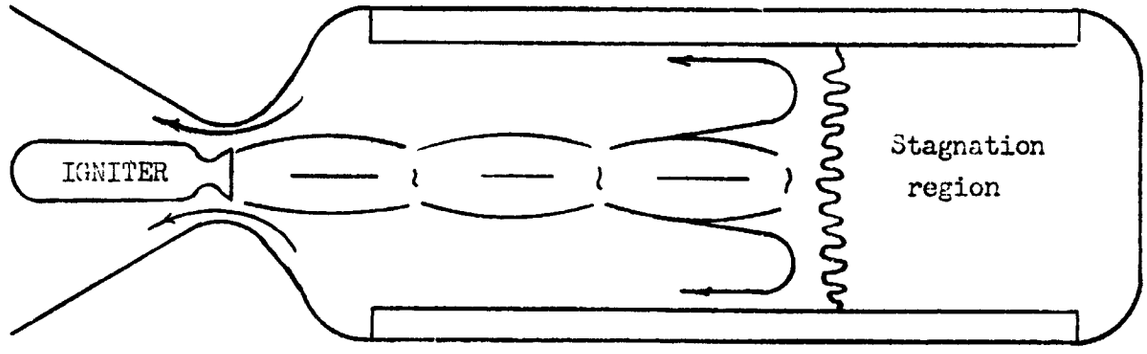

SUPERSONIC NOZZLE WITH HIGH PENETRATION

FIGURE - 49

E. The first ignition occurs within the aft region and progresses until the grain surface aft of the stagnation plane has ignited. As time progresses the ignition boundary defined by the stagnation plane propagates towards the head end of the motor under the influence of radiative heat flux from the body of hot gases in the aft-end of the motor and from the conductive and convective heat fluxes on newly exposed surface areas resulting from movement of the stagnation plane forward during buildup in motor chamber pressure.

F. Total ignition is achieved when the entire grain surface area has been ignited.

This ignition model reveals the importance of a stagnation zone in determining the character of aft-end ignition. Since the stagnation zone limits the fraction of propellant surface exposed to igniter thermal flux, the existence and position of a stagnation plane must necessarily have a profound effect on characteristic ignition times. High penetrations (70% to 80%), would give characteristic motor ignition transient times comparable to head-end ignition. Low penetration would yield longer ignition transients with slow pressure rise rates since the ignition front propagation rate into the stagnant head-end region is slow compared with propagation rates for propellants directly exposed to igniter exhaust gases.

Plumley[26] and Jensen and Cose[27] have shown experimentally that the primary factor influencing the distribution of aft-end ignition is the igniter nozzle configuration. Supersonic nozzles provide higher penetration and shorter ignition delays for comparable igniter mass flow rates.

To investigate the variations in aft-end ignition, heat flux tests were conducted using various igniter mass flows with both sonic and supersonic igniters. The effects of aluminized and nonaluminized igniter propellants were also investigated. The following paragraphs present an analysis of these data.

Analysis of the data revealed no generalized method which would adequately correlate aft-end ignition results. This difficulty arises from the complicated gas dynamic effects and the limited test data collected. To obtain a valid generalized correlation, the test data must be expressed in terms of the appropriate dimensionless similarity parameters which in general are the Reynolds, Nusselt and Prandtl numbers and dimensional similarity parameters pertaining to igniter and motor configuration. Because of unknowns in the flow and temperature fields within the duct, sufficiently accurate length determinations of the Reynolds and Nusselt numbers cannot be made to provide meaningful quantitative correlations.

As previously discussed, determination of the localized Reynolds and Prandtl numbers is highly dependent upon the local mass flux and temperature. In the case of aft-end ignition the igniter jet penetrates into the motor and is dissipated in a turbulent mixing region of undetermined length aft

of the stagnation zone. Within the turbulent mixing region the higher gas potential in the core forces the less energetic gas to the duct wall setting up a counter flowing wall jet. This produces a developing wall boundary layer which flows along the annular area between the wall and the incoming jet. The mass flux (and, hence, Reynolds number) which would be needed to correlate heat transfer from the wall jet, is indeterminate because of a variable fluid boundary and an unknown amount of stripping of gases from the igniter jet and mixing with the countercurrent wall stream. A similar problem arises in determining the localized value of the Nusselt number. Uncertainties in the length variation of wall and jet temperatures induce considerable error in this determination.

Carlson and Seader[17] used a length-dependent correlation of the form

$$Nu/Re^{0.5}\ Pr^{0.4} \tag{41}$$

Although it is not precisely clear from their report how the Nusselt and Reynolds numbers were evaluated, it is believed that the igniter mass flow, the port area, and a viscosity for some mean temperature were used such that

$$Re = \left(\frac{\dot{w}_{ign}}{A_P}\right) \frac{D}{\mu} \tag{42}$$

and

$$Nu = \frac{h\,D}{k} = \frac{q}{(T_\infty - T_w)} \cdot \frac{D}{k} \tag{43}$$

where the value of wall stream temperature (T_∞) is evaluated at some mean value. In the current studies on head-end ignition, errors in

determination of the Nusselt number resulting from assuming a constant wall temperature are in the order of 75% if the combustion temperature of the igniter is used, and 38% if a mean duct temperature is used. Similar errors may occur for the aft-end ignition case. Hence, these temperature and flow parameter uncertainties must be considered carefully in the reduction of the data.

Although a generalized correlation of length dependency is not appropriate with the present limited data, correlations to determine the location and magnitude of the maximum heat flux are desirable. The magnitude of the maximum heat flux was investigated by use of modified Reynolds and Nusselt numbers. For each test, the Reynolds number at the maximum heat flux point was determined by the equation

$$Re_{max} = \frac{(\rho_f \cdot V_{an})D}{\mu_f} \cong \left(\frac{w_{ign}}{A_{AN}}\right) \frac{D}{\mu_f} \cdot \frac{T_b}{T_f} = \left(\frac{\dot{w}_{ign}}{A_{AN}}\right) \frac{D}{\mu_f} \cdot \frac{T_b}{T_f} \qquad (44)$$

Here $\dot{w}_{ign}/A_{AN}$ is the mass flux of the annular wall jet. Assumptions are that the greater percentage of the igniter jet penetrates past the point of maximum heat flux before reversal. The annular wall stream area was approximated by reducing the duct port area by average maxima igniter jet areas as determined by the methods of Love and Grigsby.[23] These duct area reductions were approximately 20% for the sonic igniter nozzle and 10% for the supersonic igniter nozzles. The Nusselt numbers were determined by the equation

$$Nu_{max} = \frac{h\,D}{k_f} = \frac{q}{(T - T_w)} \cdot \frac{D}{k_f} \qquad (45)$$

The thermal conductivity, viscosity, and Prandtl numbers were evaluated at mean film temperatures of 2,860° and 3,220°R, respectively, for the non-aluminized and aluminized igniter propellants.

The wall temperatures were determined from heat flux versus temperature curves constructed from the computer analysis of the transient heat flux data. The wall stream temperature was assumed to be at the combustion temperature of the igniter propellants. While this is obviously not the case, the actual temperature of the wall stream being less, it is believed that because of the similarity of heat flux distance profiles that the corresponding Nusselt numbers will all be biased by approximately the same percentages.

The dimensionless data for the maximum heat flux points determined by the previously discussed method are presented in figure 50. These data appear to be adequately represented by the equations

$$Nu_{max} = 0.0745\ Re^{0.8}\ Pr^{0.3} \quad \text{(Nonaluminized)} \quad (46)$$

$$Nu_{max} = 0.0914\ Re^{0.8}\ Re^{0.3} \quad \text{(Aluminized)} \quad (47)$$

As indicated by these correlations the maximum heat transfer for the aluminized propellant is approximately 23% higher than the nonaluminized propellant which agrees well with data for axial head-end ignition (20%).

An important point noted from this data indicates that for the same Reynolds number there is no appreciable difference in Nusselt numbers for sonic and supersonic igniters. This apparently results from the fact that the annular area effect on the Reynolds number, adjusted for the mass flux in each case, was approximately correct.

No general correlation was found for the location of the maximum heat flux but, for the configurations investigated, the maxima were found to be approximately 1.5 diameters from the igniter exit plane for the sonic nozzles and 3.0 diameters for the supersonic.

4.4.4 Radiation Data

A theoretical correlation of radiation data is employed which incorporates the use of charts of previously calculated emissivities for a homogeneous cloud in a cylindrical container radiating to any point on the container's inner surface (see reference 8). These emissivities are given in terms of a dimensionless radiation parameter and the dimensionless cylindrical location. The time-varying radiation parameter is determined for each calculation interval as a function of the measured bore gas pressure assuming constant gas temperature. The corresponding emissivity is determined from the charts and the radiant heat flux is calculated by application of this value to the Stephan-Boltzman blackbody radiation law.

Comparative heat fluxes determined by test data and the theoretical correlation show fair agreement. Mullis[9] reported that the experimental data was from 50% to 80% of the theoretically calculated data. He concluded

that this discrepancy resulted from clouding of the radiometer test windows during the test; however, an investigation of the calculation methods used indicated that the effect of the igniter gas temperature loss along the duct length was not estimated correctly. This loss resulted in a significant drop in gas temperature along the duct which, when incorporated into the theoretical calculations, produces results which agree within ±30% of the experimental results.

Since the theoretical correlations agree with the experimental data within the accuracy of the test data, it is concluded that the theoretical correlation given in reference 9 adequately approximates the radiant flux level.

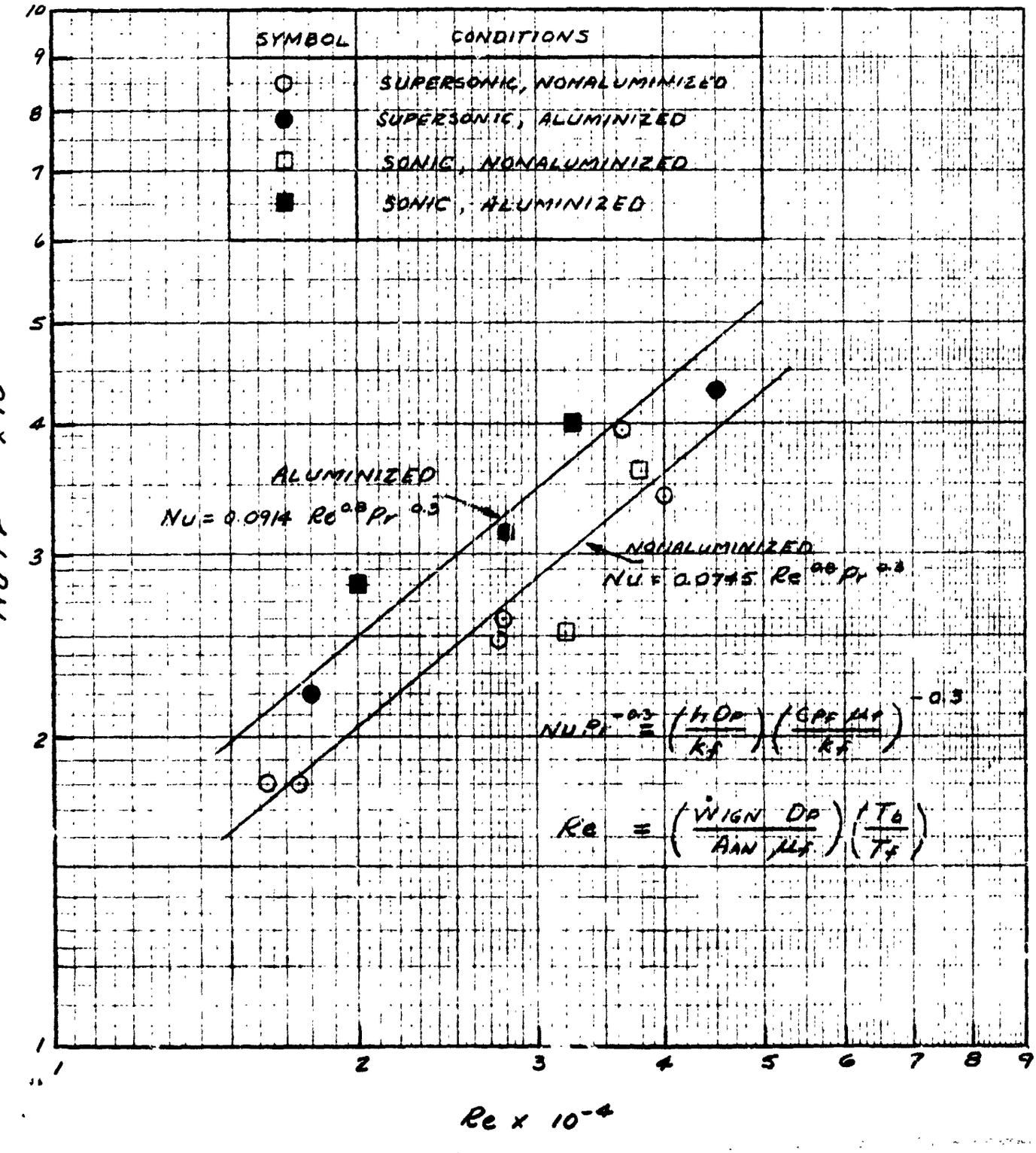

FIGURE 50. POINT OF MAXIMUM HEAT TRANSFER FOR AFT END IGNITION

5.0 CONCLUSIONS AND RECOMMENDATIONS

The present analytical studies on the heat transfer behavior of solid propellant pyrogen igniters have provided some degree of correlation between the thermal and hydrodynamic properties of the igniter exhaust, the igniter configuration, the position in the duct, and the resulting heat transfer rate to the propellant surface. Basically, the following general conclusions are defined from this study:

A. Correlations were developed for axial head-end convective heat transfer which are of use to the igniter designer. These correlations are based upon geometrically similar parameters which govern the velocity and temperature profiles in the region of developing hydrodynamic and thermal boundary layers. The location and amplitude of the heat flux maxima can be approximated by use of empirical correlations since theoretical methods for their prediction are currently inadequate. Additional empirical correlations are available for predicting the distribution of heat flux as a function of distance from the maximum. These correlations show that at distances greater than 6 diameters downstream of the region of maximum heat flux, the correlations approach values predicted by classical pipe flow correlations for fully developed turbulent flow.

Further experimental studies are required to properly develop a model to characterize head-end gas dynamics in order to theoretically define head-end heat transfer in the region from the head-end to the area of maximum heat flux.

B. Correlations similar to those for axial head-end igniters exist for canted head-end igniters. However, because of the axial asymmetry, at least two correlations are needed to map the axial heat flux distribution. Location of the maximum heat-flux region is determined by igniter jet impingement. The magnitude of the maxima is highly dependent upon jet dynamics and further studies are needed to establish accurate heat-transfer correlations for this region as well as areas upstream of the maximum heat-transfer point.

C. Further characterization of the fluid dynamics of aft-end ignition is necessary before accurate length dependent correlations can be obtained. Current data are sufficient to provide only approximate quantitative information on steady-state flux levels. Limited test data indicate that the transient phenomena during aft-end ignition varies more widely over the ignition interval than head-end igniter dynamics. To adequately analyze and correlate aft-end ignition tests, studies should be undertaken to determine igniter fluid dynamics in conjunction with heat transfer tests with a high speed surface heat flux measurement capability.

D. Application of the experimental correlations to igniter design and calculation of ignition transient depend upon the rationale that steady-state heat transfer correlations can be applied to a transient phenomena. This is believed to be the case, but high response heat flux measurements should be conducted in test apparatus with wall thermal properties similar to propellant thermal properties so that the correspondence of driving thermal potential and consequential heat transfer distribution can be determined.

E. The effects of aluminum content in the igniter propellant on heat transfer were found to correlate in part with the thermal properties of the propellants. However, additional studies are necessary to arrive at theoretical and analytical descriptions of the effects of particle impingement and condensation as well as two phase flow effects on heat transfer characteristics, particularly in the case of canted head-end igniter exhausts.

F. No usable radiation correlation could be obtained from available igniter test data. To achieve a proper correlation, a more comprehensive investigation is needed and measurement techniques should be improved to provide data to derive a more complete radiation model.

6.0 REFERENCES

1. Baer, A. D., and N. W. Ryan, "Ignition of Composite Propellant by Low Radiant Fluxes," presented at the American Institute of Aeronautics and Astronautics Solid Propellant Rocket Conference, Palo Alto, California, January 1964.

2. Anderson, R., R. S. Brown, G. T. Thompson, and R. W. Ebeling, "Theory of Hypergolic Ignition of Solid Propellants," presented at the American Institute of Aeronautics and Astronautics Heterogeneous Combustion Conference, Palm Beach, Florida, December 1963.

3. Anderson, R., R. S. Brown, and L. J. Shannon, "Ignition Theory of Solid Propellants," presented at the American Institute of Aeronautics and Astronautics Solid Rocket Conference, Palo Alto, California, January 1964.

4. Price, E. W., H. H. Bradley, Jr., J. D. Hightower, and R. O. Fleming, Jr., "Ignition of Solid Propellants," presented at the American Institute of Aeronautics and Astronautics Solid Propellant Rocket Conference, Palo Alto, California, January 1964.

5. Beyer, R. B., "Ignition of Solid Propellant Motors Under Vacuum (U)," Final Report, Contract No. AF 04(611)-9701. United Technology Center, April 1965. (CONFIDENTIAL)

6. Lewis, C. H., Jr., and D. J. Carlson, "Normal Shock Location in Underexpanded Gas and Gas Particle Jets," AIAA Journal, 2, 776-777, 1964.

7. Love, E. S. and C. E. Grigsby, "Some Studies of Axisymmetric Free Jets Exhausting from Sonic and Supersonic Nozzles into Still Air and into Supersonic Streams." NACA RML54L31, 10 May 1955.

8. Henderson, H. P., "One-Dimensional Axisymmetric Heat Conduction Program, Revision 1," UTC Aerothermal Report, dated 6 June 1966.

9. Mullis, B. G., "Heat Transfer Studies of Solid Rocket Igniter," Final Technical Report, Contract No. NAS7-302. United Technology Center, September 1965.

10. Mullis, B. G. and D. Cose, "Heat Transfer Studies of Solid Rocket Igniters," Second Quarterly Technical Report, Contract No. NAS7-302. United Technology Center, 15 January 1965.

11. Bastress, E. K., D. S. Allan, and D. L. Richardson, "Solid Propellant Ignition Studies," Technical Documentary Report No. RP:-TDR-64-65, 30 October 1964.

12. Fullman, C. H. et al., "Theoretical and Experimental Investigations of Ignition Systems for Very Large Solid-Propellant Motors (U)," Final Report, UTC 2012-FR, Contract No. AF 04(611)-7559. United Technology Center, May 1963. (CONFIDENTIAL)

13. Reid, R. C., and T. K. Sherwood, "The Properties of Gases and Liquids."

14. Still, D. R., et al., "JANAF Thermochemical Tables," Dow Chemical Company Research Laboratory, Air Force Contract No. AF 04(611)-755, July 1964.

15. Humble, L. V., W. H. Lowdermilk and L. G. Desmon, "Measurements of Average Heat-Transfer and Friction Coefficients for Subsonic Flow of Air in Smooth Tubes at High Surface and Fluid Temperatures, NACA Report 1020, 1951.

16. Wrubel, J. A., "Studies of Heat Transfer Characteristics of Hot Gas Igniters," Second Quarterly Progress Report, AFRPL-TR-66-358, Rocketdyne, December 1966.

17. Carlson, L. W. and J. D. Seader, "A Study of Heat Transfer Characteristics of Hot-Gas Ignition," proceeding of the Interagency Chemical Rocket Propulsion Group Second Combustion Conference, Vol. I, (CPIA Publication No. 105, 580, May 1966.

18. Brown, R. S. and G. E. Jensen, "Investigation of Fundamental Hypergolic Ignition Phenomena Under Dynamic Flow Environments," Final Report, Contract No. NAS 7-156, United Technology Center, February 1965.

19. Jensen, G. E. and D. A. Cose, "Studies in Ignition and Flame Propagation of Solid Propellants," Final Report UTC 2117-FR, United Technology Center, June 1966.

20. Boelter, L. M. K., G. Young, and H. W. Iverson, "An Investigation of Aircraft Heaters XXVII-Distribution of Heat Transfer Rate in the Entrance Section of a Circular Tube," NACA TN1451, July 1948.

21. Kays, W. M., "Convective Heat and Mass Transfer." (Lecture Note Series, Stanford University)

22. Kays, W. M., "Convective Heat and Mass Transfer." (Lecture Note Series, Stanford University)

23. Love, E. S., C. E. Grigsby, L. P. Lee, and M. J. Woodling, "Experimental Theoretical Studies of Axisymmetric Free Jets," NASA TR R-6 1959.

24. Zumwalt, G. W., "Analytical and Experimental Study of the Axially-Symmetric Supersonic Base Pressure Problem," University of Illinois, Doctoral Thesis, 1959.

25. Neissen, W. R., and M. Bretting, "The Study of an Ignition Technique for Large Solid Rocket Motors," Eleventh Annual AFSC Science and Engineering Symposium, Brooks AFB, Texas, 21-22, October 1964.

26. Plumley, Arnold G., "Development of an Analytical Model to Determine Aft Igniter Design Parameters," Aerojet General Corporation Technical Paper 136 SRP, Contract No. AF 04(695)-350, March 1964.

27. Jensen, G. E., "Studies in Ignition and Flame Propagation of Solid Propellants," First Semiannual Report, Contract No. NAS 7-329, United Technology Center, May 1965.